Development of Ocular Surface Tribometer and Computational Program for Determining Frictional Characteristics of Human Ocular Surfaces

Sarwo Pranoto

June 2018

Summary

Dry eye syndrome is considered to be related to friction on human ocular surfaces. In dry eye, a deficiency of the tear fluid causes continuous friction between the eyelid and the ocular surface during blinking. As the tear fluid is decreased, the friction between the eyelid and the ocular surface is increased. Then the friction during blinks can damage the ocular surface. Therefore, many researchers have been interested in examining the mechanical friction on human ocular surfaces to contribute to practitioners in treating dry eye syndrome patients. However, the problem of friction is very complex. Although many researchers have examined the mechanical friction on human ocular surfaces, frictional characteristics of the human ocular surface have not been clarified. Therefore, it is necessary to investigate the plight of ocular surfaces where friction is generated and the associated frictional characteristics in order to solve the dry eye problem.

Hence, the main purpose of this research is to determine frictional characteristics of human ocular surfaces. In this research, frictional coefficient of the human ocular surface is considered related to the viscosity of tear film, the velocity of nictation, and the palpebral pressure. Then an ocular surface tribometer capable of measuring the moving velocity of the probe, normal forces, and frictional forces on human ocular surfaces was developed. A new number that capable of calculating the frictional coefficient of the human ocular surface was proposed. Then by incorporating the proposed new number, a mathematical model describing frictional coefficient of the human ocular surface was also proposed.

The ocular surface tribometer developed in this research consists of two main parts, namely hardware and software. The hardware consists of an electrostatic capacity sensor as a two-axis force sensor, a frame to fix a face, an encoder, a microcontroller, and a laptop-computer. The software consists of a data logger software. In this research, the ocular surface tribometer was used to measure normal forces, frictional forces, and displacements of the probe on six healthy subjects. The data logger was used to process the measured data. By using the data logger, the data on normal forces, frictional forces, and displacements of the probe were sampled synchronously.

In this research, the computational program employing BSG-Starcraft of PSO and LSM was developed. Using the proposed new number in employing the BSG-Starcraft of PSO and LSM, the frictional characteristic curves of human ocular surfaces were determined. In addition, the frictional characteristic curves of human ocular surfaces were also determined by using other methods: the Hersey Number in employing Least-Squares Method (LSM) and the proposed new number in employing the Genetic Algorithm and LSM. Then the obtained frictional characteristic curves were compared.

This research has shown that the frictional characteristics of human ocular surfaces could be classified into three types: the fluid lubrication where the eyelid and ocular surfaces are fully separated by the tear layer, the mixed lubrication where a part of the eyelid and ocular surfaces is supported by the tear layer and in the other part, the eyelid surface may be in contact with the ocular surface, and the lubrication containing both the mixed and fluid ones. In both the mixed lubrication and the lubrication containing the mixed and fluid ones, the appropriate frictional characteristic curves could be obtained for the three methods. While, in the fluid lubrication, the appropriate frictional characteristic curves could be obtained for the two methods using the proposed new number, but the appropriate ones could not be obtained for the method using the Hersey Number.

Contents

Chapter 1

Introduction

1.1 Background

In recent years, dry eye syndrome has been recognized as common health problems that need to be treated in eye cares. Dry eye syndrome is a very common condition that is characterized by a disturbance of the tear fluid and caused by a deficiency of tear fluid. Dry eyes may lead to eye inflammation, scarring on the surface of the corneas and vision problems. Dry eye syndrome can be experienced by various age groups. It has been diagnosed not only among the middle-aged and older people but also among the young-aged that generally are office workers.

The increasing of dry eye syndrome has driven many studies in order to provide contributions for practitioners to formulate appropriate treatment. Some researchers examined the cause of dry eye syndrome. The use of digital electronic devices has been recognized as one of the significant causes of dry eye symptoms. Nowadays, as the use of computers and digital electronic devices has significantly increased, most of the people's daily activities cannot be separated from the use of digital electronic devices such as computer and smartphone. During the use of digital devices, people tend to reduce their blinking rate. Lack of blinking rate may lead to disturbance of tear film. Thus, people who stare at computer monitors or smartphones for a long time may experience a change in their tear production, which is a symptom of dry eye syndrome.

Moreover, many studies have also been conducted to examine the mechanical friction on human ocular surfaces. The friction may happen when there is a deficiency of tear fluid to separate the eyelid and the ocular surface. The deficiency of tear fluid causes continuous friction between the eyelid and the ocular surface during blinking. As the tear fluid is decreased, the friction between the eyelid and the ocular surface is increased. The increase in friction is thought to cause the increase in the severity of blink associated disorder such as LWE (Lid Wiper Epitheliopathy) and LIPCOF (Lid-Parallel Conjunctival Folds). Then the friction during blinks can damage the ocular surface. Also, in dry eye, the pressures of the upper and lower eyelids were significantly higher than those in normal ones. Therefore, the eyelid pressure may change the shape of the cornea during blinking. Besides, various instruments have been developed by researchers to measure the pressure of the eyelid on the ocular surface. Some researchers have also conducted measurements on frictional coefficients of human ocular surfaces. Although many studies have been conducted in mechanical friction, the frictional characteristics of human ocular surfaces have not been clearly determined.

Based on this background, the main objective of this research is to determine frictional characteristics of human ocular surfaces. This research is composed of three main parts. The first part is the development of ocular surface tribometer that composed of hardware and software. The second part is developing computational program employing the BattleStar Galactica (BSG) – Starcraft of Particle Swarm Optimization (PSO) for determining frictional characteristics of human ocular surfaces based on the data measured by the developed ocular surface tribometer. The third part is the comparison of frictional characteristic curves of human ocular surfaces that determined by using the Hersey Number and a proposed new number.

1.2 Literature Review

A review of published papers dealing with the studies on frictional characteristics of human ocular surfaces is presented in this section. The papers were reviewed based on the purposes of this research. The summary of the literature review is shown in Fig. 1.1.
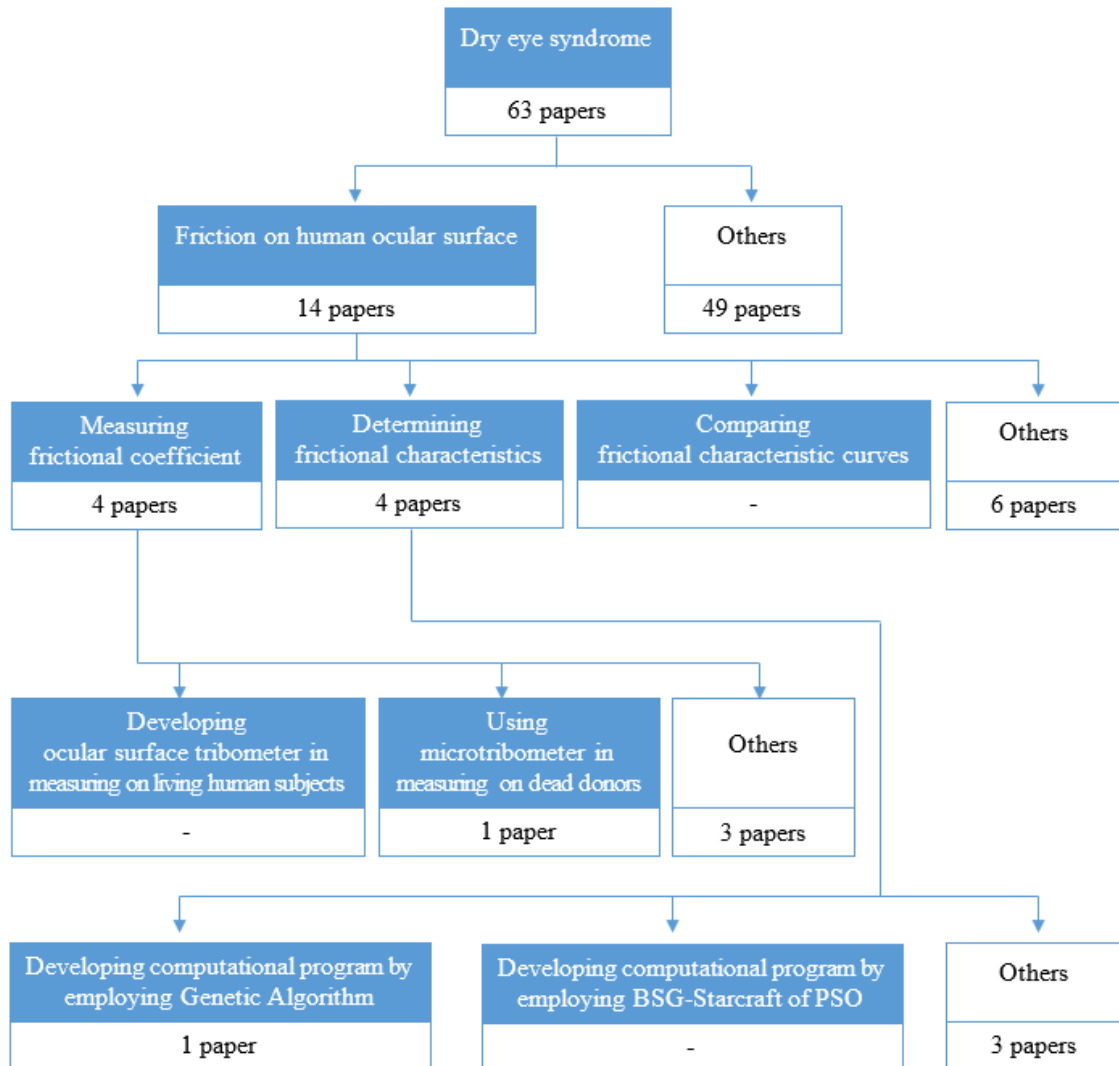

Fig. 1.1 Summary of the literature review

There are 63 [1 – 63] papers discussed about dry eye syndrome reached by the author. As far as the author reached, there are 14 of the reviewed papers [1 - 14] dealt

with friction related to dry eye syndrome. There are four papers [1 – 4] reported on the measurement of frictional coefficients and four papers [5 – 8] reported on determining frictional characteristics. As for the measurement of frictional coefficients, only one paper by T. Wilson et al. [1] reported on the measurement of frictional coefficients of human ocular surfaces. In their paper, the measurements of frictional coefficients were conducted on ocular surfaces of twenty eight dead donors. The ocular surfaces used in the measurements were taken from the dead donors within seven hours after the donors' death. Two papers [2 – 3] reported on the measurement of frictional coefficients on contact lenses and one paper [4] reported the measurement of frictional coefficient of the ocular surface in a murine.

As for the determining frictional characteristics of human ocular surfaces, there are four papers [5 – 8] reported on determining of frictional characteristics of human ocular surfaces. Jones et al. [5] developed an elastohydrodynamic model of the human eyelid wiper. Dunn et al. [6] examined the lubrication regions in contact lens wear during blinking. Pult et al. [7] discussed the friction between upper eyelid and cornea or between upper eyelid and surfaces of a contact lens during spontaneous blinking. Recently, Okamoto et al. [8] developed a physical apparatus and computational program employing a genetic algorithm and least-squares method for measuring frictional coefficients of human ocular surfaces and for determining frictional characteristics of human ocular surfaces.

As for the authors reached, there is no report on developing an ocular surface tribometer that uses an electrostatic capacity type force sensor as a two-axis force sensor for measuring frictional coefficient on living healthy subjects. There is no report developing computational program employing BSG-Starcraft of PSO for determining

frictional characteristics of human ocular surfaces. Furthermore, there is no report comparing frictional characteristic curves of human ocular surfaces that determined by three methods: using the Hersey Number in employing LSM, using the proposed new number in employing the BSG-Starcraft of PSO and LSM, and using the proposed new number in employing the Genetic Algorithm and LSM were used.

1.3 Purposes of Research

The purposes of this research are listed as follows

1. To develop ocular surface tribometer for measuring frictional coefficients of human ocular surfaces.

2. To determine frictional characteristics of human ocular surfaces by implementing BSG-Starcraft of Particle Swarm Optimization and LSM.

3. To compare frictional characteristic curves of human ocular surfaces determined by using the Hersey Number and a proposed new number.

1.4 Structure of Dissertation

The dissertation is structured in the following manner. Chapter 1 presents the background of the research, literature review, purposes of the research and structure of the dissertation. The literature review is addressed to measure frictional coefficients on human ocular surfaces and to determine frictional characteristics of human ocular surfaces.

Chapter 2 presents a study on the development of ocular surface tribometer for measuring frictional coefficients of human ocular surfaces. The development of ocular surface tribometer in order to obtain data that used to calculate frictional coefficients of

human ocular surfaces is firstly described in this chapter. Then, the measurement method of frictional coefficients of human ocular surfaces is presented.

As for the development of ocular surface tribometer, the hardware of the ocular surface tribometer is firstly presented. Then, the software development of ocular surface tribometer is also presented. The hardware of ocular surface tribometer is presented by describing frictional measuring apparatus of the ocular surface tribometer and device to measure moving velocity of the probe, respectively. In addition, the electronic circuit of the ocular surface to process the signal obtained by the frictional measuring apparatus is also described. In this chapter, the development of software for data logger using VB Net is also explained. Then, the measurement method of frictional coefficients of human ocular surfaces is described. After that, the experimental data obtained by the ocular surface tribometer during the research is presented at the end of this chapter.

Chapter 3 presents a study on determining frictional characteristics of human ocular surfaces by employing BattleStarGalactica-Starcraft of Particle Swarm Optimization (BSG-Starcraft of PSO). In this chapter, a mathematical model describing frictional coefficient of human ocular surfaces is firstly explained. Then, the overview of BSG-Starcraft of PSO is explained. Parameters of the frictional characteristic curves of the human ocular surface are also explained in this chapter. After that, the procedure for determining parameters of the frictional characteristic curves of the human ocular surface is presented. Finally, frictional characteristic curves of human ocular surfaces determined by the BSG-Starcraft of PSO and Least-Squares Method (LSM) are presented.

Chapter 4 presents a study on a comparison of frictional characteristic curves of the human ocular surface determined by using the Hersey Number and a proposed new number. In this chapter, the frictional characteristic curves are determined by using three

methods: the Hersey Number in employing LSM, the proposed new number in employing the BSG-Starcraft of PSO and LSM, and the proposed new number in employing Genetic Algorithm and LSM. Then the obtained frictional characteristic curves are compared.

Finally, chapter 5 presents the summary of conclusions of the research. In addition, list of references of reviewed literature and publications as the core of dissertation are given at the end of this dissertation.

Chapter 2

Development of Ocular Surface Tribometer for Measuring Frictional Coefficients of Human Ocular Surfaces

2.1 Introduction

In the field of mechanical engineering, to identify the frictional coefficients on journal bearings, the Hersey Number is commonly applied. The Hersey Number is shown as in (2.1).

$$H_s = \frac{\eta \omega}{p} \tag{2.1}$$

Where η is the viscosity of lubricating oil, ω the rotational speed of a shaft, and p the pressure of lubricating oil behind the location of the minimum separation between the bearing and the shaft.

2.2 Frictional Coefficients of Human Ocular Surfaces

In this research, the frictional coefficient, μ of a human ocular surface is considered to be related to the viscosity, η of tear fluid, the velocity, V_n of nictation, and the palpebral pressure, P. Then, a new ocular surface tribometer capable of measuring the moving velocity, V of the probe, the normal force, N, and the frictional force, F was developed. The measured data of normal forces and frictional forces are used to calculate frictional coefficient, μ of a human ocular surface. The frictional coefficient, μ of a human ocular surface is calculated using equation as shown in (2.2).

$$\mu = \frac{F}{N} \tag{2.2}$$

2.3 Development of Ocular Surface Tribometer

The development of ocular surface tribometer is divided into two main parts, namely development of hardware and development of software.

2.3.1 Development of Hardware

In this research, the hardware of ocular surface tribometer consists of the frictional coefficient measuring apparatus and the device to measure the moving velocity of the probe.

Figure 2.1 shows the frictional coefficient measuring apparatus. The frictional coefficient measuring apparatus consists of an amplifier and an electrostatic capacity type force sensor as a two-axis force sensor (Tech Alpha, Japan). The frictional coefficient measuring apparatus is used to measure normal force and frictional force acquired by the probe. The probe is made of stainless steel and has a spherical ball of 3 [mm] diameter on its tip.
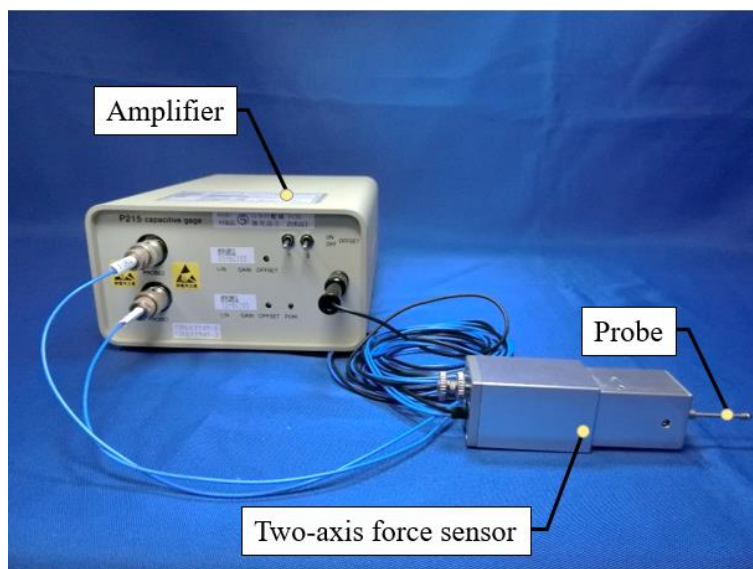

Fig. 2.1 Frictional coefficient measuring apparatus

Table 2.1 shows the specifications of the two-axis force sensor. The two-axis force sensor is used to measure normal force and frictional force in the range of 0 ~ 4.6 [gf] and

± 2.7 [gf], respectively. The sensitivity of the sensor to measure normal force is 1.96 [V/gf] and the sensitivity of the sensor to measure frictional force is 2.13 [V/gf]. The output voltages of the sensor are in the range – 2 [V] ~ 14 [V] for both normal force and frictional force. However, the guaranteed output voltage for both normal force and frictional force are in the range of 0 ~ 10 [V].

Table 2.1 Specifications of the two-axis force sensor

	Normal force	Frictional force
Channel	1	2
Measurement range [gf]	0 ~ 4.6	± 2.7
Sensitivity [V/gf]	1.96	2.13
Measurement upper limit [V]	10	10
Measurement lower limit [V]	0	0

Figure 2.2 shows the device to measure moving velocity of the probe. The device to measure moving velocity of the probe was designed in order to be able to move the probe of a two-axis force sensor in Z and X directions. The device to measure V of the probe consists of a frame to fix a face, two pulleys, a belt, slide rails to adjust probe position in Z, a slide rail to adjust probe position in X, slide rail blocks, a stainless steel plate, an encoder, a microcontroller, and a laptop computer.

Figure 2.3 shows the parts of the device to measure moving velocity of the probe that capable of moving in Z direction. The parts consist of slide rails, slide rail blocks, a linear guide clamper, a screw, springs, and a sensor mounting base.
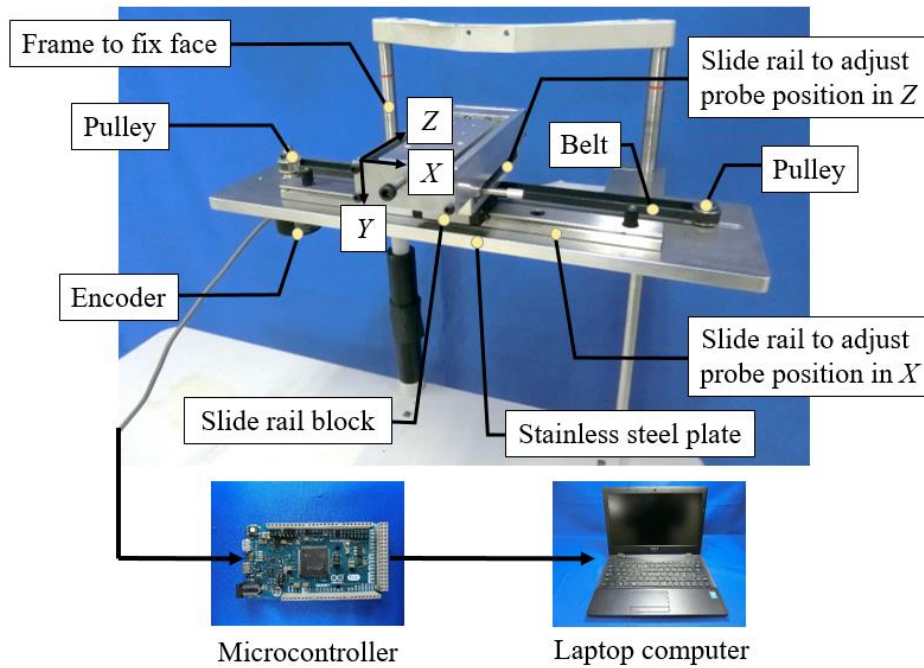
Fig. 2.2 Device to measure moving velocity of probe
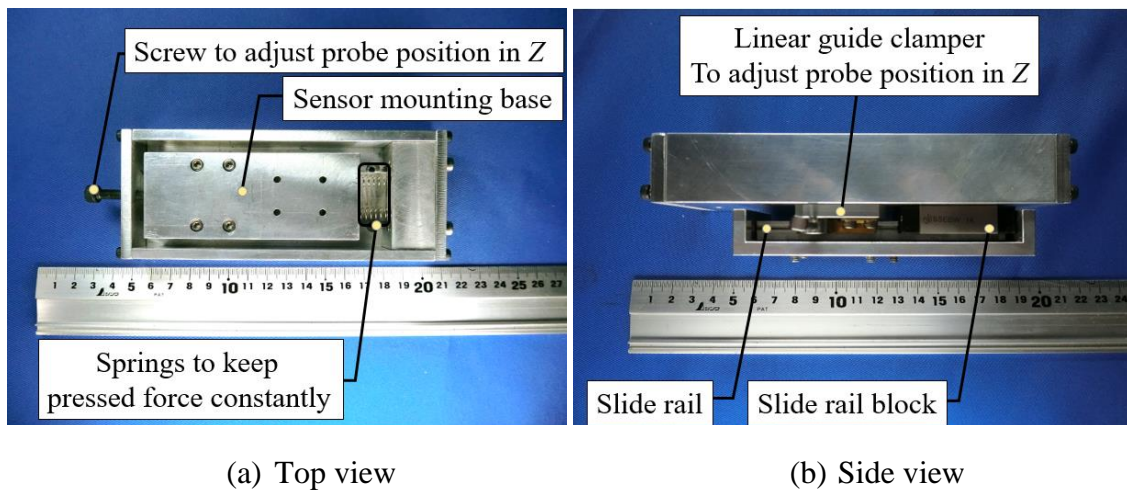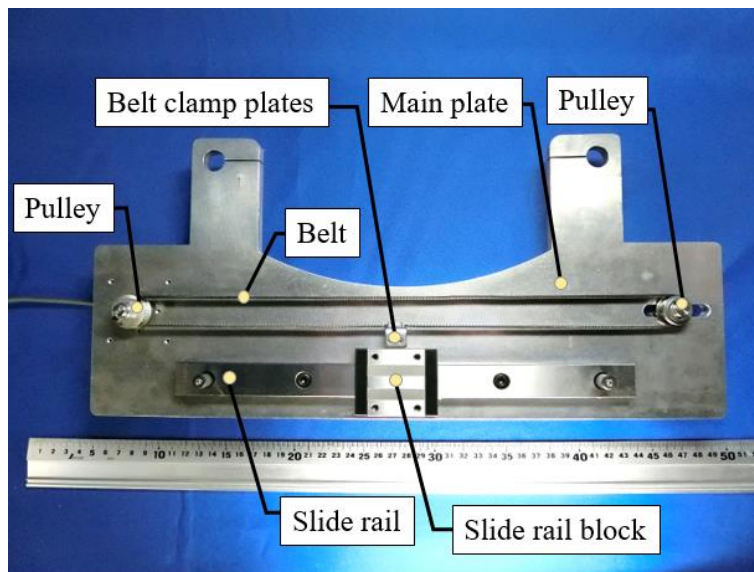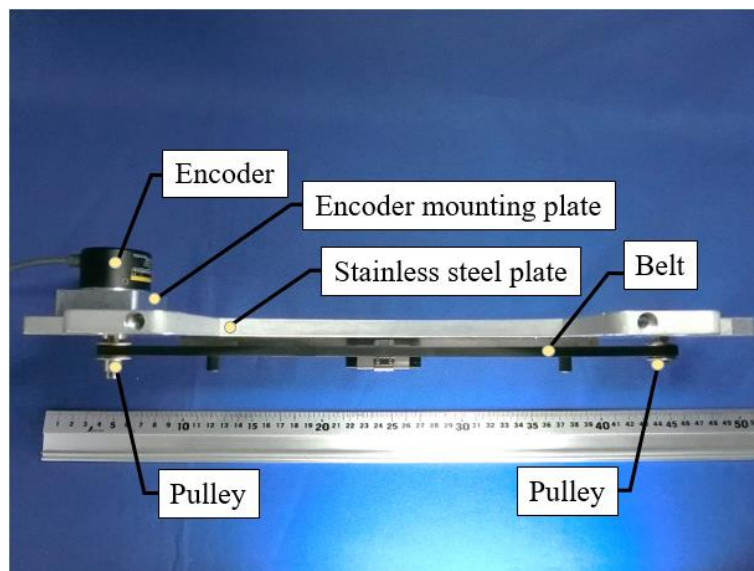

(a) Top view   (b) Side view

Fig. 2.3 Parts of the device to measure moving velocity of the probe that

capable of moving in Z direction

Figure 2.4 shows the parts of the device to measure moving velocity of the probe that capable of moving in X directions. The parts consist of a stainless steel plate, a slide rail, a slide rail block, a belt, a belt clamp plates, two pulleys, a bearing, and an encoder.
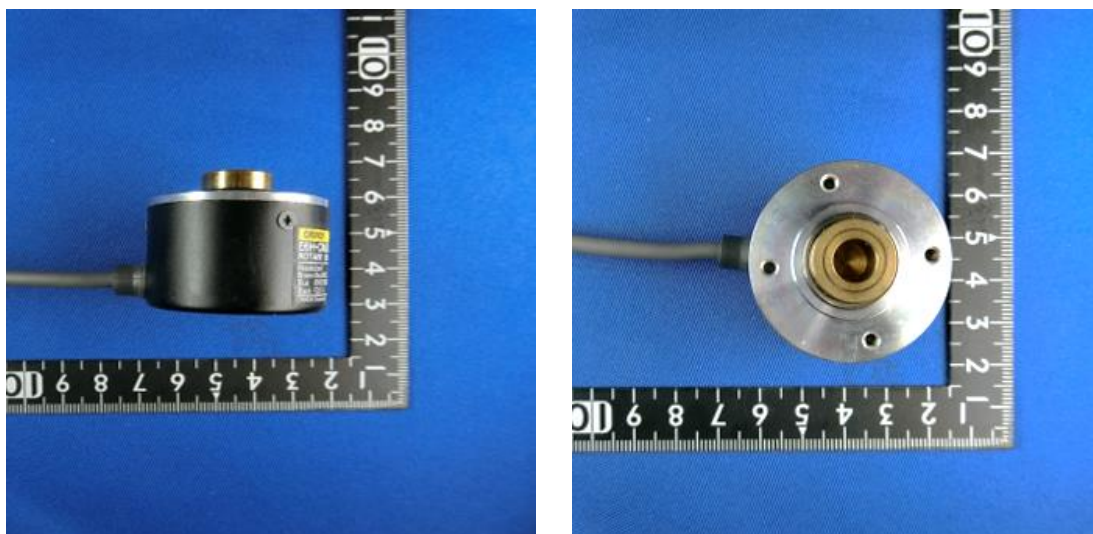
(a) Top view

(b) Side view

Fig. 2.4 Parts of the device to measure moving velocity of the probe that capable

of moving in X directions

Figure 2.5 and Figure 2.6 show the encoder (E6H-CWZ6C, Omron, Co.) used for measuring moving velocity of the probe and the encoder mounting plate, respectively. Table 2.2 shows the specifications of the encoder.

(a) Side view   (b) Top view

Fig. 2.5 Encoder (E6H-CWZ6C, Omron, Co.)

Fig. 2.6 Encoder mounting plate

Table 2.2 Specifications of encoder

Model number (OMRON Co.)	E6H-CWZ6C
Power supply voltage	DC 5 ~ 24 [V]
Output form	Open collector
Resolution	1,000 [pulse/rev]
Maximum permissible speed	10,000 [rpm]

Figure 2.7 shows the bearing with housing. The bearing with housing (SBACR698ZZ, Misumi Group Inc.) is used as a part of the device to measure moving velocity of the probe.
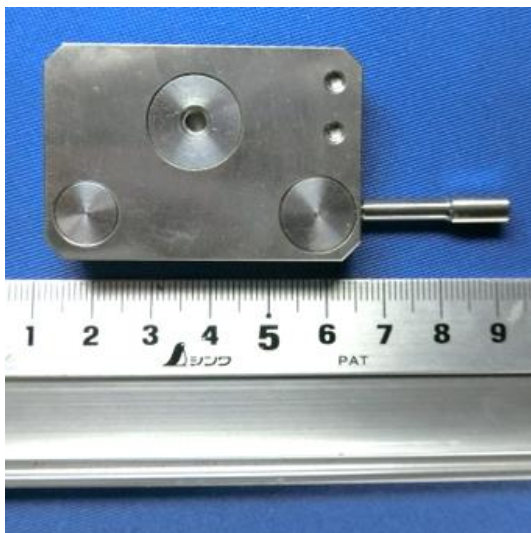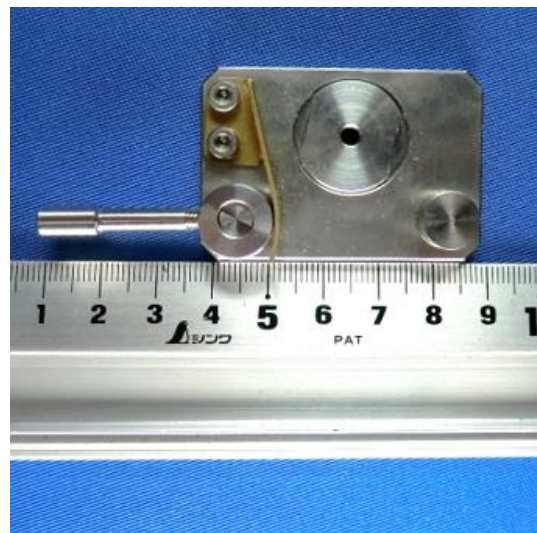

(a) Top view　　　　　　　　　　　(b) Side view

Fig. 2.7 Bearing with housing

Figure 2.8 shows slide rail clamper. Slide rail clamper is used to tight and set the position of the probe in Z direction when applying normal force on human ocular surfaces.

(a) Top view　　　　　　　　　　　(b) Bottom view

Fig. 2.8 Slide rail clamper

Figure 2.9 shows the slide rails and slide rail blocks. Slide rails and slide rail blocks (SSEBWL14G-100, SSEBWL14G-130, Misumi Group Inc.) are used in mechanism for moving the probe in Z direction. Slide rail and slide rail block (SSEBV20-280, Misumi Group Inc.) is used in mechanism for moving the probe in X directions.
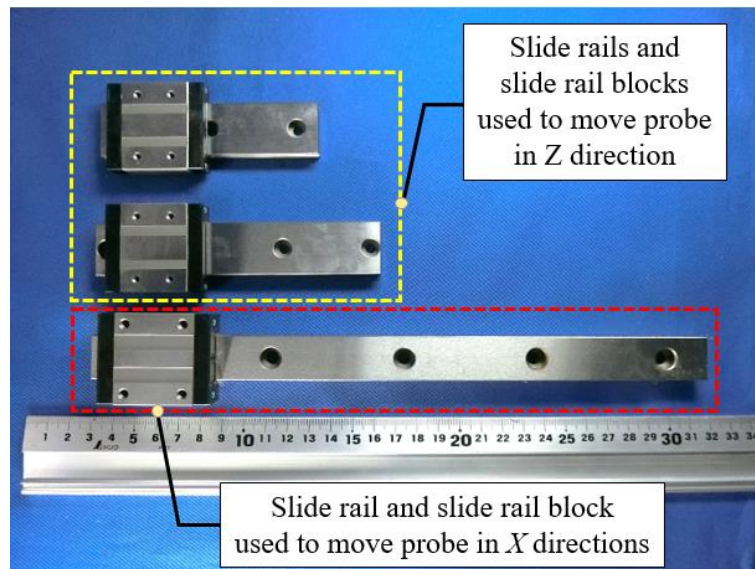

Fig. 2.9 Slide rails and slide rail blocks

Figure 2.10 shows the moving directions of the probe in ocular surface tribometer on the left eye. The moving direction of the probe in Z direction is needed in order to apply normal forces by pushing the probe on the ocular surface. The moving direction of the probe in X directions is needed in order to obtain data on frictional force and displacement of the probe.

In addition, the device for measuring moving velocity of the probe composed of electronic parts, namely microcontroller (Arduino Due Board) and laptop computer. Figure 2.11 shows the Arduino Due Board. The specifications of the Arduino Due Board are shown in Table 2.3.

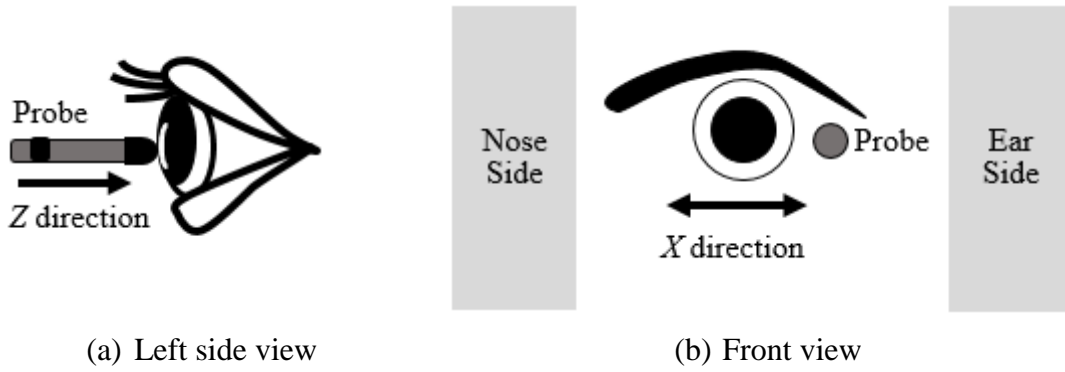(a) Left side view   (b) Front view

Fig. 2.10 Moving directions of the probe in ocular surface tribometer on the left eye

Fig. 2.11 Arduino Due Board

Table 2.3 Specifications of Arduino Due Board

Microcontroller	AT91SAM3X8E
Operating Voltage	3.3V
Flash Memory	512 KB
SRAM	96 KB
Clock Speed	84 MHz

Figure 2.12 shows laptop computer. The specifications of the laptop computer are shown in Table 2.4.

Fig. 2.12 Laptop computer

Table 2.4 Specifications of laptop computer

Manufacturer	Mouse computer
Processor	Intel(R) Core(TM) i7-5500U CPU @2.4GHz
RAM	8 GB
OS	Windows 10 Home 64 bit

On the developed ocular surface tribometer, the output signals of the sensor from the amplifier need to be inputted to the microcontroller in order to be processed using the data logger software. However, the microcontroller can only take in the signals in the range of 3.3 volt of DC as input. To address this issue, a suitable voltage signal conditioning circuit is needed to be designed which can convert the output voltages of the sensor to the range of 3.3 volt of DC input. For this purpose, a signal conditioner has been

designed as shown in Figure 2.13. Figure 2.14 shows the schematic of the signal conditioner. The wiring diagram of the electronic circuit used on the ocular surface tribometer is shown in Figure 2.15.
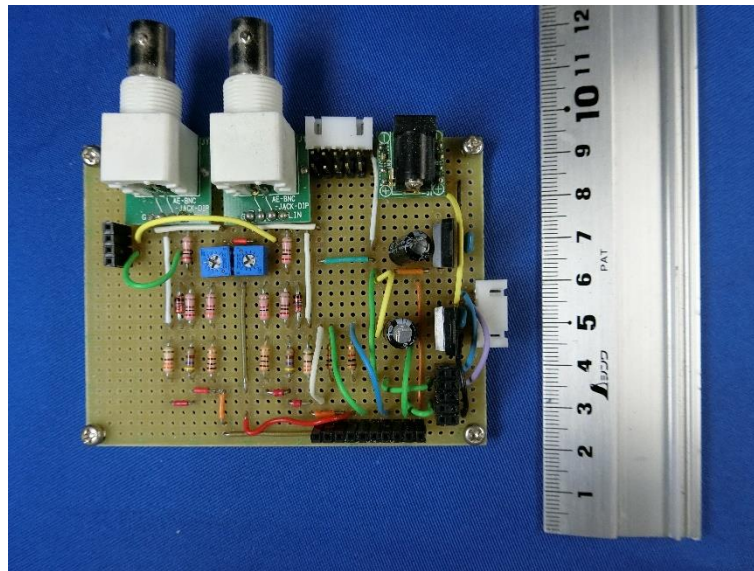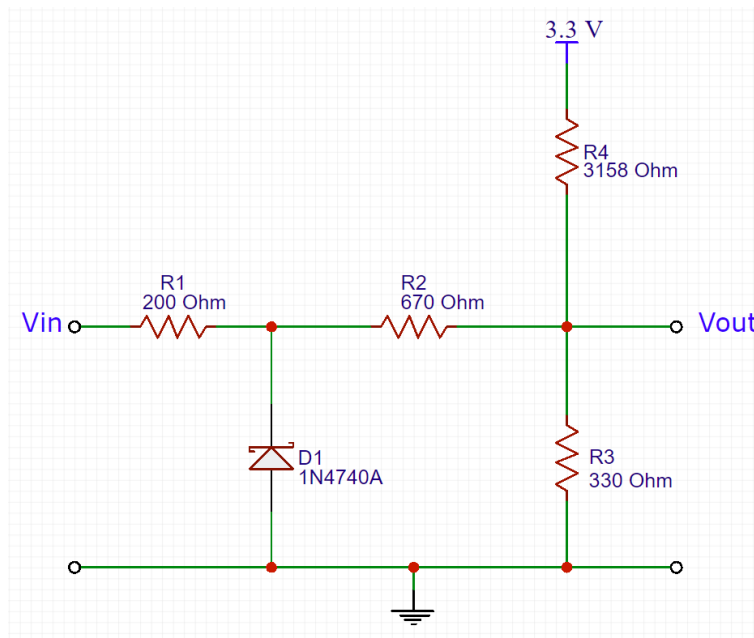

Fig. 2.13 Signal Conditioner

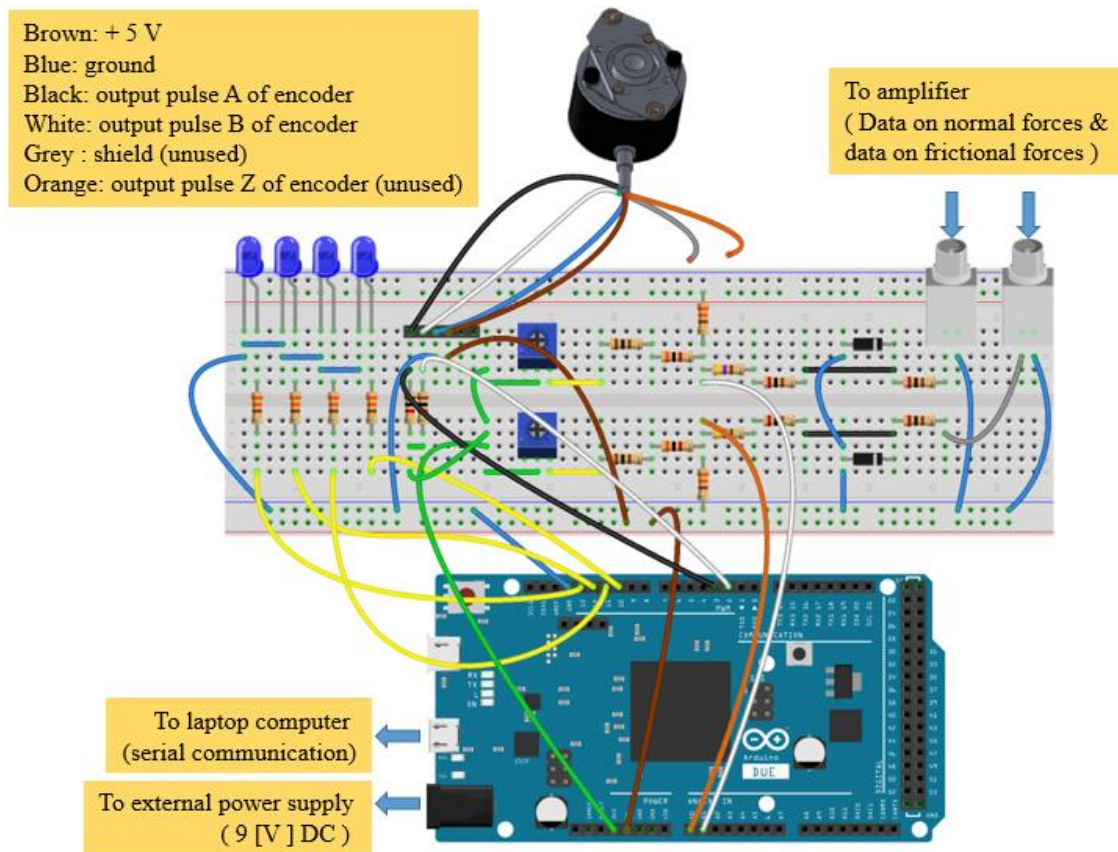Fig. 2.14 Electronic circuit of signal conditioner

Fig. 2.15 Wiring diagram of electronic circuit used on ocular surface tribometer

Figure 2.16 shows the block diagram of measurement process on ocular surface tribometer. The analog values of normal forces and frictional forces from the signal conditioner are converted to digital ones by using the ADC module in the microcontroller. The microcontroller is used to send digital data of normal forces, frictional forces, and encoder to PC via serial communication to be further processed using data logger software. A display consisting of LEDs is used to indicate the value of normal forces applied on the ocular surface.
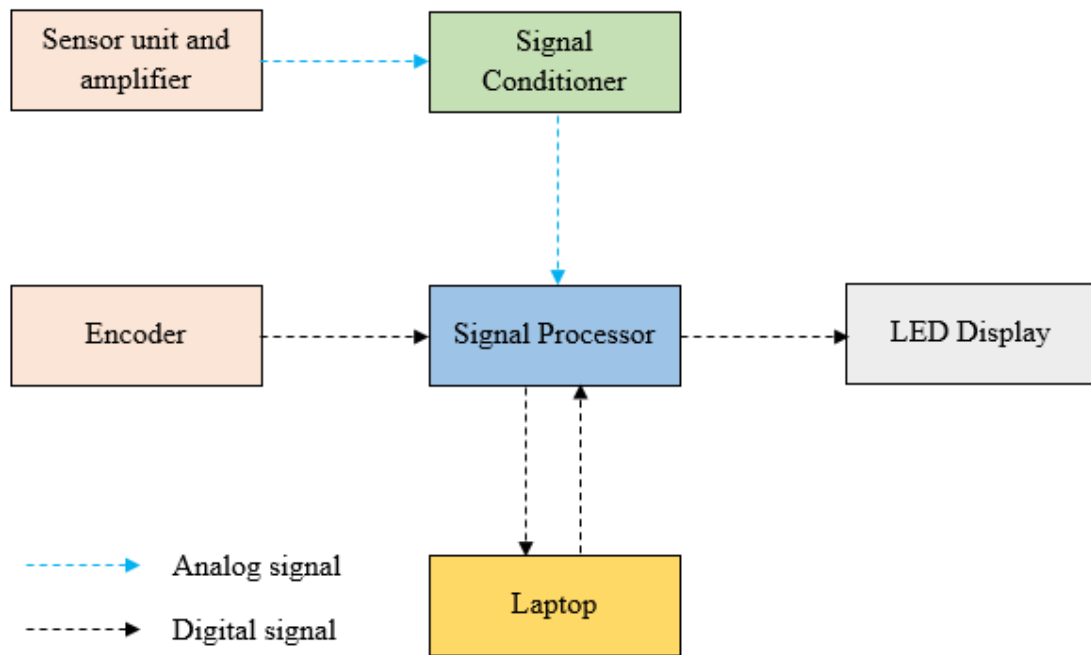
Fig. 2.16 Block diagram of measurement process on ocular surface tribometer

2.3.2 Development of Software

The developed software of ocular surface tribometer consists of two parts. The first part is the software used to process the measured data in the microcontroller. The second part is the software used to process the measured data on the laptop computer.

In the previous section of this dissertation, it was mentioned that the Arduino Due Board is used in the research. Then, in order to program Arduino Due Board, the Arduino IDE (Integrated Development Environment) is used. In this research, Arduino IDE 1.6.9 was used to write code and upload it to the Arduino Due Board.

Figure 2.17 shows the environment of the Arduino IDE 1.6.9. The Arduino development environment contains a text editor, a message area, a menu and a toolbar.
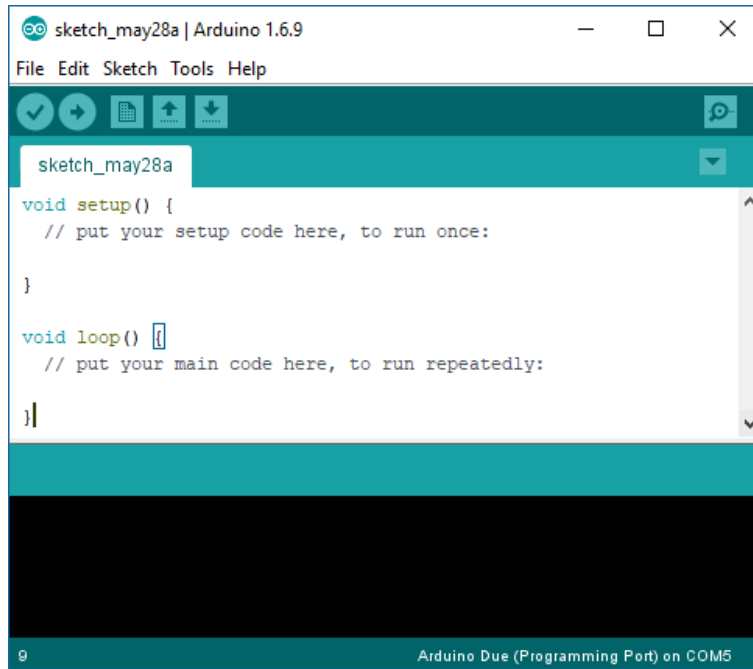
Fig. 2.17 Arduino Integrated Development Environment (IDE) 1.6.9

The second part of the developed software, namely data logger software is used to process measured data in the laptop computer. In this research, the data logger software was developed by using Visual Studio 2015. Visual Studio 2015 used in this research has a comprehensive collection of tools and services to develop the application of data logger for running in Microsoft Windows operating system. The data logger provides a graphical user interface which gives the user access to some features. The application program was created in Visual Basic.NET and uses a Structured Query Language (SQL) for database maintenance. Table 2.5 shows the GUI windows of the data logger.

Table 2.5 GUI windows of the data logger

Window	Function
Splash Screen	To show opening data logger software
Main Menu	To record measured data, display measurement in real time,
Setting	To set connection between PC and microcontroller
Calibration	To calibrate the sensor

Figure 2.18 and Figure 2.19 show the splash screen of the eye data logger and the main window of the eye data logger, respectively. The splash screen will be loaded for about 5 seconds when the software is running for the first time. Then the main window will be displayed. The main window consists of four parts: menu bar, toolbar, charts area, and tab pages. The menu bar and toolbar provide interfaces to the user such as record, open file, save file, print, view statistic data, setting serial communication and view each measured data. The chart areas are used for plotting data of normal forces, frictional forces and displacements of the probe. Each measured data can be viewed using the button on the left side of the main window. The tab pages consist information about the values of normal forces, frictional forces, displacements of the probe, frictional coefficients, velocity of the probe, date and time when the measurement of frictional coefficient of the human ocular surface was taken.

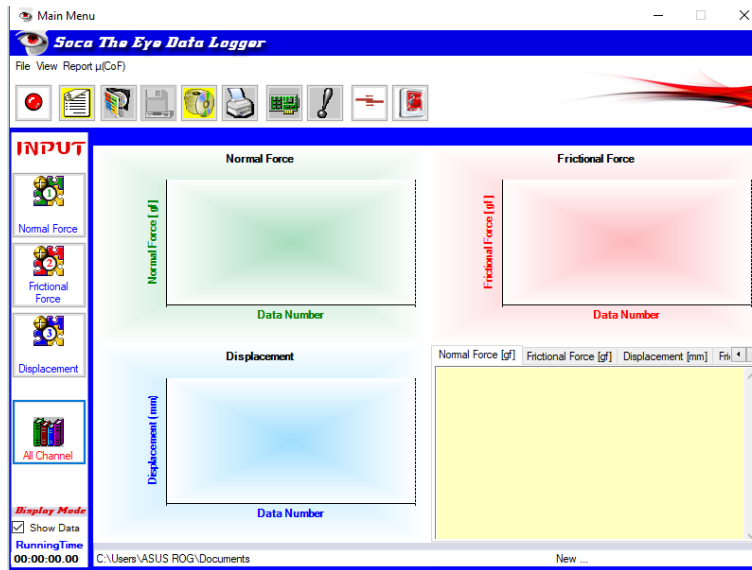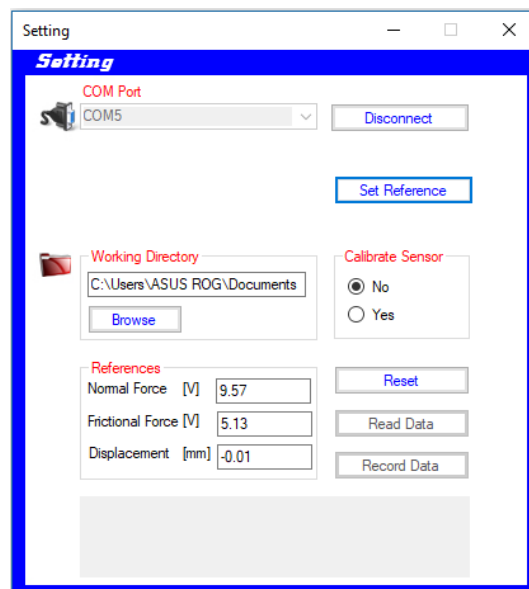Fig. 2.18 Splash screen of the eye data logger

Fig. 2.19 Main window of the eye data logger

Figure 2.20 shows the setting window. The setting window is used to connect the PC and microcontroller, set voltages reference for measuring normal forces and frictional forces, reset normal force data, frictional force data and displacement of probe data to zero values, set the working directory and open the calibration window.
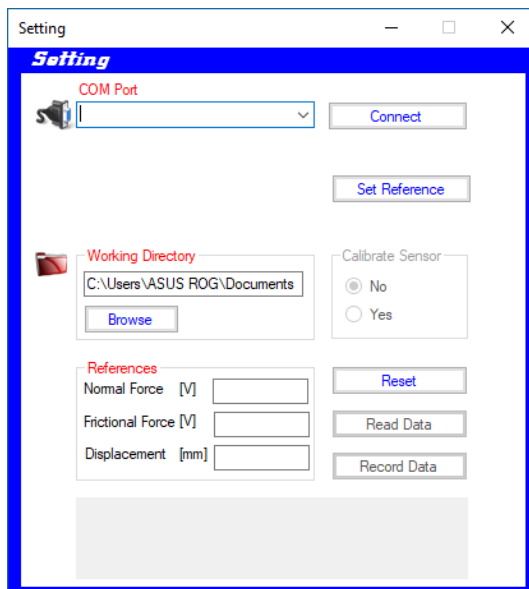
(a) Connect to microcontroller   (b) Set voltages reference

(c) Reset voltages reference   (d) Read measured data

Fig. 2.20 Setting window

Figure 2.21 shows the calibration window. The calibration window is used to calibrate the sensitivity of the two-axis force sensor.
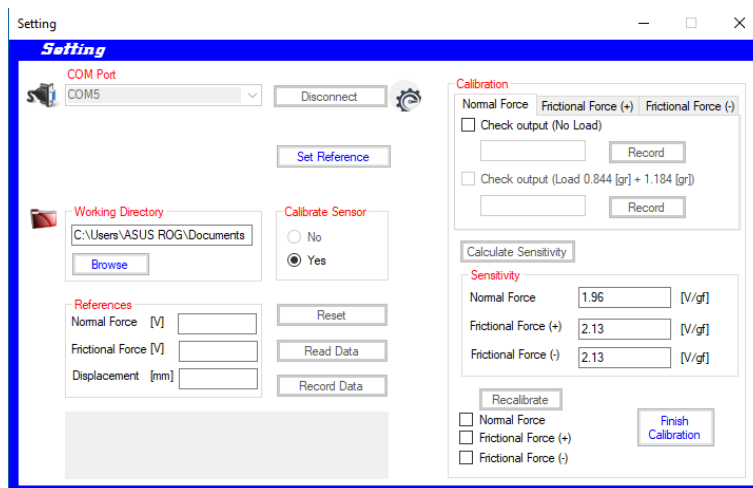

Fig. 2.21 Calibration window

Figures 2.22 to 2.25 show the GUI windows for opening the saved file, plotting the measured data, selecting the measured data, saving the selected measured data.

24

Fig. 2.22 Window for
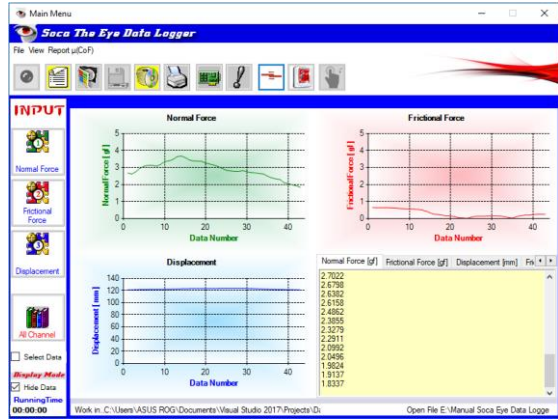opening the saved file

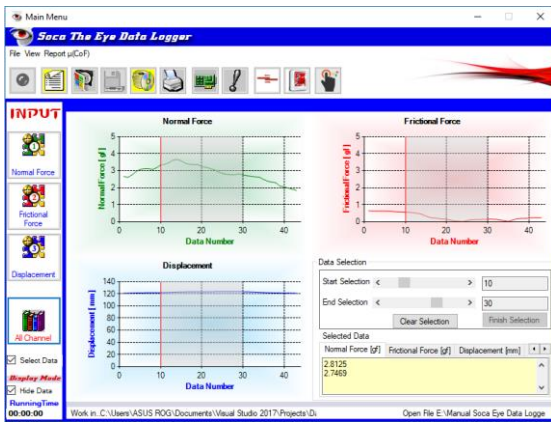Fig. 2.23 Window for
plotting the measured data

Fig. 2.24 Window for
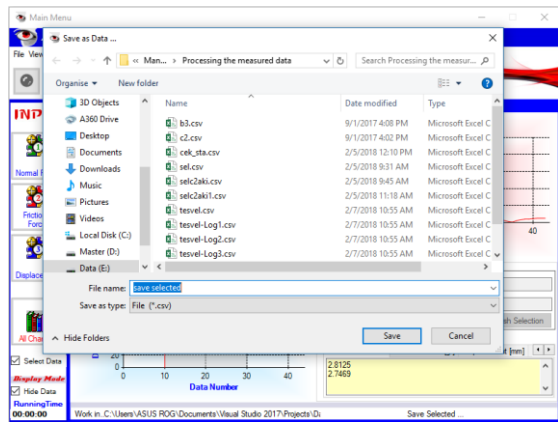selecting the measured data

Fig. 2.25 Window for
saving the selected measured data

Figure 2.26 shows the ocular surface tribometer. The ocular surface tribometer consist of hardware and software.

① Frame to fix face
② Data on normal force & frictional force
③ Pulley
④ Encoder
⑤ Data on rotational angle measured with encoder
⑥ Amplifier
⑦ Signal conditioner & signal processor
⑧ Two-axis force sensor
⑨ Camera
⑩ LED
⑪ Belt
⑫ Slide rail to adjust probe position in X
⑬ Laptop computer
⑭ Data on normal force, frictional force & rotational angle measured with encoder via serial cable
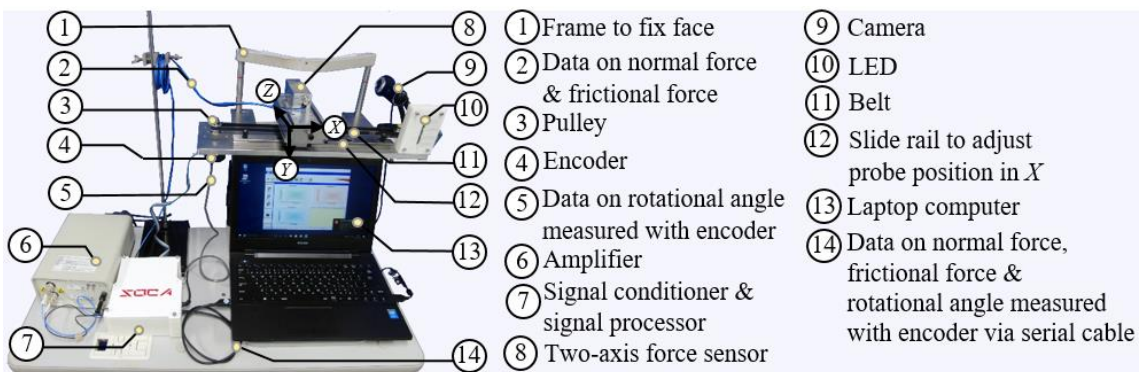
Fig. 2.26 Ocular surface tribometer

2.4 Measurement Method of Frictional Coefficients of Human Ocular Surfaces

In this research, the measurement of frictional coefficients of human ocular surfaces was conducted on six healthy subjects (A, B, C, D, E, and F). The frictional coefficients on the cornea and the bulbar conjunctiva near the ear side were measured on the left eye of the subjects. Figure 2.27 shows the measurement positions and slide directions of the probe on the human ocular surface.
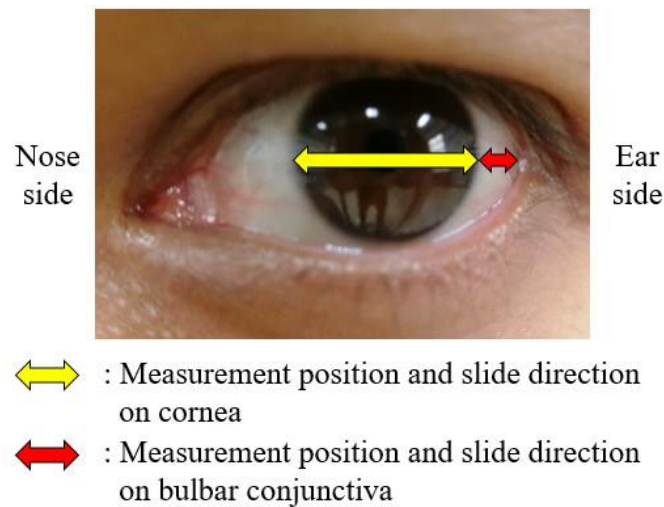

Fig. 2.27 Measurement positions and slide directions of probe on human ocular surfaces

Figure 2.28 shows the flowchart of the measurement procedure. The procedure to measure frictional coefficients of human ocular surfaces consists of several steps. First, in order to eliminate the pain during the measurement of the frictional coefficients, an anesthetic solution (0.4% of Benoxyl eye drop, Santen) was dropped to the eye of the subject. Figure 2.29 shows the anesthetic solution (0.4% of Benoxyl ophthalmic anesthetic, Santen).
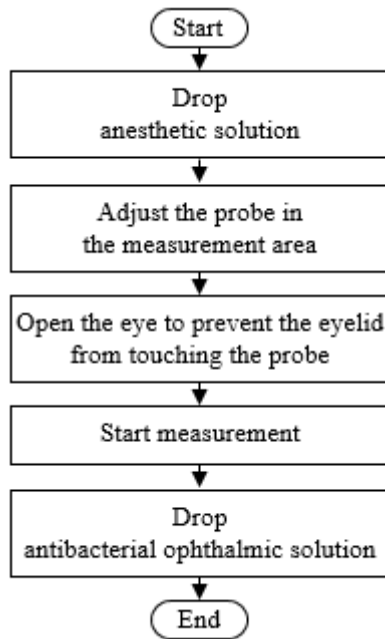
Fig. 2.28 Flowchart of the measurement procedure

Fig. 2.29 Ophthalmic anesthetic used in the experiment

Second, after 15 to 20 seconds since the dropping of the anesthetic solution, the face of the subject is fixed on the frame. The face of the subject was fixed on the frame by adjusting the height of the frame and the position of the probe in the X direction so that the tip of the probe is located in front of the left eye as shown in Figure 2.30.
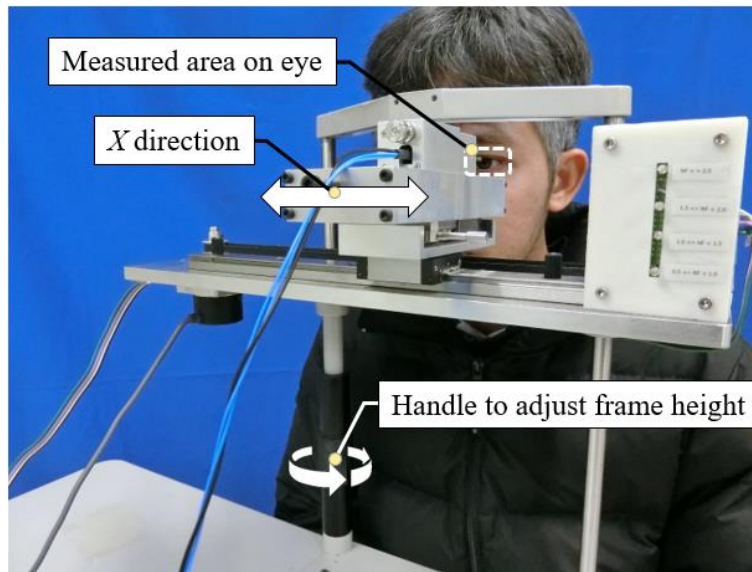
Fig. 2.30 Adjustment of probe in X direction

Third, the probe position was adjusted in Z direction as shown in Figure 2.31. The probe was adjusted by moving the probe in Z direction until the probe nearly touch the eye of the subject. The slide rail clamper is used to tight the probe position.
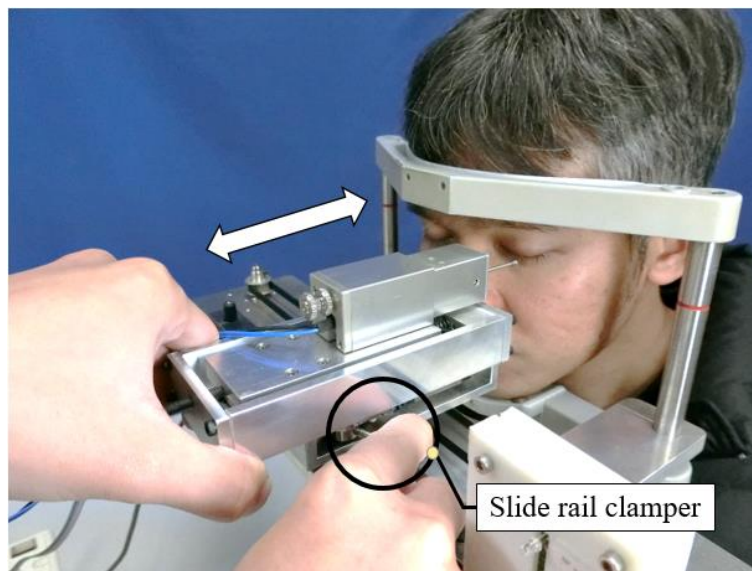

Fig. 2.31 Adjustment of probe in Z direction using slide rail clamper

Next, using a screw as shown in Figure 2.32, the probe was moved in Z direction until the tip of the probe touch the eye surface.
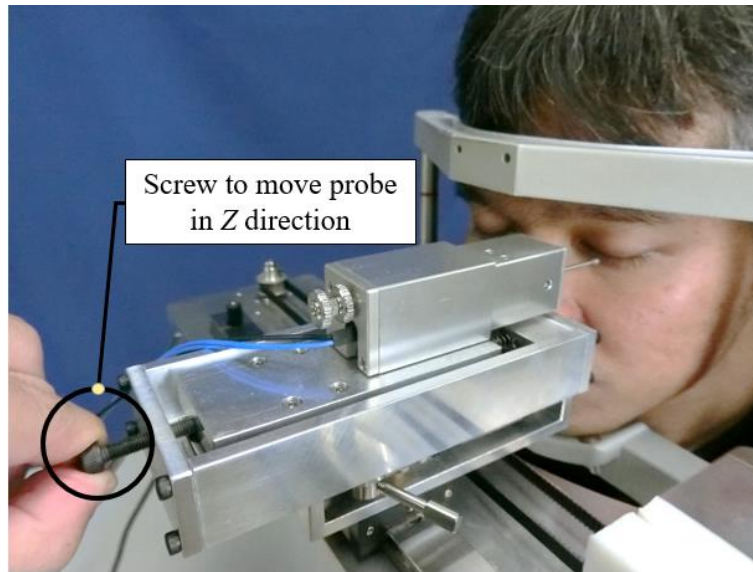
Fig. 2.32 Screw to move probe in Z direction

Then, the measurement is started by opening the eye in order to prevent the eyelid from touching the probe as shown in Figure 2.33. In this step, the applied normal force was controlled in the range below 4.6 [gf] and the probe is moved in X direction in order to obtained data on frictional force and displacement of the probe.
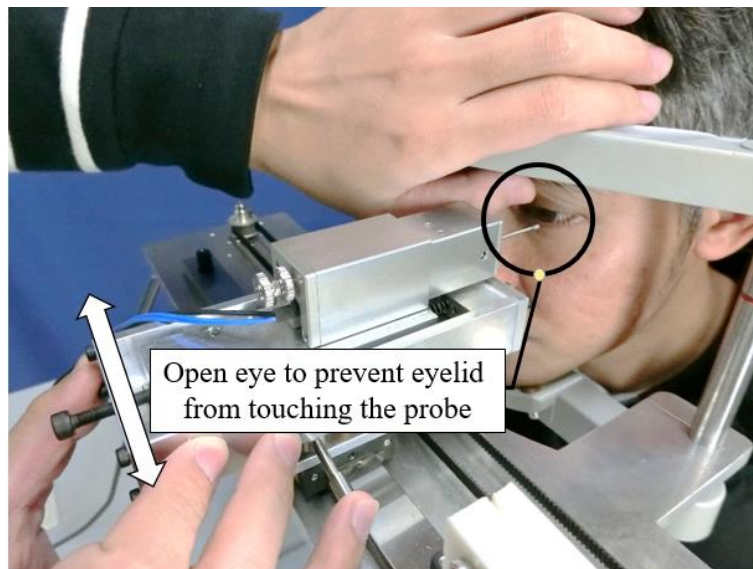
Fig. 2.33 Start measurement

Figure 2.34 shows the examples of measurements of frictional coefficients on the cornea and bulbar conjunctiva of healthy subjects.

(a) Measurement of frictional coefficients on cornea of the left eye
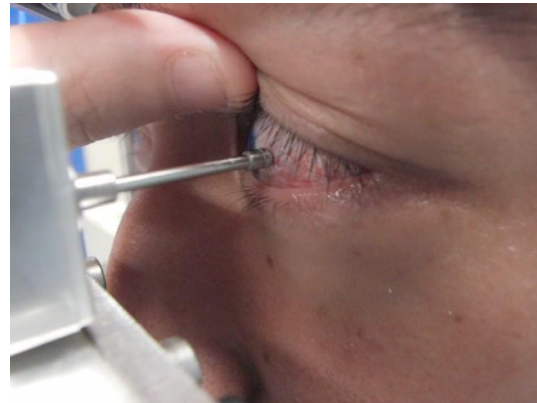
(b) Measurement of frictional coefficients on bulbar conjunctiva of the left eye

Fig 2.34 Examples of measurements of frictional coefficients on the cornea and bulbar conjunctiva of healthy subjects

Finally, after the measurement, an antibacterial ophthalmic solution (0.3% gatifloxacin ophthalmic solution, Senju Pharmaceutical Co., Ltd.) as shown in Figure 2.35 was instilled into the eye of the subject.

Fig. 2.35 Antibacterial ophthalmic solution (0.3% gatifloxacin ophthalmic solution, Senju Pharmaceutical Co., Ltd.)

2.5 Experimental Results

Figures 2.36 to 2.41 show the examples of experimental data measured by the ocular surface tribometer on the cornea of six healthy subjects (A, B, C, D, E, and F), respectively. In all experiments, time history responses of N, F, and d were measured at the same time using the developed ocular surface tribometer.

Figure 2.36 shows the examples of experimental data measured by the ocular surface tribometer on the cornea of subject A. In this experiment, normal forces were applied to the cornea within the range of 1.83 [gf] to 3.67 [gf]. Frictional forces were measured in the range of 0.01 [gf] to 0.64 [gf]. The average values of normal forces and frictional forces are 2.87 [gf] and 0.29 [gf], respectively. The displacements of the probe were measured by the encoder and controlled to be within the maximum range of 2.56 [mm].

Figure 2.37 shows the examples of experimental data measured by the ocular surface tribometer on the cornea of subject B. In this experiment, normal forces were applied to the cornea within the range of 0.75 [gf] to 1.96 [gf]. Frictional forces were measured in the range of 0.01 [gf] to 0.22 [gf]. The average values of normal forces and frictional forces are 1.51 [gf] and 0.13 [gf], respectively. The displacements of the probe were measured by the encoder and controlled to be within the maximum range of 2.80 [mm].
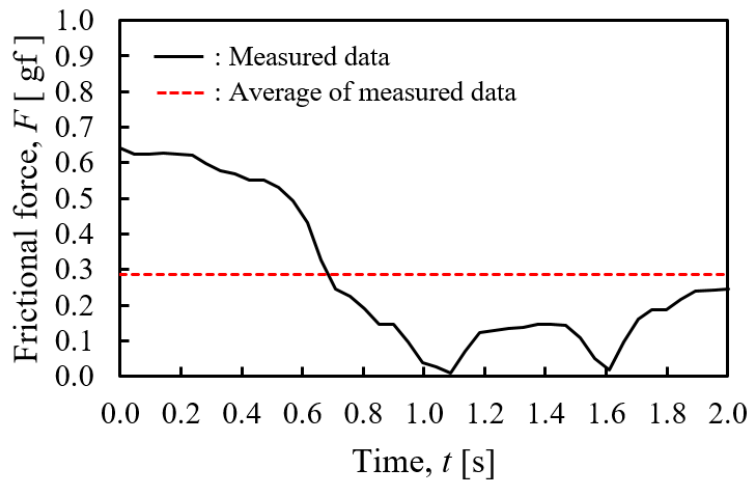
Figure 2.38 shows the examples of experimental data measured by the ocular surface tribometer on the cornea of subject C. In this experiment, normal forces were applied to the cornea within the range of 0.43 [gf] to 2.11 [gf]. Frictional forces were measured in the range of 0.01 [gf] to 0.49 [gf]. The average values of normal forces and frictional forces are 1.30 [gf] and 0.12 [gf], respectively. The displacements of the probe were measured by the encoder and controlled to be within the maximum range of 3.14 [mm].
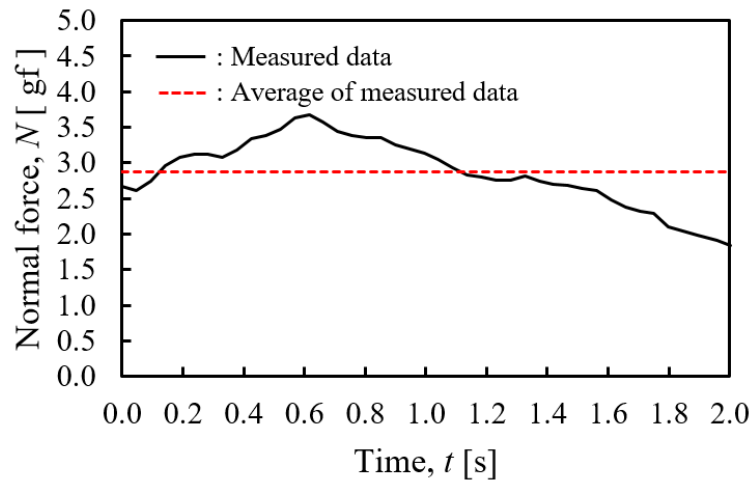
(a) Normal force

(b) Frictional Force

(c) Displacement

Fig. 2.36 Examples of cornea's data measured by the ocular surface tribometer on subject A

(a) Normal force

(b) Frictional force

(c) Displacement

Fig. 2.37 Examples of cornea's data measured by the ocular surface tribometer on subject B

(a) Normal force

(b) Frictional force

(c) Displacement

Fig. 2.38 Examples of cornea's data measured by the ocular surface tribometer on subject C
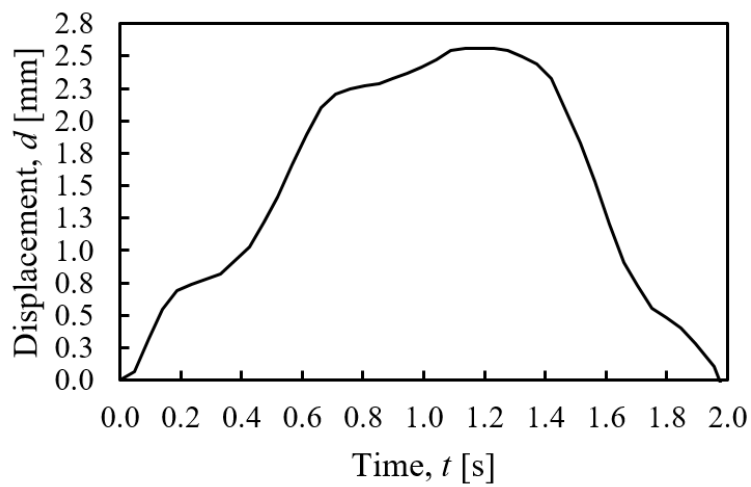
Figure 2.39 shows the examples of experimental data measured by the ocular surface tribometer on the cornea of subject D. In this experiment, normal forces were applied to the cornea within the range of 0.59 [gf] to 1.20 [gf]. Frictional forces were measured in the range of 0.01 [gf] to 0.11 [gf]. The average values of normal forces and frictional forces are 0.97 [gf] and 0.07 [gf], respectively. The displacements of the probe were measured by the encoder and controlled to be within the maximum range of 2.62 [mm].

Figure 2.40 shows the examples of experimental data measured by the ocular surface tribometer on the cornea of subject E. In this experiment, normal forces were applied to the cornea within the range of 1.02 [gf] to 1.51 [gf]. Frictional forces were measured in the range of 0.01 [gf] to 0.14 [gf]. The average values of normal forces and frictional forces are 1.21 [gf] and 0.08 [gf], respectively. The displacements of the probe were measured by the encoder and controlled to be within the maximum range of 1.55 [mm].

Figure 2.41 shows the examples of experimental data measured by the ocular surface tribometer on the cornea of subject F. In this experiment, normal forces were applied to the cornea within the range of 1.98 [gf] to 2.30 [gf]. Frictional forces were measured in the range of 0.03 [gf] to 0.25 [gf]. The average values of normal forces and frictional forces are 2.08 [gf] and 0.17 [gf], respectively. The displacements of the probe were measured by the encoder and controlled to be within the maximum range of 2.12 [mm].
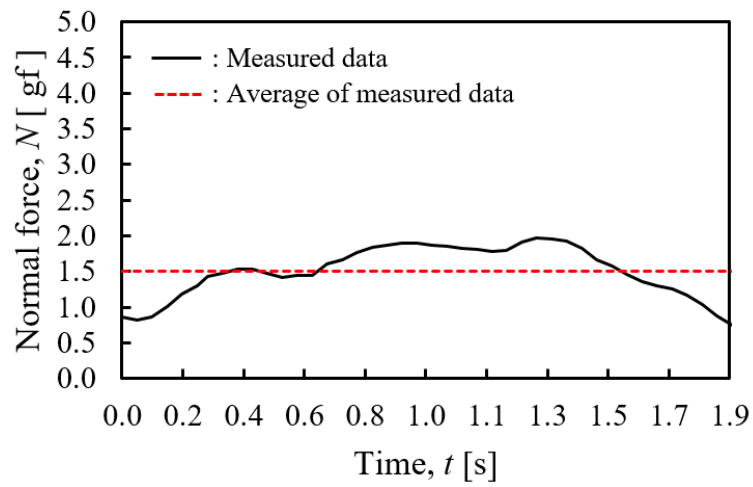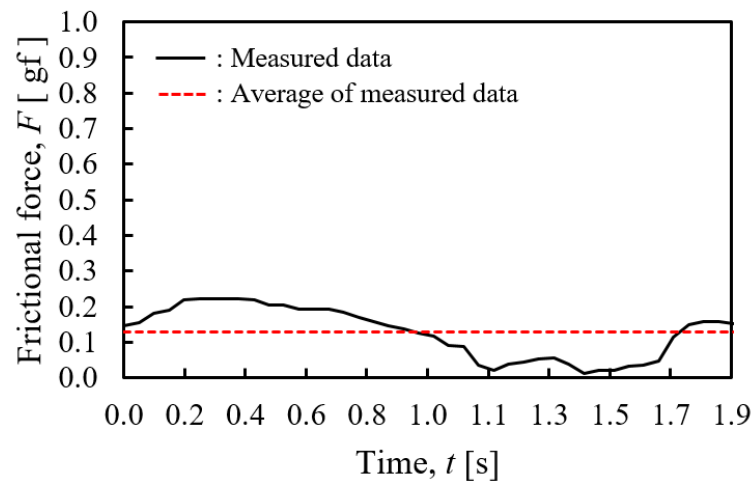
(a) Normal force

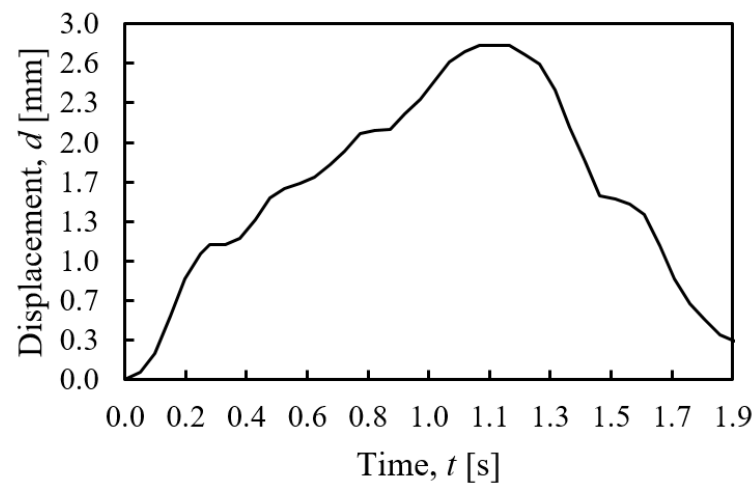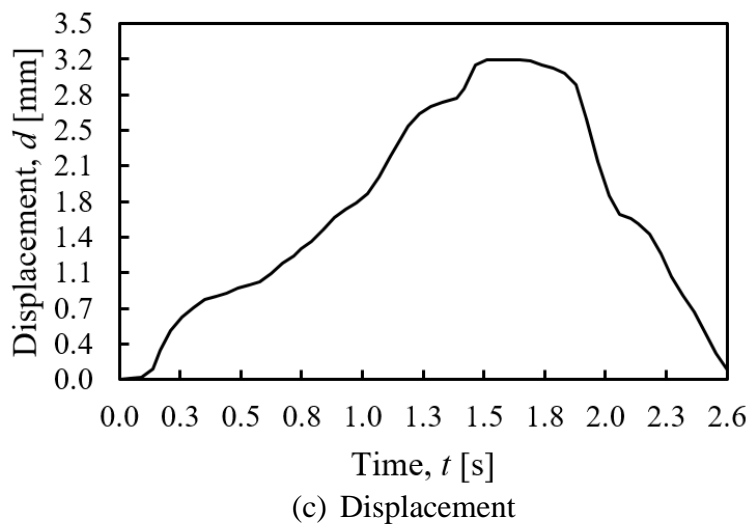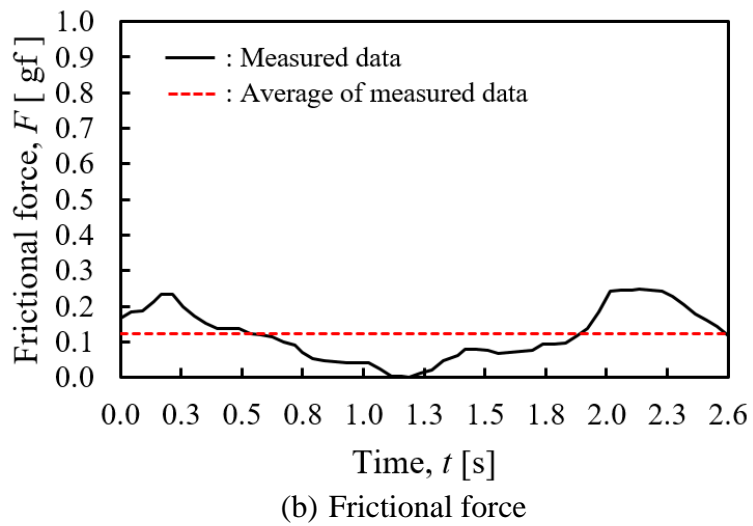

(b) Frictional force

(c) Displacement

Fig. 2.39 Examples of cornea's data measured by the ocular surface tribometer on subject D

(a) Normal force

(b) Frictional force

(c) Displacement

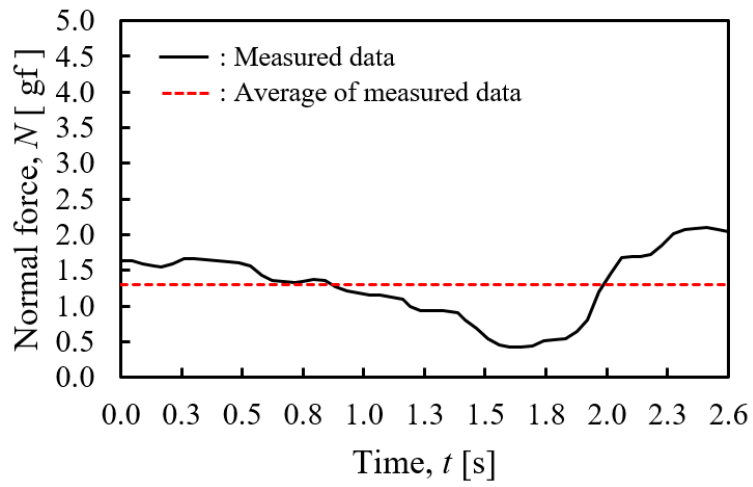Fig. 2.40 Examples of cornea's data measured by the ocular surface tribometer on subject E

(a) Normal force

(b) Frictional force

(c) Displacement

Fig. 2.41 Examples of cornea's data measured by the ocular surface tribometer on subject F

Figures 2.42 to 2.47 show the examples of experimental data measured by the ocular surface tribometer on the bulbar conjunctiva of six healthy subjects (A, B, C, D, E, and F), respectively. In all experiments, time history responses of N, F, and d were measured at the same time using the developed ocular surface tribometer.

Figure 2.42 shows the examples of experimental data measured by the ocular surface tribometer on the bulbar conjunctiva of subject A. In this experiment, normal forces were applied to the bulbar conjunctiva within the range of 2.43 [gf] to 4.13 [gf]. Frictional forces were measured in the range of 0.01 [gf] to 0.74 [gf]. The average values of normal forces and frictional forces are 3.43 [gf] and 0.30 [gf], respectively. The displacements of the probe were measured by the encoder and controlled to be within the maximum range of 2.13 [mm].

Figure 2.43 shows the examples of experimental data measured by the ocular surface tribometer on the bulbar conjunctiva of subject B. In this experiment, normal forces were applied to the bulbar conjunctiva within the range of 1.24 [gf] to 2.86 [gf]. Frictional forces were measured in the range of 0.01 [gf] to 0.32 [gf]. The average values of normal forces and frictional forces are 2.16 [gf] and 0.16 [gf], respectively. The displacements of the probe were measured by the encoder and controlled to be within the maximum range of 2.57 [mm].
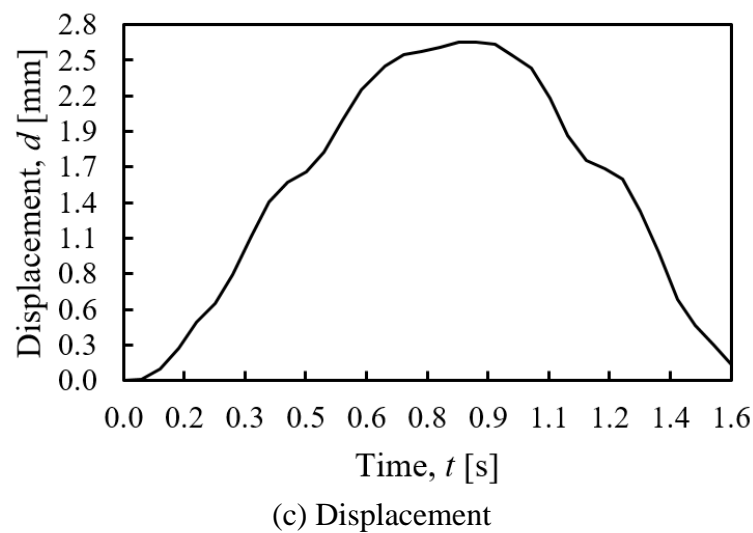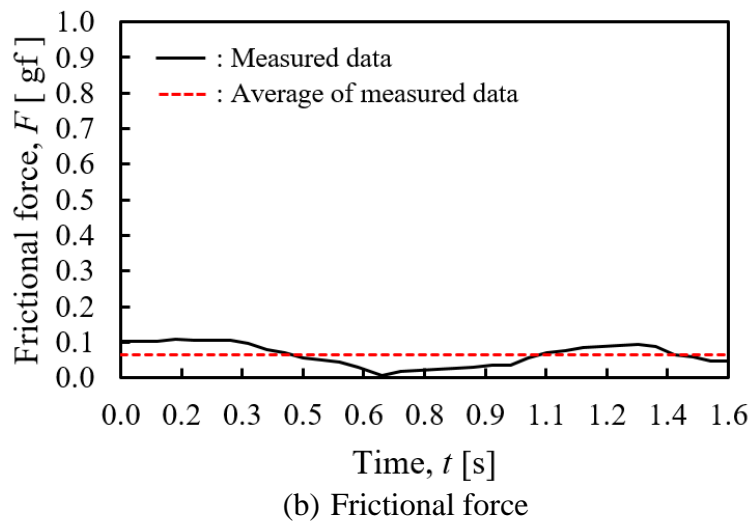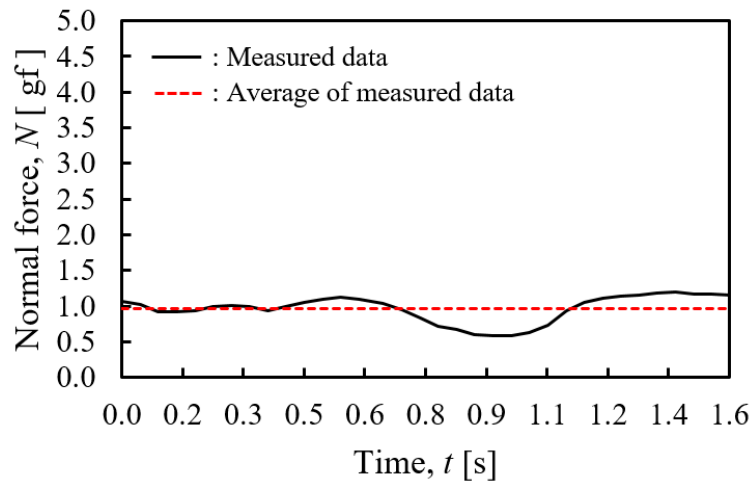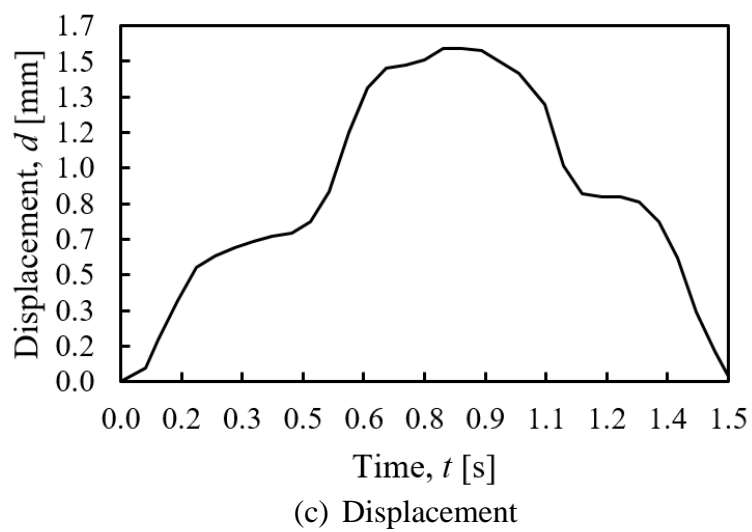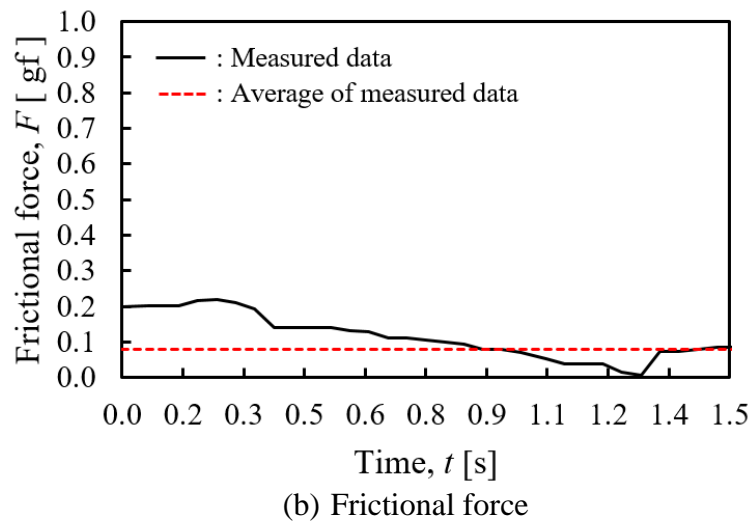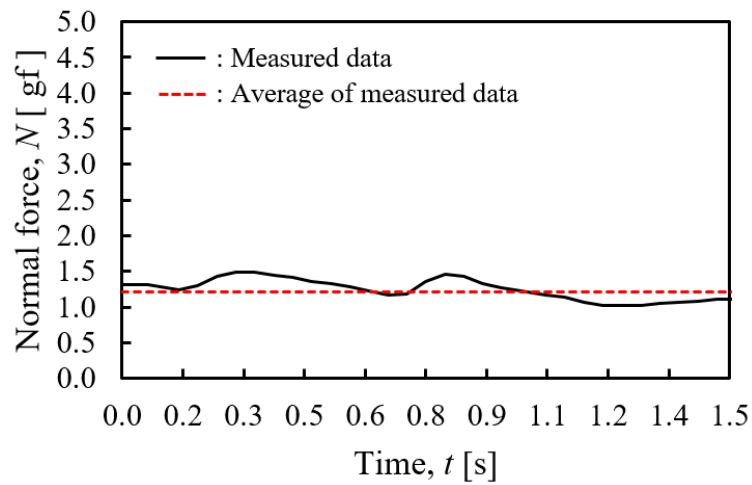
Figure 2.44 shows the examples of experimental data measured by the ocular surface tribometer on the bulbar conjunctiva of subject C. In this experiment, normal forces were applied to the bulbar conjunctiva within the range of 1.46 [gf] to 4.90 [gf]. Frictional forces were measured in the range of 0.02 [gf] to 0.72 [gf]. The average values of normal forces and frictional forces are 3.80 [gf] and 0.39 [gf], respectively. The displacements of the probe were measured by the encoder and controlled to be within the maximum range of 3.16 [mm].

(a) Normal force

(b) Frictional force
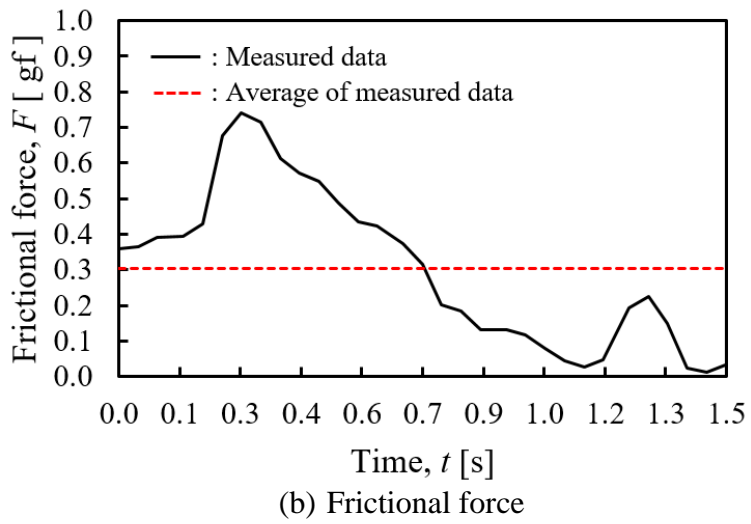
(c) Displacement

Fig. 2.42 Examples of bulbar conjunctiva's data measured by

the ocular surface tribometer on subject A

(a) Normal force

(b) Frictional force

(c) Displacement

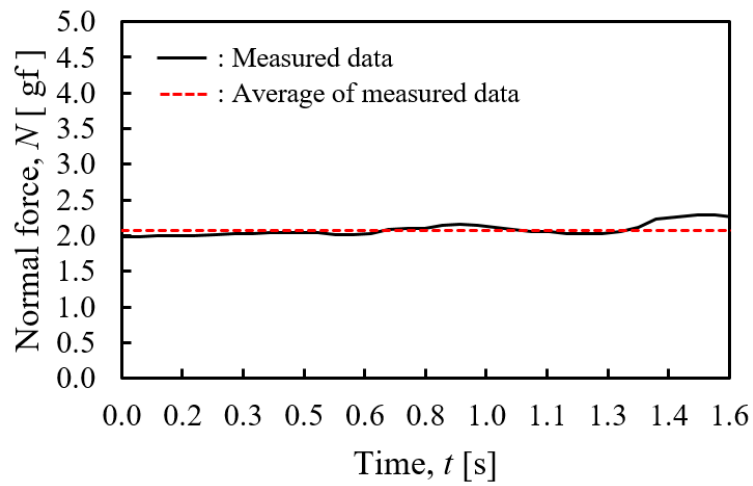Fig. 2.43 Examples of bulbar conjunctiva's data measured by
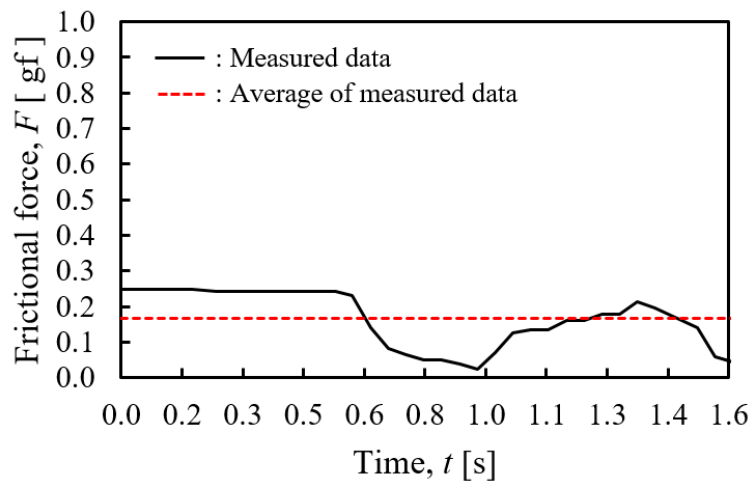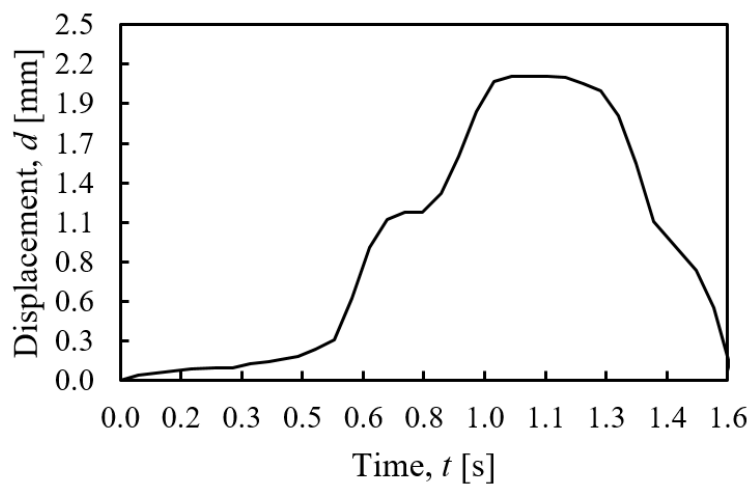
the ocular surface tribometer on subject B

41

(a) Normal force

(b) Frictional force

(c) Displacement
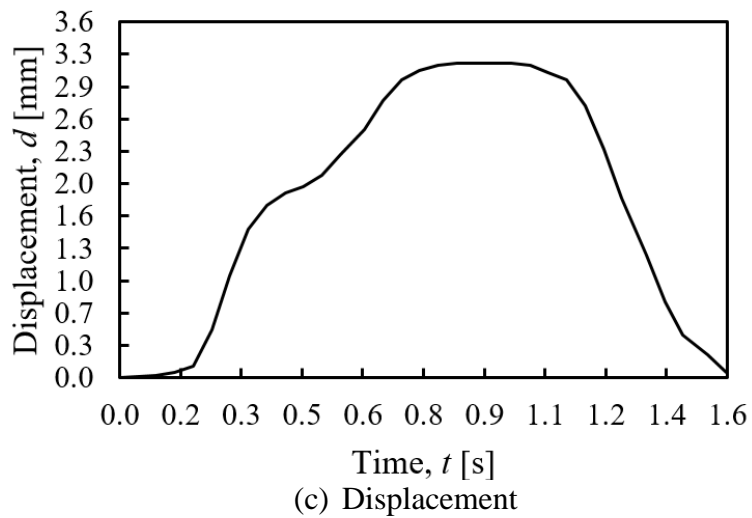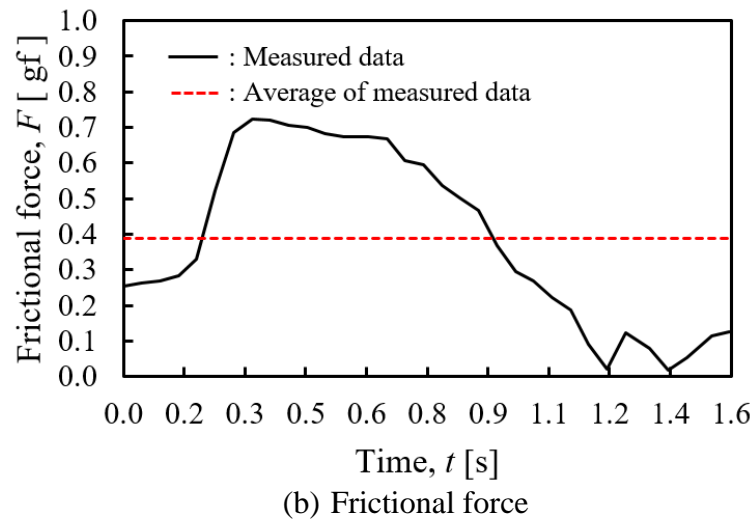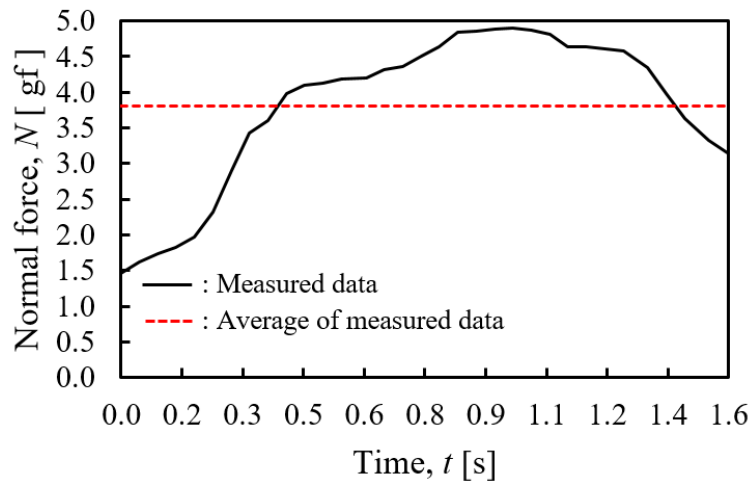
Fig. 2.44 Examples of bulbar conjunctiva's data measured by

the ocular surface tribometer on subject C

Figure 2.45 shows the examples of experimental data measured by the ocular surface tribometer on the bulbar conjunctiva of subject D. In this experiment, normal forces were applied to the bulbar conjunctiva within the range of 0.49 [gf] to 2.61 [gf]. Frictional forces were measured in the range of 0.09 [gf] to 0.23 [gf]. The average values of normal forces and frictional forces are 1.54 [gf] and 0.12 [gf], respectively. The displacements of the probe were measured by the encoder and controlled to be within the maximum range of 1.28 [mm].

Figure 2.46 shows the examples of experimental data measured by the ocular surface tribometer on the bulbar conjunctiva of subject E. In this experiment, normal forces were applied to the bulbar conjunctiva within the range of 0.25 [gf] to 3.82 [gf]. Frictional forces were measured in the range of 0.04 [gf] to 0.15 [gf]. The average values of normal forces and frictional forces are 2.41 [gf] and 0.15 [gf], respectively. The displacements of the probe were measured by the encoder and controlled to be within the maximum range of 3.09 [mm].

Figure 2.47 shows the examples of experimental data measured by the ocular surface tribometer on the bulbar conjunctiva of subject F. In this experiment, normal forces were applied to the bulbar conjunctiva within the range of 0.25 [gf] to 3.82 [gf]. Frictional forces were measured in the range of 0.02 [gf] to 0.55 [gf]. The average values of normal forces and frictional forces are 3.07 [gf] and 0.20 [gf], respectively. The displacements of the probe were measured by the encoder and controlled to be within the maximum range of 3.99 [mm].
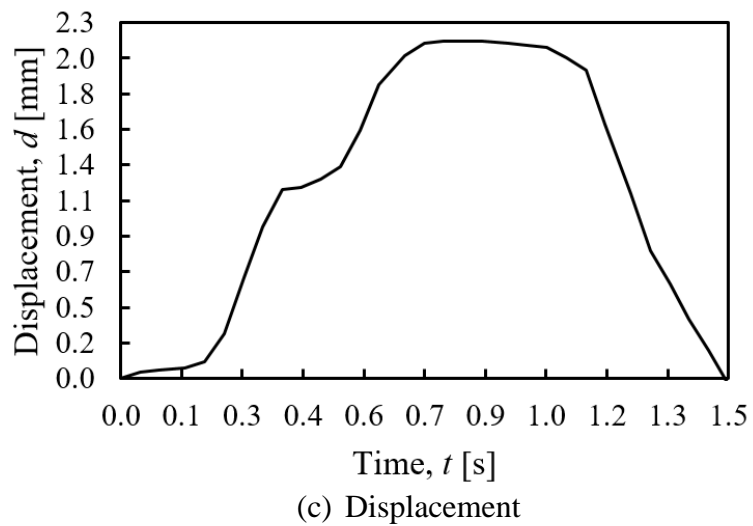
(a) Normal force

(b) Frictional force
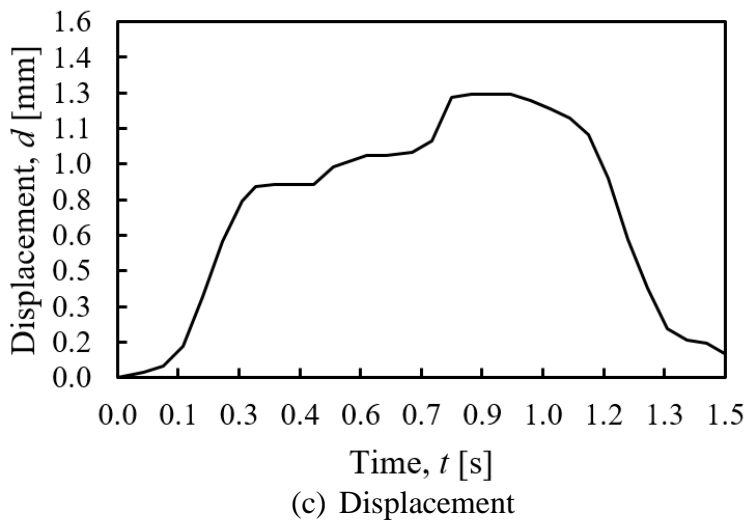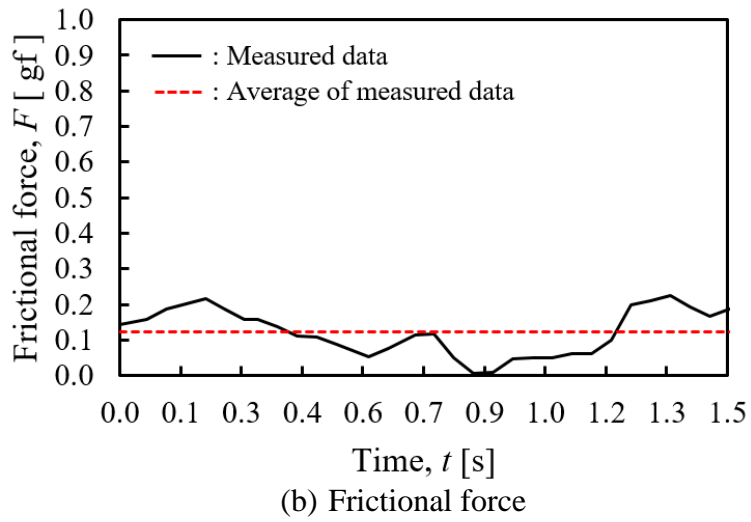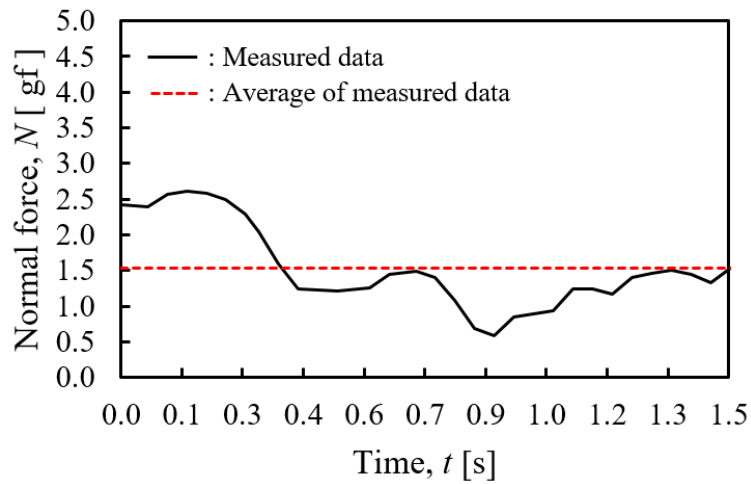
(c) Displacement

Fig. 2.45 Examples of bulbar conjunctiva's data measured by

the ocular surface tribometer on subject D
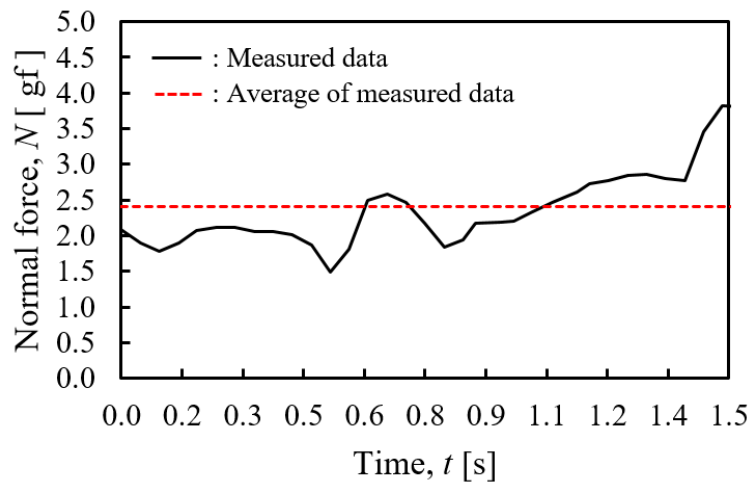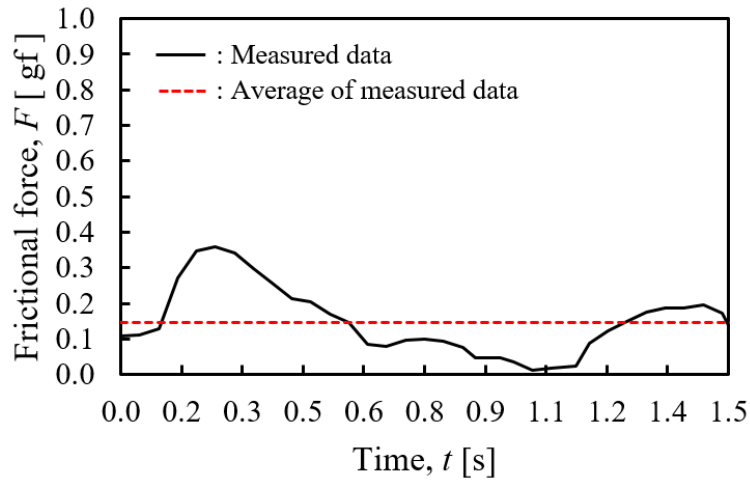
(a) Normal force
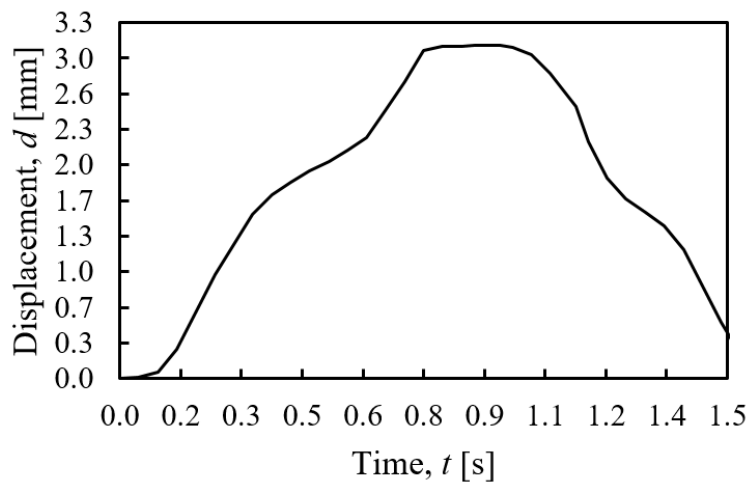
(b) Frictional force

(c) Displacement

Fig. 2.46 Examples of bulbar conjunctiva's data measured by

the ocular surface tribometer on subject E
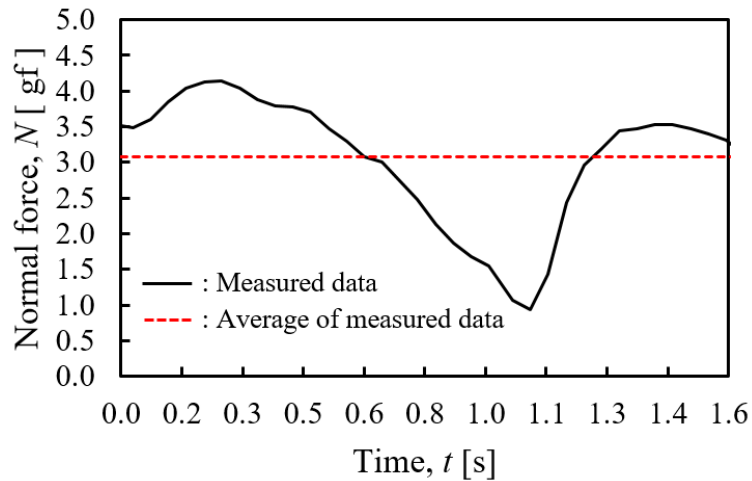
(a) Normal force
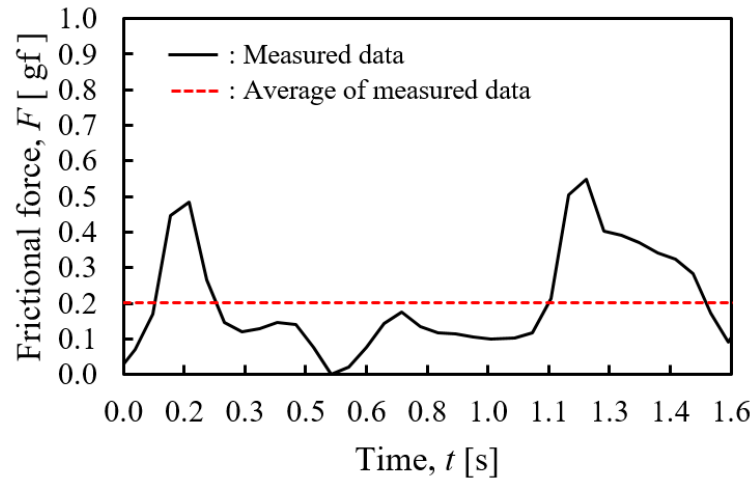
(b) Frictional force
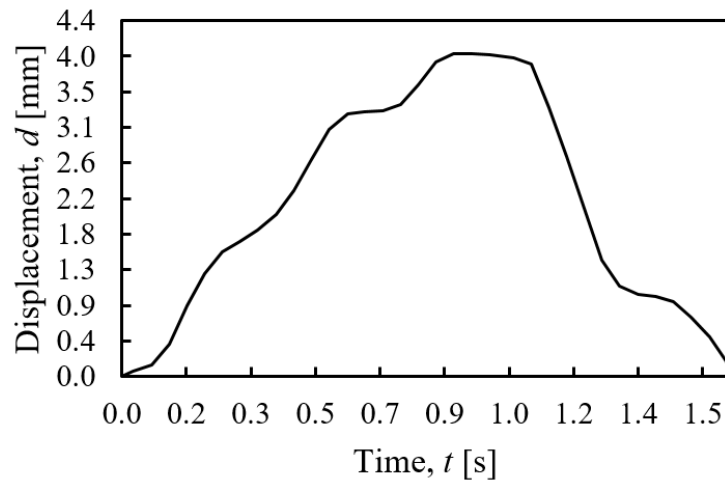
(c) Displacement

Fig. 2.47 Examples of bulbar conjunctiva's data measured by
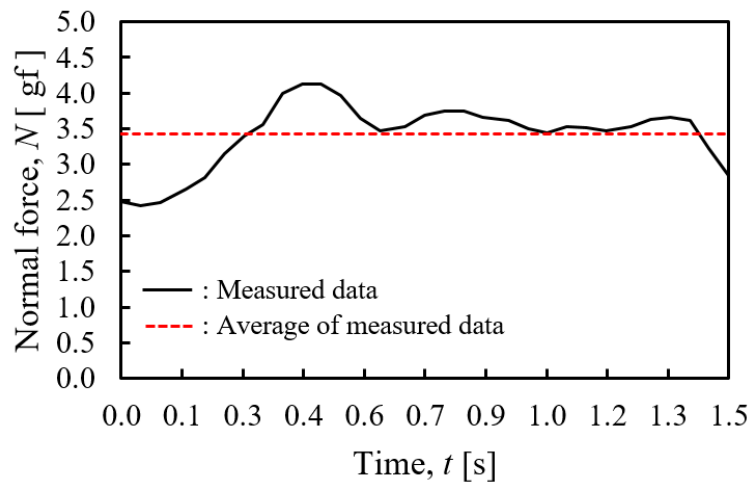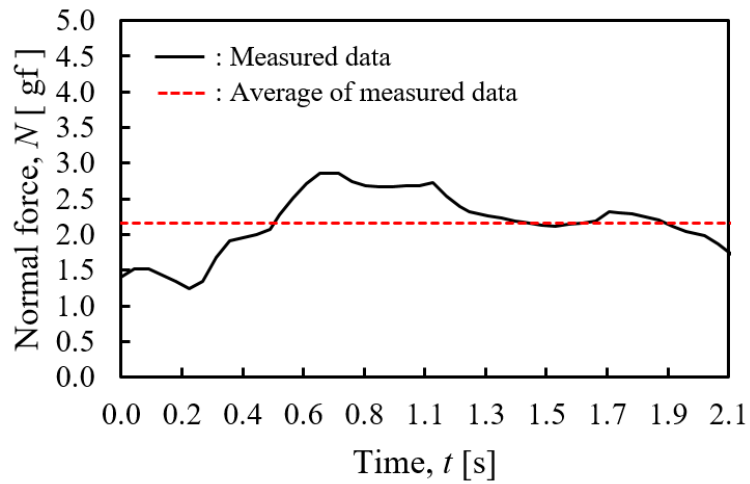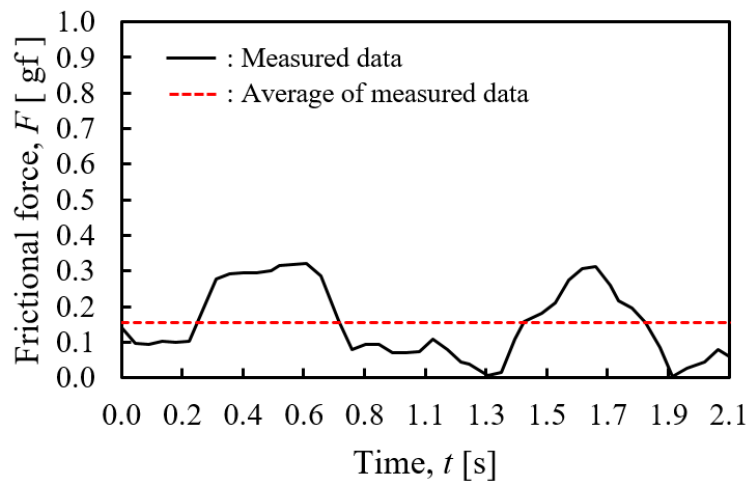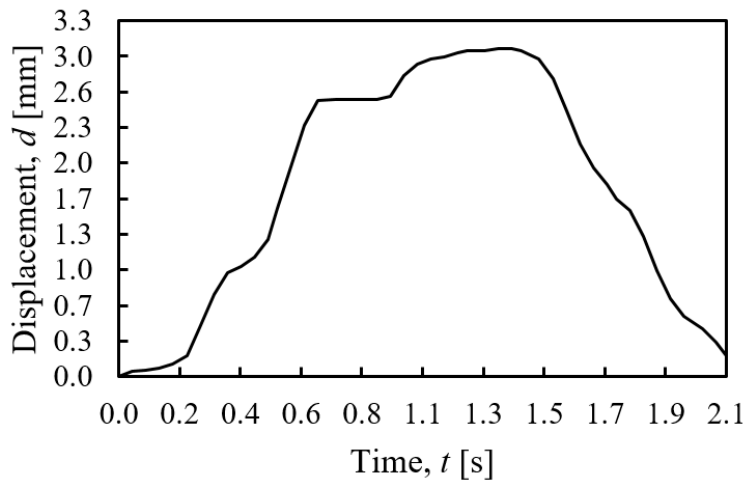
the ocular surface tribometer on subject F

Figure 2.48 shows the examples of cornea's results calculated by using the measured data on subject A. The average values of μ and average absolute values of V in this calculation are 0.10 and 2.61 [mm/s], respectively. The average values of μ on the cornea of subject A varied within the range of 0.04 to 0.11. The average absolute values of V of the probe on the cornea of subject A varied within the range of 2.21 [mm/s] to 5.68 [mm/s]. The average values of μ and average absolute values of V of the probe were used to determine the frictional characteristics of the human ocular surface.
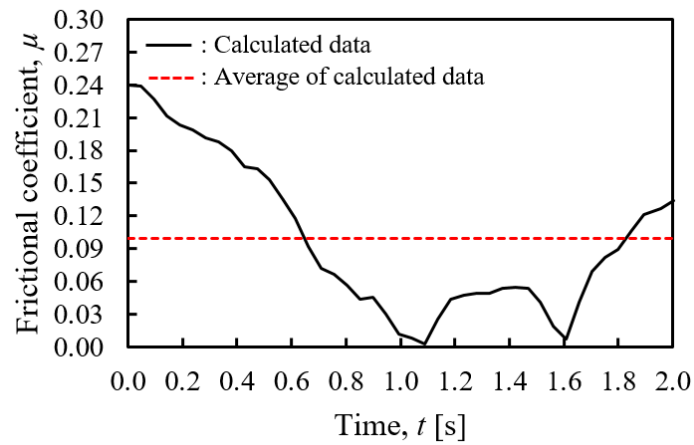
(a) Frictional coefficient on cornea of subject A
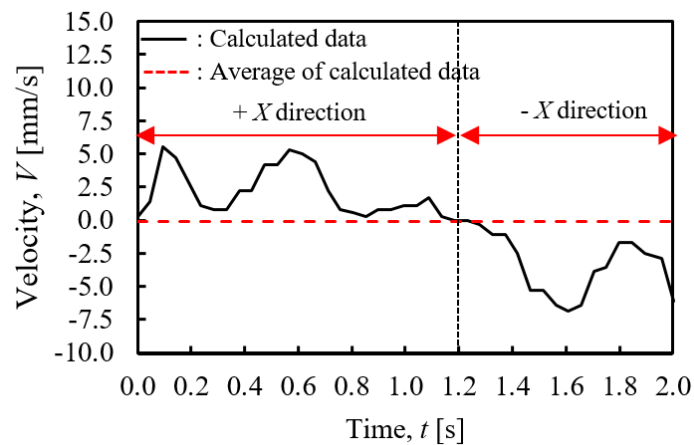
(b) Velocity of the probe on cornea of subject A

Fig. 2.48 Examples of cornea's results calculated by using the measured data on subject A

Figure 2.49 shows the examples of cornea's results calculated by using the measured data on subject B. The average values of μ and average absolute values of V in this calculation are 0.10 and 2.69 [mm/s], respectively. The average values of μ on the cornea of subject B varied within the range of 0.08 to 0.18. The average absolute values of V of the probe on the cornea of subject B varied within the range of 1.98 [mm/s] to 4.37 [mm/s]. The average values of μ and average absolute values of V of the probe were used to determine the frictional characteristics of the human ocular surface.

(a) Frictional coefficient on cornea of subject B

(b) Velocity of the probe on cornea of subject B

Fig. 2.49 Examples of cornea's results calculated by using the measured data on

subject B

Figure 2.50 shows the examples of cornea's results calculated by using the measured data on subject C. The average values of μ and average absolute values of V in this calculation are 0.10 and 2.41 [mm/s], respectively. The average absolute values of μ on the cornea of subject C varied within the range of 0.07 to 0.17. The average absolute values of V of the probe on the cornea of subject C varied within the range of 1.72 [mm/s] to 3.54 [mm/s]. The average values of μ and average absolute values of V of the probe were used to determine the frictional characteristics of the human ocular surface.
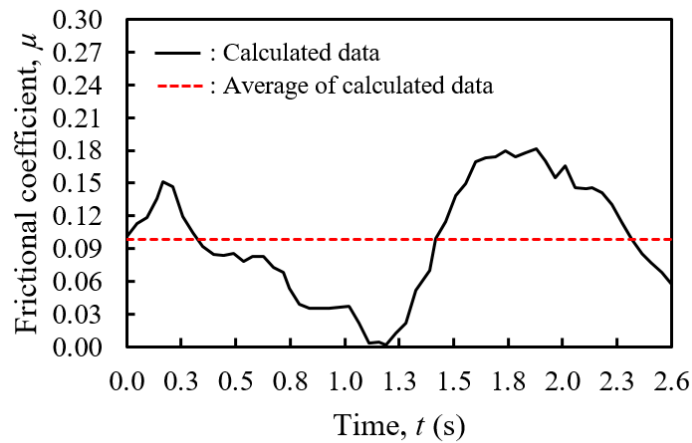
(a) Frictional coefficient on cornea of subject C
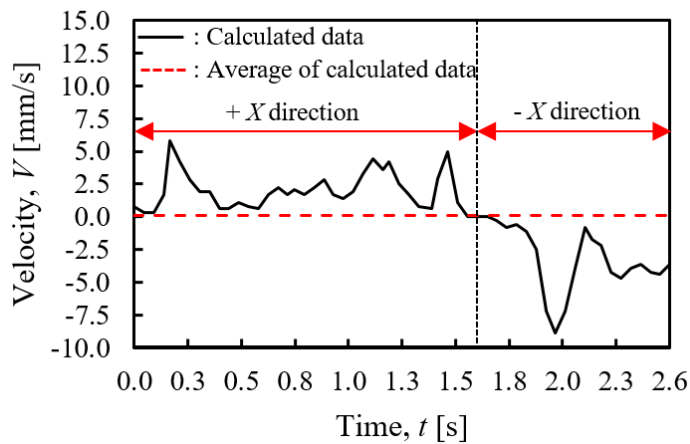
(b) Velocity of the probe on cornea of subject C

Fig. 2.50 Examples of cornea's results calculated by using the measured data on subject C

Figure 2.51 shows the examples of cornea's results calculated by using the measured data on subject D. The average values of μ and average absolute values of V in this calculation are 0.07 and 3.17 [mm/s], respectively. The average values of μ on the cornea of subject D varied within the range of 0.04 to 0.13. The average absolute values of V of the probe on the cornea of subject D varied within the range of 1.70 [mm/s] to 3.85 [mm/s]. The average values of μ and average absolute values of V of the probe were used to determine the frictional characteristics of the human ocular surface.
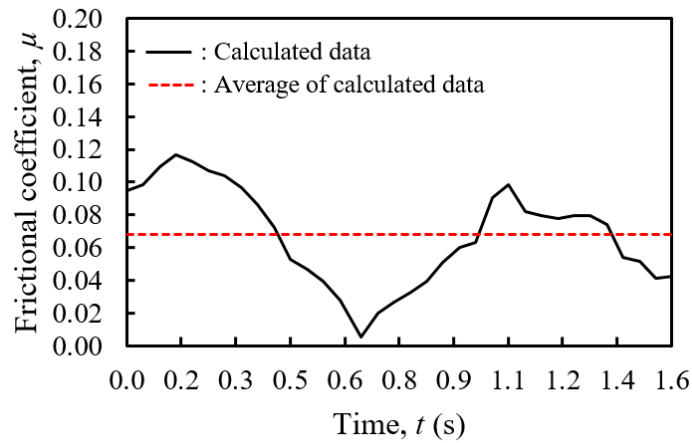
(a) Frictional coefficient on cornea of subject D
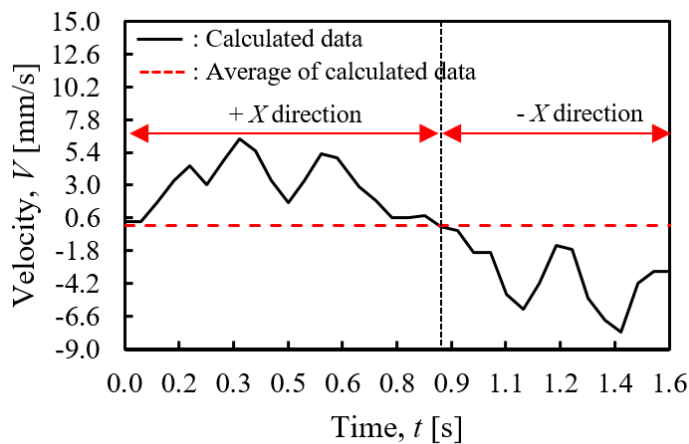
(b) Velocity of the probe on cornea of subject D

Fig. 2.51 Examples of cornea's results calculated by using the measured data on subject D

Figure 2.52 shows the examples of cornea's results calculated by using the measured data on subject E. The average values of μ and average absolute values of V in this calculation are 0.06 and 2.03 [mm/s], respectively. The average values of μ on the cornea of subject E varied within the range of 0.06 to 0.19. The average absolute values of V of the probe on the cornea of subject E varied within the range of 1.47 [mm/s] to 3.31 [mm/s]. The average values of μ and average absolute values of V of the probe were used to determine the frictional characteristics of the human ocular surface.
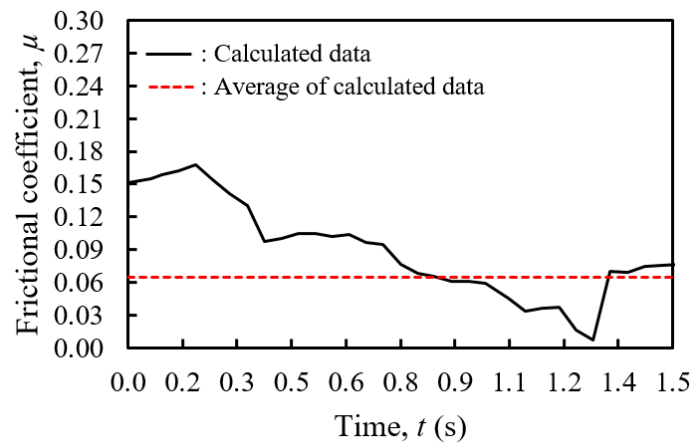
(a) Frictional coefficient on cornea of subject E
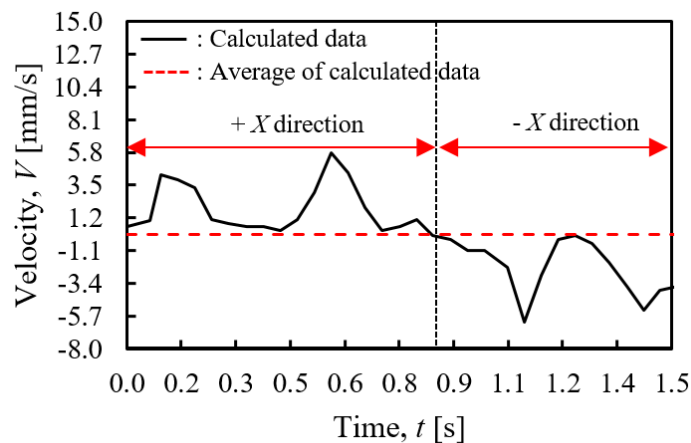
(b) Velocity of the probe on cornea of subject E

Fig. 2.52 Examples of cornea's results calculated by using the measured data on subject E

Figure 2.53 shows the examples of cornea's results calculated by using the measured data on subject F. The average values of μ and average absolute values of V in this calculation are 0.08 and 2.51 [mm/s], respectively. The average values of μ on the cornea of subject F varied within the range of 0.06 to 0.16. The average absolute values of V of the probe on the cornea of subject F varied within the range of 1.69 [mm/s] to 5.84 [mm/s]. The average values of μ and average absolute values of V of the probe were used to determine the frictional characteristics of the human ocular surface.
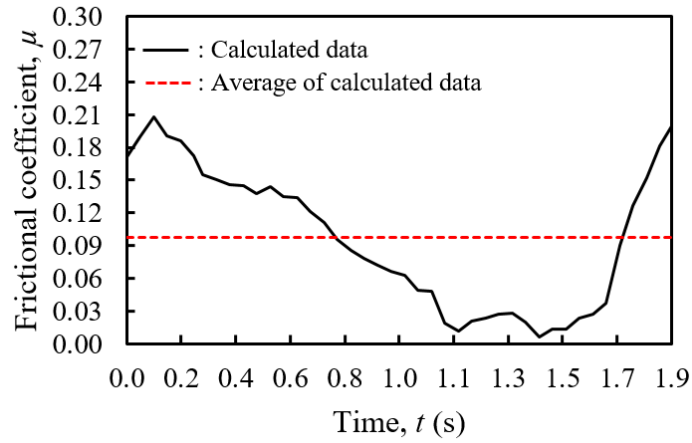

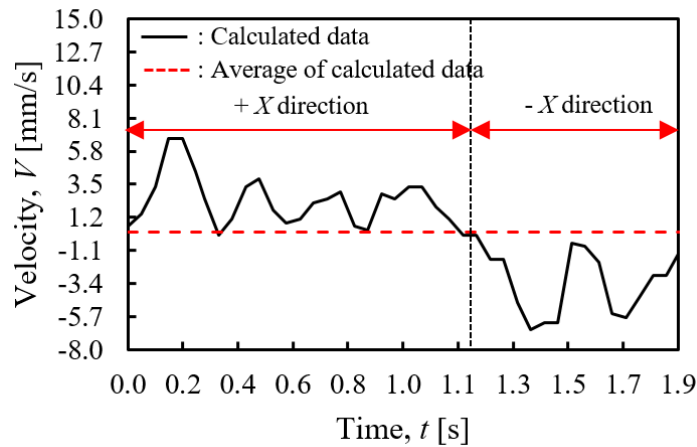(a) Frictional coefficient on cornea of subject F

(b) Velocity of the probe on cornea of subject F

Fig. 2.53 Examples of cornea's results calculated by using the measured data on subject F

Figure 2.54 shows the examples of bulbar conjunctiva's results calculated by using the measured data on subject A. The average values of μ and average absolute values of V in this calculation are 0.09 and 2.84 [mm/s], respectively. The average values of μ on the bulbar conjunctiva of subject A varied within the range of 0.06 to 0.10. The average absolue values of V of the probe on the bulbar conjunctiva of subject A varied within the range of 1.97 [mm/s] to 5.37 [mm/s]. The average values of μ and average absolute values of V of the probe were used to determine the frictional characteristics of the human ocular surface.

(a) Frictional coefficient on bulbar conjunctiva of subject A

(b) Velocity of the probe on bulbar conjunctiva of subject A

Fig. 2.54 Examples of bulbar conjunctiva's results calculated by

using the measured data on subject A

Figure 2.55 shows the examples of bulbar conjunctiva's results calculated by using the measured data on subject B. The average values of μ and average absolute values of V in this calculation are 0.07 and 2.83 [mm/s], respectively. The average values of μ on the bulbar conjunctiva of subject B varied within the range of 0.06 to 0.11. The average absolute values of V of the probe on the bulbar conjunctiva of subject B varied within the range of 2.71 [mm/s] to 5.25 [mm/s]. The average values of μ and average absolute values of V of the probe were used to determine the frictional characteristics of the human ocular surface.
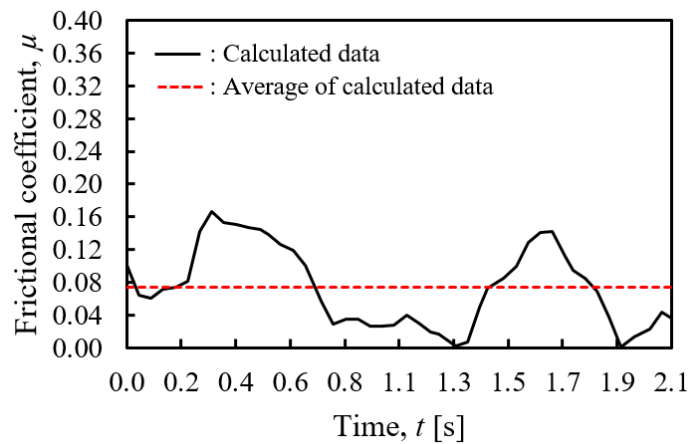

(a) Frictional coefficient on bulbar conjunctiva of subject B
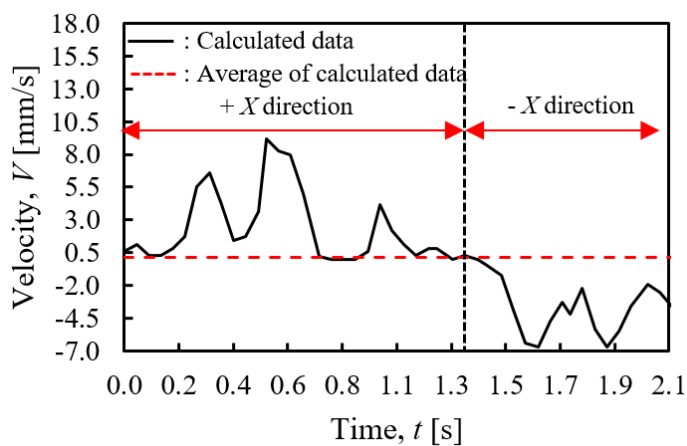
(b) Velocity of the probe on bulbar conjunctiva of subject B

Fig. 2.55 Examples of bulbar conjunctiva's results calculated by

using the measured data on subject B

Figure 2.56 shows the examples of bulbar conjunctiva's results calculated by using the measured data on subject C. The average values of μ and average absolute values of V in this calculation are 0.11 and 3.88 [mm/s], respectively. The average values of μ on the bulbar conjunctiva of subject C varied within the range of 0.07 to 0.13. The average absolute values of V of the probe on the bulbar conjunctiva of subject C varied within the range of 1.50 [mm/s] to 5.30 [mm/s]. The average values of μ and average absolute values of V of the probe were used to determine the frictional characteristics of the human ocular surface.
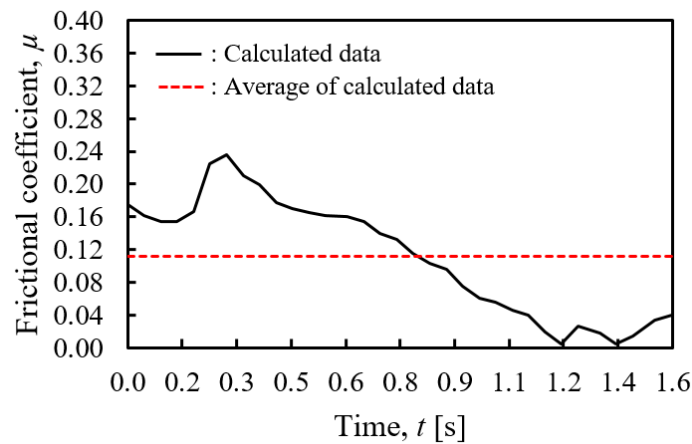

(a) Frictional coefficient on bulbar conjunctiva of subject C
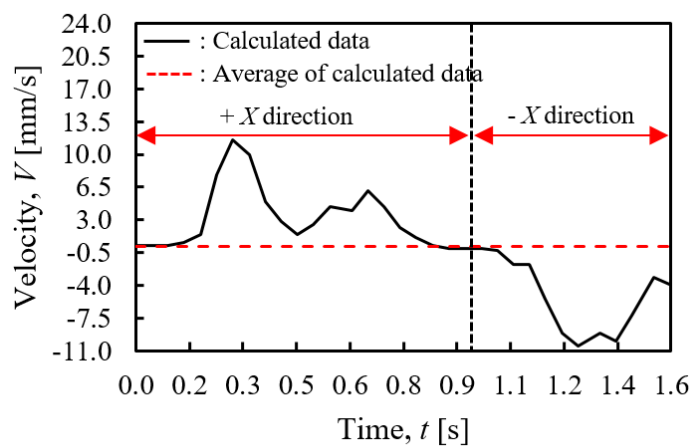
(b) Velocity of probe on bulbar conjunctiva of subject C

Fig. 2.56 Examples of bulbar conjunctiva's results calculated by using the measured data on subject C

Figure 2.57 shows the examples of bulbar conjunctiva's results calculated by using the measured data on subject D. The average values of μ and average absolute values of V in this calculation are 0.08 and 1.68 [mm/s], respectively. The average values of μ on the bulbar conjunctiva of subject D varied within the range of 0.07 to 0.16. The average absolute values of V of the probe on the bulbar conjunctiva of subject D varied within the range of 1.33 [mm/s] to 3.70 [mm/s]. The average values of μ and average absolute values of V of the probe were used to determine the frictional characteristics of the human ocular surface.
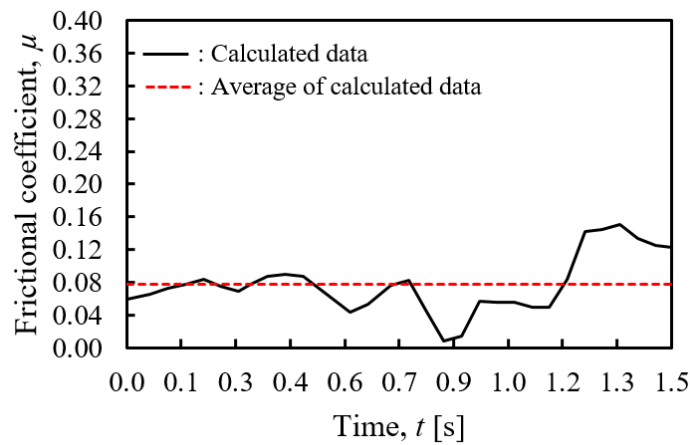

(a) Frictional coefficient on bulbar conjunctiva of subject D
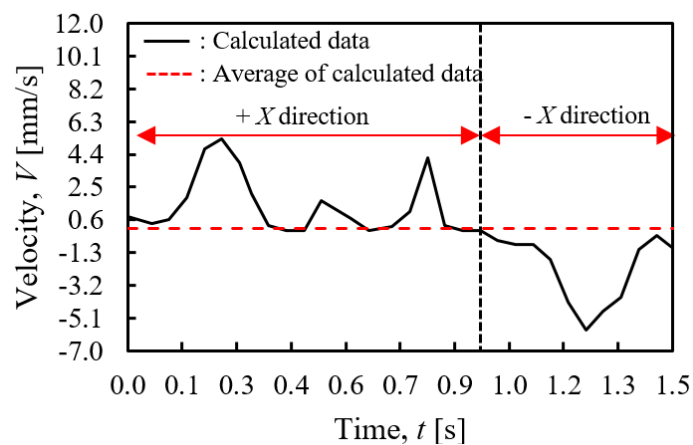
(b) Velocity of probe on bulbar conjunctiva of subject D

Fig. 2.57 Examples of bulbar conjunctiva's results calculated by

using the measured data on subject D

Figure 2.58 shows the examples of bulbar conjunctiva's results calculated by using the measured data on subject E. The average values of μ and average absolute values of V in this calculation are 0.07 and 3.80 [mm/s], respectively. The average values of μ on the bulbar conjunctiva of subject E varied within the range of 0.07 to 0.13. The average absolute values of V of the probe on the bulbar conjunctiva of subject E varied within the range of 1.80 [mm/s] to 3.80 [mm/s]. The average values of μ and average absolute values of V of the probe were used to determine the frictional characteristics of the human ocular surface.
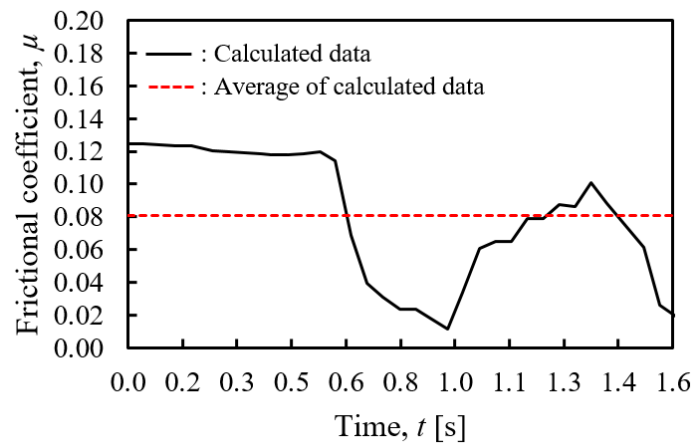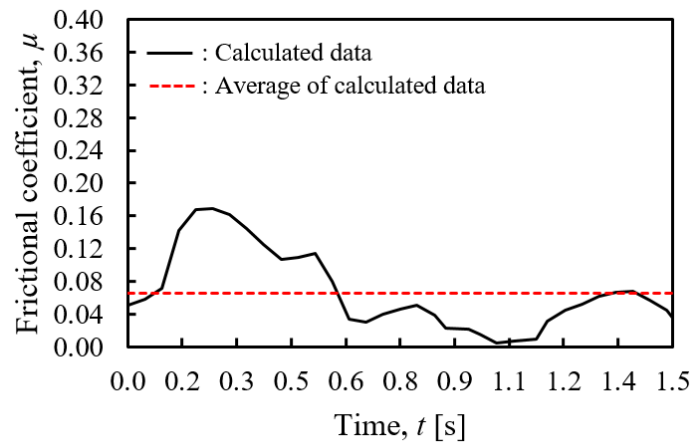

(a) Frictional coefficient on bulbar conjunctiva of subject E
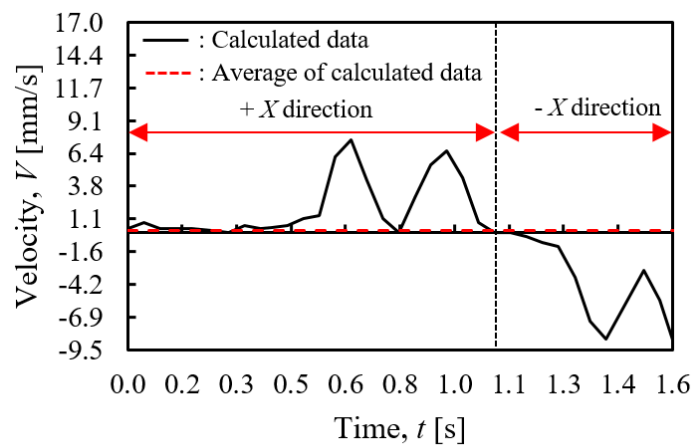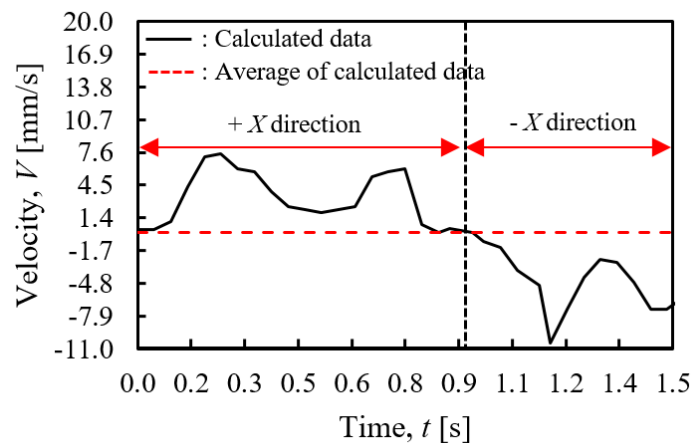

(b) Velocity of probe on bulbar conjunctiva of subject E

Fig. 2.58 Examples of bulbar conjunctiva's results calculated by

using the measured data on subject E

57

Figure 2.59 shows the examples of bulbar conjunctiva's results calculated by using the measured data on subject F. The average values of μ and average absolute values of V in this calculation are 0.07 and 4.92 [mm/s], respectively. The average values of μ on the bulbar conjunctiva of subject F varied within the range of 0.06 to 0.10. The average absolute values of V of the probe on the bulbar conjunctiva of subject F varied within the range of 2.09 [mm/s] to 5.51 [mm/s]. The average values of μ and average absolute values of V of the probe were used to determine the frictional characteristics of the human ocular surface.
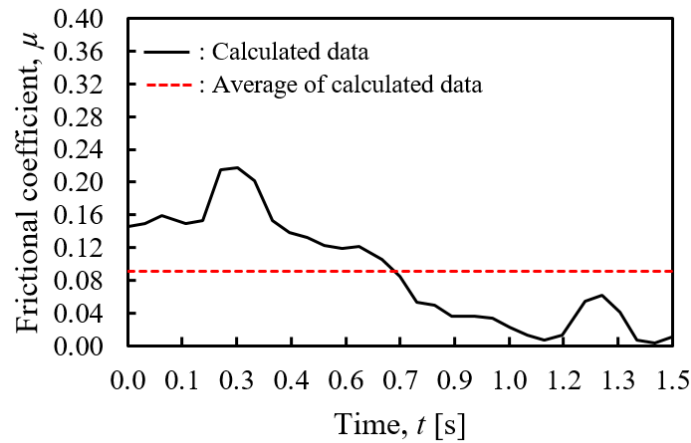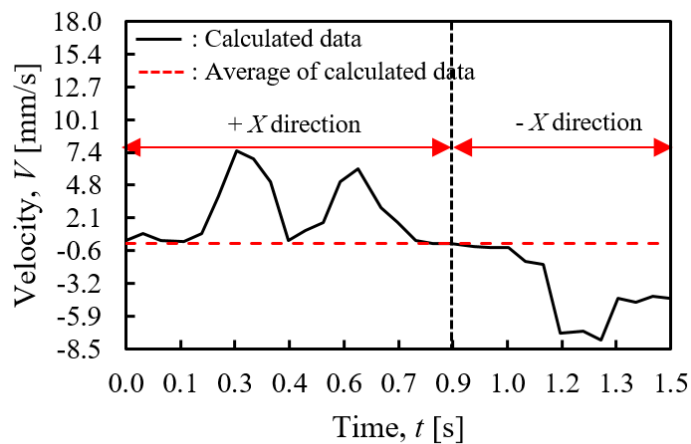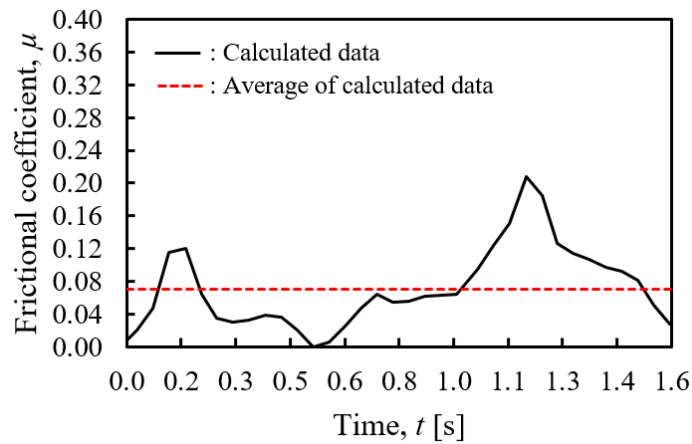

(a) Frictional coefficient on bulbar conjunctiva of subject F
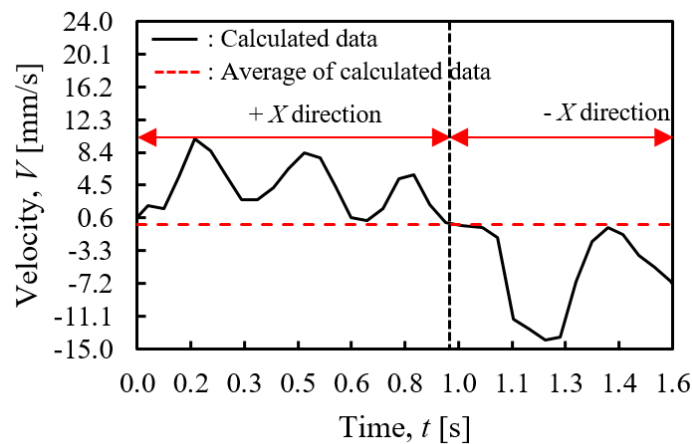
(b) Velocity of probe on bulbar conjunctiva of subject F

Fig. 2.59 Examples of bulbar conjunctiva's results calculated by using the measured data on subject F

2.6 Conclusion

The summary of results is shown below.

(1) The new ocular surface tribometer for measuring normal forces, frictional forces, and displacements of the probe had been developed.

(2) The measurements of normal forces, frictional forces, and displacements of the probe had been successfully conducted on the cornea and bulbar conjunctiva of six healthy subjects.

Chapter 3

Development of Computational Program Employing BSG-Starcraft of PSO and LSM for Determining Frictional Characteristics of Human Ocular Surfaces

3.1 Introduction

The purpose of the study presented in this chapter is to determine frictional characteristics of the human ocular surface. A mathematical model describing frictional coefficient of the human ocular surface was proposed. In order to determine frictional characteristics of the human ocular surface, a computational program employing the BSG-Starcraft of PSO and LSM was developed. The BSG-Starcraft of PSO and LSM were used to determine the optimal parameters in a mathematical model proposed in the research.

3.2 Proposed New Number and Mathematical Model for Frictional Coefficients of Human Ocular Surfaces

A tear layer exists between the eyelid and the ocular surface in a normal eye. However, some areas of the eyelid and the ocular surface directly contact each other in a dry eye. Thus, when the eyelid and the ocular surface are fully separated by the tear layer, μ on a human ocular surface is considered to be within the range of fluid lubrication. While in the condition of the ocular surface is dry, μ on a human ocular surface is considered to be within the range of mixed lubrication.

In this research, a new number, X was proposed to calculate μ on the human ocular surface as given in (3.1).

$$X = \frac{\eta^{p_1} V^{p_2}}{N^{p_3}} \tag{3.1}$$

Where parameters, p_1, p_2, and p_3 are arbitrary real numbers. Then by incorporating the proposed number, X, a mathematical model was proposed to describe μ of the human ocular surface as given in (3.2).

$$\mu = p_4 X^{n-4} + p_5 X^{n-5} + \ldots + p_{n-1} X + p_n \tag{3.2}$$

Where parameters, p_4, p_5, …, and p_n are arbitrary real numbers. In this paper, it is assumed that η is constant and equal to 1, in other words, $p_1 = 0$.

3.3 BSG – Starcraft of PSO

3.3.1 Parameters of Frictional Characteristic Curve on Human Ocular Surfaces

In this research, an optimization method was used in determining parameters, p_1, …, p_n in (3.1) and (3.2). Then, a computational program combining the BSG-Starcraft of PSO and the LSM developed by the authors was applied to achieve the optimization. The computational program was applied through six steps.

In the first step, the positions, velocities, and inertia weights of all particles in the swarm were initialized. The position and velocity of particle i at iteration j in the n-dimensional search space were represented as $x_i^j = \left(x_{i,1}^j, x_{i,2}^j, \ldots, x_{i,n}^j \right) = (p_1, p_2, \ldots, p_n)$ and $v_i^j = \left(v_{i,1}^j, v_{i,2}^j, \ldots, v_{i,n}^j \right)$, respectively. In this research, the dimensional space, n was set to 6 indicating the total number of parameters in the proposed new number and the mathematical model. The initial positions, x_i^0 and velocities, v_i^0 of all particles were randomly generated within pre-defined ranges as expressed in (3.3) and (3.4).

$$x_i^0 = x_{min} + rand\,(x_{max} - x_{min}) \tag{3.3}$$

$$v_i^0 = v_{min} + rand\,(v_{max} - v_{min}) \tag{3.4}$$

Here $x_{min} = -3.2767$ and $x_{max} = 3.2767$ are the lower and upper bounds on x. While $v_{min} = 0.1 \times x_{min}$ and $v_{max} = 0.1 \times x_{max}$ are the lower and upper bounds on v. The inertia weight, w^j was calculated as in (3.5).

$$w^j = w_{max} - \left(\frac{w_{max} - w_{min}}{j_{max}}\right) j \tag{3.5}$$

Where w_{min} and w_{max} are the minimum and maximum inertia weights. The inertia weight, w^j decreased linearly from 0.9 to 0.4. The maximum number of iterations, j_{max} was set to 200. In the second step, the objective function was evaluated. The objective function, F_i^j of particle i at iteration j was given as in (3.6).

$$F_i^j = \sum_{l=1}^{n_e} \sqrt{(\mu_i - \mu_l)^2} \qquad (i = 1 \sim n_s) \tag{3.6}$$

Here μ_i and μ_l are the value of frictional coefficient on the human ocular surface that obtained by BSG-Starcraft of PSO and the actual experimental value of frictional coefficient on the human ocular surface, respectively. n_e and n_s are the number of experimental values and the number of particles in a swarm. In this research, the number of experimental values, n_e were set to range of 17 to 23 and the number of particles in a swarm, n_s was set to 20. Then the BSG-Starcraft of PSO algorithm was applied to minimize the value of the objective function, F_i^j.

In the third step, the personal best position of particle i, $P_{Best,\,i}$ and the best global position in the current swarm, G_{Best} were determined. The $P_{Best,\,i}$ was the smallest value of the objective function, F_i^j obtained by the particle i at all previous iterations. The smallest value of the objective function among $P_{Best,\,i}$ was determined as G_{Best}.

In the fourth step, the G_{Best} was determined as the carrier, $X_{Carrier}$. The $X_{Carrier}$ was used in each iteration to send some new particles called raptors with the probability 0.9. The position of raptor k at iteration j in the n-dimensional search space was represented as $x^j_{Raptor\ k} = \left(x^j_{Raptor\ k,\ 1}, x^j_{Raptor\ k,\ 2}, ..., x^j_{Raptor\ k,\ n} \right)$. The objective function, $F^j_{Raptor\ k}$ of raptor k at iteration j was evaluated by using the formula as given in (3.7).

$$F^j_{Raptor\ k} = \sum_{l=1}^{n_e} \sqrt{\left(\mu_k - \mu_l \right)^2} \qquad (k = 1 \sim n_r) \qquad (3.7)$$

Here n_r are the number of raptors in each iteration. In this research, the number of raptors in each iteration, n_r was set to 20.

Figure 3.1 shows the schematics of raptors exploring the space. If a raptor with better value of objective function than $x_{Carrier}$ reaches the better position, a jump vector, namely *Jump* is defined. Then, the swarm jumps to the new position by the translation of the vector *Jump*. Thus, the new position of $x_{Carrier}$ is now the raptor with the best position. Therefore, due to the new position of the swarm, the $P_{Best,\ i}$ and G_{Best} are updated.

Fig. 3.1 Schematics of raptors exploring the space

In the fifth and sixth steps, the velocity and position of particle i were updated as in (3.8) and (3.9), respectively.

$$v_i^{j+1} = w^j v_i^j + c_1 r_1 \left(P_{Best,\, i} - x_i^j\right) + c_2 r_2 \left(G_{Best} - x_i^j\right) \tag{3.8}$$

$$x_i^{j+1} = x_i^j + v_i^{j+1} \tag{3.9}$$

Here c_1 is the self-confidence factor and c_2 the swarm confidence factor. The value of the constants c_1 and c_2 are set to be same and equal to 2. The r_1 and r_2 were the random numbers uniformly distributed in the range (0, 1).

Figure 3.2 shows the updating velocity and position of a particle. As expressed in (3.8), the velocity, v_i^j of the particle i is updated by combining G_{Best} and $P_{Best,\, i}$ with w^j, c_1, c_2, r_1, and r_2. The position, x_i^{j+1} of the particle i in the next iteration is affected by the current velocity, v_i^j of the particle i, G_{Best} and $P_{Best,\, i}$.

Current velocity effect v_i^j

Global best effect

v_i^{j+1}

Personal best effect

⬤ Position of particle i at iteration j, x_i^j

◯ Position of particle i at iteration $j+1$, x_i^{j+1}

⊜ The best global position among all the particles in the swarm, G_{Best}

◎ The personal best position of the particle i, $P_{Best,\, i}$

v_i^j = Velocity of particle i at iteration j

v_i^{j+1} = Velocity of particle i at iteration $j+1$

Fig. 3.2 Updating velocity and position of a particle

3.3.2 Procedure for Determining Parameters in the Frictional Characteristic Curve of Human Ocular Surfaces

The procedure for determining parameters in the frictional characteristic curve of the human ocular surface using the BSG-Starcraft of PSO is given by the pseudo-code as follows:

1: Randomly initialize x_i^0, w^j, and v_i^0 of all particles

2: Evaluate the objective function of all particles, F_i^0

3: Determine the personal best position of particle i, $P_{Best, i} = x_i^0$

4: Determine the best global position in the current swarm, G_{Best}

5: **while** $j \leq j_{max}$ **do**

6:   **for** $i = 1$ to n_s **do**

7:     Set the G_{Best} as the carrier, $x_{Carrier}$

8:     Randomly create n_r raptors, with a probability $= 0.9$ to explore the space

9:     Evaluate the objective function, $F_{Raptor\,k}^j$ of raptor k at iteration j

10:     **if** $\exists k / F_{Raptor\,k}^j \leq F_{x_{Carrier}}^j$ **then**

11:     Set the jump vector as $Jump = x_{Raptor\,k}^j - x_{Carrier}$ and jump the swarm to the new position

12:     Evaluate the objective function for the swarm at the new position

13:   **Else**

14:     Evaluate the objective function of the swarm at the original position

15:   **end if**

16:   Update the $P_{Best, i}$

17:   Update the G_{Best}

18:      Update the velocity of particle i according to Eq. (3.8)

19:      Update the position of particle i according to Eq. (3.9)

20:   **end for**

21: **end while**

3.4 Frictional Characteristic Curves of Human Ocular Surfaces Determined by Employing BSG-Starcraft of PSO and LSM

In this research, 127 data were measured by the developed ocular surface tribometer. The measurements were performed on the cornea and bulbar conjunctiva of six healthy subjects (A, B, C, …, and F) by using the developed ocular surface tribometer. For each subject, the measurements on cornea were firstly conducted. The measurements on bulbar conjunctiva were secondly done. In both measurements, N, F, and displacement, d were measured.

It was possible to use 96% of the measurement data for determining the frictional characteristics of the human ocular surfaces. Then the frictional characteristic curves of the human ocular surface were determined by using the proposed new number and employing the BSG-Starcraft of PSO and LSM.

Figures 3.3 shows the example of the frictional characteristic curve of the cornea and bulbar conjunctiva in fluid lubrication region of subject A. The frictional characteristic curve is described based on the measured data obtained from the subject A. The calculations were carried out using the computational program of the BSG-Starcraft of PSO and LSM by setting the number, $n_s = 20$ of particles in a swarm. The parameters, $p_2 = 0.68$ and $p_3 = 0.01$ were obtained when the objection function value, $F_i^j = 0.068$.

The objective function value, $F_i^j = 0.068$ was achieved within the maximum iteration

number, $j_{max} = 200$. As for the subject A, the frictional coefficients on both cornea and

bulbar conjunctiva fall within the fluid lubrication where the eyelid and ocular surfaces

are fully separated by the tear layer. Then the curve in the fluid lubrication shows an

upward-sloping characteristic.
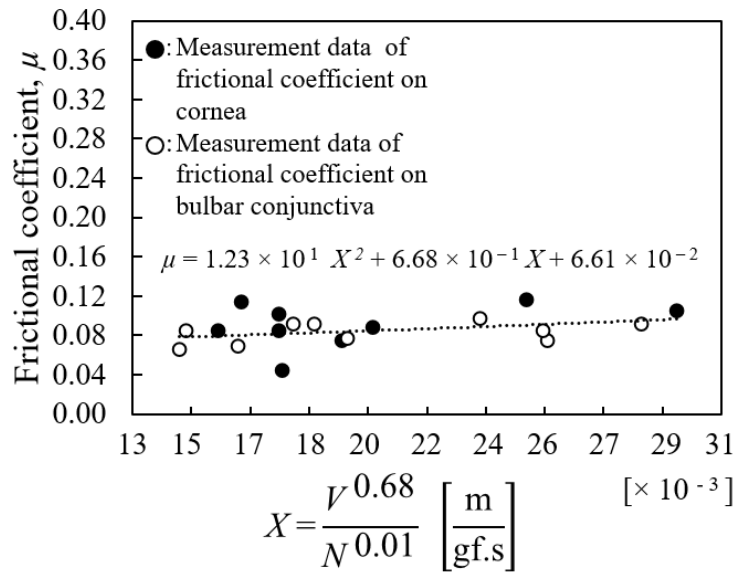
Fig. 3.3 Example of frictional characteristic curve of cornea and bulbar conjunctiva

in fluid lubrication region of subject A ($0.04 < \mu < 0.11$; $\bar{\mu} = 0.08$)

Figures 3.4 shows the example of the frictional characteristic curve of the cornea

and bulbar conjunctiva in mixed lubrication region of subject B. The frictional

characteristic curve is described based on the measured data obtained from the subject B.

The calculations were carried out using the computational program of the BSG-Starcraft

of PSO and LSM by setting the number, $n_s = 20$ of particles in a swarm. The parameters,

$p_2 = 0.35$ and $p_3 = 0.20$ were obtained when the objection function value, $F_i^j = 0.122$.

The objective function value, $F_i^j = 0.122$ was achieved within the maximum iteration

number, $j_{max} = 200$. As for the subject B, the frictional coefficients on both cornea and bulbar conjunctiva fall within the mixed lubrication where a part of the eyelid and ocular surfaces is supported by the tear layer, and in the other part, the eyelid surface may be in contact with the ocular surface. Then the curve in the mixed lubrication shows a downward-sloping characteristic.

Fig. 3.4 Example of frictional characteristic curve of cornea and bulbar conjunctiva in mixed lubrication region of subject B ($0.06 < \mu < 0.18$; $\bar{\mu} = 0.10$)

Figures 3.5 shows the example of the frictional characteristic curve of the cornea and bulbar conjunctiva in fluid lubrication region of subject C. The frictional characteristic curve is described based on the measured data obtained from the subject C. The calculations were carried out using the computational program of the BSG-Starcraft of PSO and LSM by setting the number, $n_s = 20$ of particles in a swarm. The parameters, $p_2 = 0.35$ and $p_3 = 0.93$ were obtained when the objection function value, $F_i^j = 0.097$. The objective function value, $F_i^j = 0.097$ was achieved within the maximum iteration

number, $j_{max} = 200$. As for the subject C, the frictional coefficients on both cornea and bulbar conjunctiva fall within the fluid lubrication where the eyelid and ocular surfaces are fully separated by the tear layer. Then the curve in the fluid lubrication shows an upward-sloping characteristic.

Fig. 3.5 Example of frictional characteristic curve of cornea and bulbar conjunctiva in fluid lubrication region of subject C ($0.07 < \mu < 0.17$; $\overline{\mu} = 0.11$)

Figures 3.6 shows the example of the frictional characteristic curve of the cornea and bulbar conjunctiva in mixed and fluid lubrication regions of subject D. The frictional characteristic curve is described based on the measured data obtained from the subject D. The calculations were carried out using the computational program of the BSG-Starcraft of PSO and LSM by setting the number, $n_s = 20$ of particles in a swarm. The parameters, $p_2 = 0.93$ and $p_3 = 1.21$ were obtained when the objection function value, $F_i^j = 0.110$. The objective function value, $F_i^j = 0.110$ was achieved within the maximum iteration number, $j_{max} = 200$. As for the subject D, the concave upward curve was obtained as the

69

frictional characteristic one. The frictional coefficients on the cornea fall within the fluid lubrication where the eyelid and the cornea are fully separated by the tear layer. Then the curve in the fluid lubrication shows an upward-sloping characteristic. The frictional coefficients on the bulbar conjunctiva fall within the mixed lubrication where a part of the eyelid and bulbar conjunctiva is supported by the tear layer, and in the other part, the eyelid surface may be in contact with the bulbar conjunctiva. Then the curve in the mixed lubrication shows a downward-sloping characteristic.

Fig. 3.6 Example of frictional characteristic curve of cornea and bulbar conjunctiva in mixed and fluid lubrication regions of subject D ($0.04 < \mu < 0.16$; $\overline{\mu} = 0.09$)

Figures 3.7 shows the example of the frictional characteristic curve of the cornea and bulbar conjunctiva in fluid lubrication region of subject E. The frictional characteristic curve is described based on the measured data obtained from the subject E. The calculations were carried out using the computational program of the BSG-Starcraft of PSO and LSM by setting the number, $n_s = 20$ of particles in a swarm. The parameters, $p_2 = 0.63$ and $p_3 = 0.81$ were obtained when the objection function value, $F_i^j = 0.097$. The objective function value, $F_i^j =$

0.097 was achieved within the maximum iteration number, $j_{max} = 200$. As for the subject E, the frictional coefficients on both cornea and bulbar conjunctiva fall within the fluid lubrication where the eyelid and ocular surfaces are fully separated by the tear layer. Then the curve in the fluid lubrication shows an upward-sloping characteristic.


The plot shows frictional coefficient μ (y-axis, from 0.00 to 0.40) versus $X = \dfrac{V^{0.63}}{N^{0.81}}\left[\dfrac{\text{m}}{\text{gf·s}}\right]$ (x-axis, 0.8 to 3.6 $[\times 10^{-2}]$).

●: Measurement data of frictional coefficient on cornea
○: Measurement data of frictional coefficient on bulbar conjunctiva

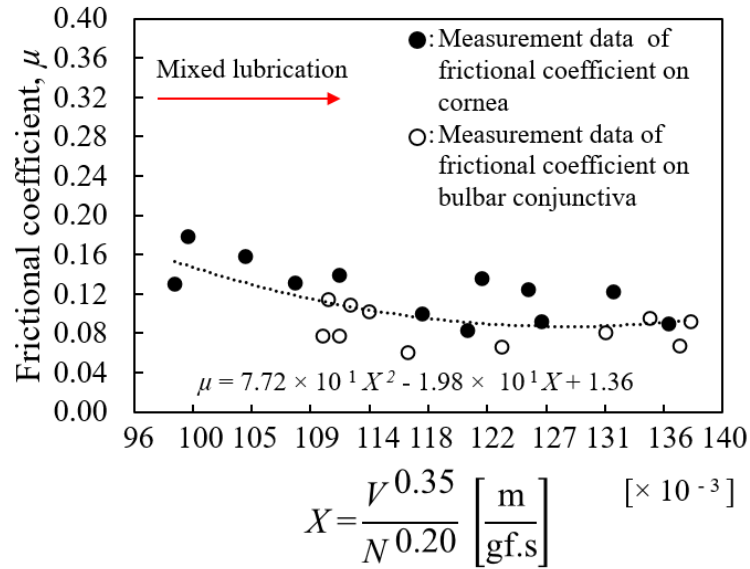$\mu = 1.55\,X^2 + 2.66\,X + 4.60 \times 10^{-2}$
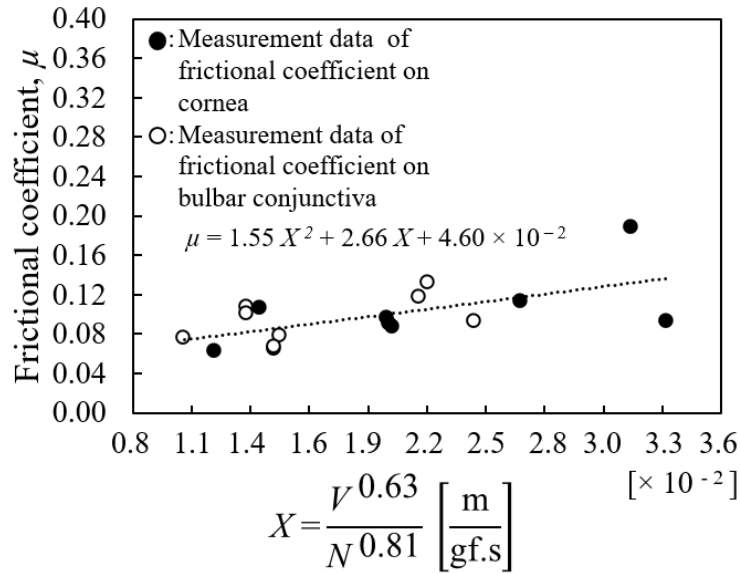
Fig. 3.7 Example of frictional characteristic curve of cornea and bulbar conjunctiva in fluid lubrication region of subject E ($0.06 < \mu < 0.19$; $\overline{\mu} = 0.10$)

Figures 3.8 shows the example of the frictional characteristic curve of the cornea and bulbar conjunctiva in fluid lubrication region of subject F. The frictional characteristic curve is described based on the measured data obtained from the subject F. The calculations were carried out using the computational program of the BSG-Starcraft of PSO and LSM by setting the number, $n_s = 20$ of particles in a swarm. The parameters, $p_2 = 0.70$ and $p_3 = 0.09$ were obtained when the objection function value, $F_i^j = 0.109$. The objective function value, $F_i^j = 0.109$ was achieved within the maximum iteration number, $j_{max} = 200$. As for the subject F, the frictional coefficients on both cornea and

bulbar conjunctiva fall within the fluid lubrication where the eyelid and ocular surfaces are fully separated by the tear layer. Then the curve in the fluid lubrication shows an upward-sloping characteristic.
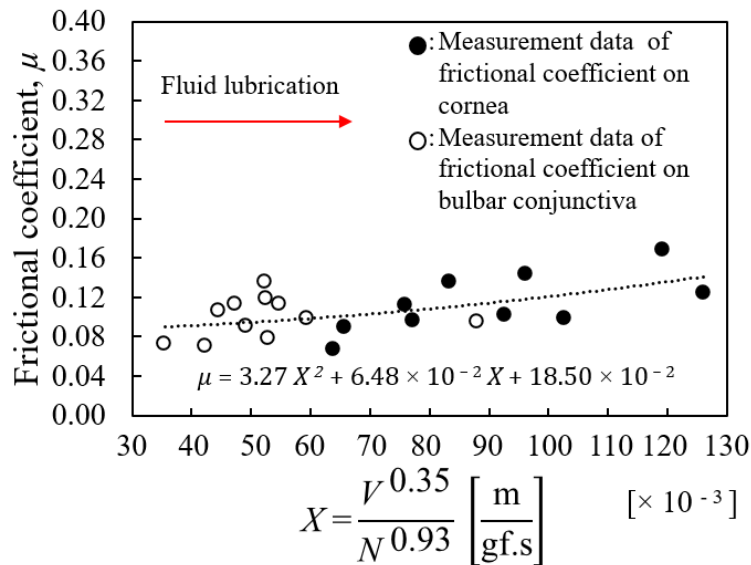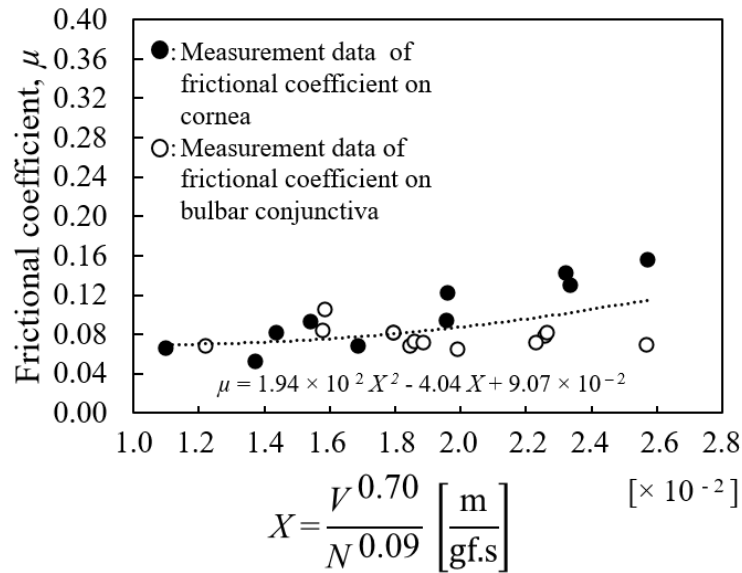

Fig. 3.8 Example of frictional characteristic curve of cornea and bulbar conjunctiva

in fluid lubrication region of subject F (0.05 < μ < 0.16; $\bar{\mu}$= 0.09)

3.5 Conclusion

The summary of the results is shown below.

(1) A new number relating to the tear viscosity, blink velocity, and the palpebral pressure was proposed in order to identify the frictional coefficient of the human ocular surface.

(2) A mathematical model describing the frictional coefficient on the human ocular surface was proposed by incorporating the new number.

(3) A computational program combining the BSG-Starcraft of PSO and the least-squares method was developed to find optimal parameters on the new number and the mathematical model.

(4) Frictional characteristic curves of the human ocular surfaces had been calculated by using the computational program employing the BSG-Starcraft of PSO and LSM.

(5) The frictional characteristics of human ocular surfaces could be classified into three types: the fluid lubrication where the eyelid and ocular surfaces are fully separated by the tear layer, the mixed lubrication where a part of the eyelid and ocular surfaces is supported by the tear layer and in the other part, the eyelid surface may be in contact with the ocular surface, and the lubrication containing both the mixed and fluid lubrications.

Chapter 4

Comparison of Frictional Characteristic Curves of Human Ocular Surfaces Determined by Using Hersey Number and Proposed New Number

4.1 Introduction

The purpose of this chapter is to investigate such appropriate parameters that the friction characteristic curves of the human ocular surface can be arranged well. The frictional characteristic curves were determined by using three methods: the Hersey Number in employing LSM, the proposed new number in employing the BSG-Starcraft of PSO and LSM, and the proposed new number in employing the Genetic Algorithm and LSM.

4.2 Procedure for Determining Frictional Characteristic Curves of Human Ocular Surfaces

4.2.1 In Using Hersey Number by Employing LSM

Figure 4.1 shows the procedure for determining frictional characteristic curves of human ocular surfaces in using Hersey Number by employing LSM. Using the Hersey Number, the parameters p_2, and p_3 in Eq. (3.1) were set to be constant and equal to 1. Then by incorporating the Hersey Number into the mathematical model in Eq. (3.2), the parameters p_4, p_5, ..., and p_n were determined by employing the LSM.

Fig. 4.1 Procedure for determining frictional characteristic curves of human ocular surfaces in using Hersey Number by employing LSM

4.2.2 In Using Proposed New Number by Employing BSG-Starcraft of PSO and LSM

Figure 4.2 shows the procedure for determining frictional characteristic curves of human ocular surfaces in using the proposed new number by employing the BSG-Starcraft of PSO and LSM. The procedure was started by using the proposed new number, X. Then the proposed new number, X was incorporated in the mathematical model in Eq. (3.2). The parameters p_2, …, p_n in Eq. (3.1) and Eq. (3.2) were determined by employing the BSG-Starcraft of PSO and LSM. The algorithm of the BSG-Starcraft of PSO used in this chapter is similar to the one in the third chapter. The BSG-Starcraft of PSO would terminate when the maximum number of iteration was reached. Then using parameters p_2 and p_3 obtained by the BSG-Starcraft of PSO, the parameters p_4, p_5,…, and p_n were determined by employing the LSM. In this research, the determination of optimal parameters in the mathematical model would terminate when the stopping criterion, namely the $p_4 > 0$ was met.

Fig. 4.2 Procedure for determining frictional characteristic curves of human ocular surfaces in using proposed new number by employing the BSG-Starcraft of PSO and LSM

4.2.3 In Using Proposed New Number by Employing Genetic Algorithm and LSM

Figure 4.3 shows the procedure for determining frictional characteristic curves of the human ocular surfaces in using the proposed new number by employing the Genetic Algorithm and LSM as in [8]. The procedure was started by using the proposed new number, X. Then the proposed new number, X was incorporated in the mathematical model in Eq. (3.2). The parameters p_2, …, p_n in Eq. (3.1) and Eq. (3.2) were determined by employing the Genetic Algorithm and LSM. The Genetic Algorithm would terminate

when the maximum number of generation was reached. Then using parameters p_2 and p_3 obtained by the Genetic Algorithm, the parameters p_4, p_5,…, and p_n were determined by employing the LSM. In this research, the determination of optimal parameters in the mathematical model would terminate when the stopping criterion, namely the $p_4 > 0$ was met.

```
                        ( Start )
                            |
                            v
                    +-------------------+
                    |      Apply        |
                    | proposed new number|
                    +-------------------+
                            |
                            v
                  +---------------------+
                  | Incorporate new number in|
                  |  mathematical model |
                  +---------------------+
                            |
                            v
                    +-------------------+
                    |      Apply        |
                    | Genetic Algorithm |
                    +-------------------+
                            |
                            v
                      / Generation >  \   No
                      \ Max. generation ? /
                            |
                           Yes
                            |
                            v
                    +-------------------+
                    |     Apply LSM     |
                    +-------------------+
                            |
                No          v
                      /   Satisfying    \
                      \ stopping criterion ? /
                            |
                           Yes
                            |
                          ( End )
```
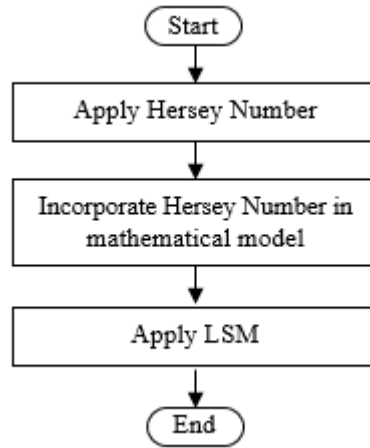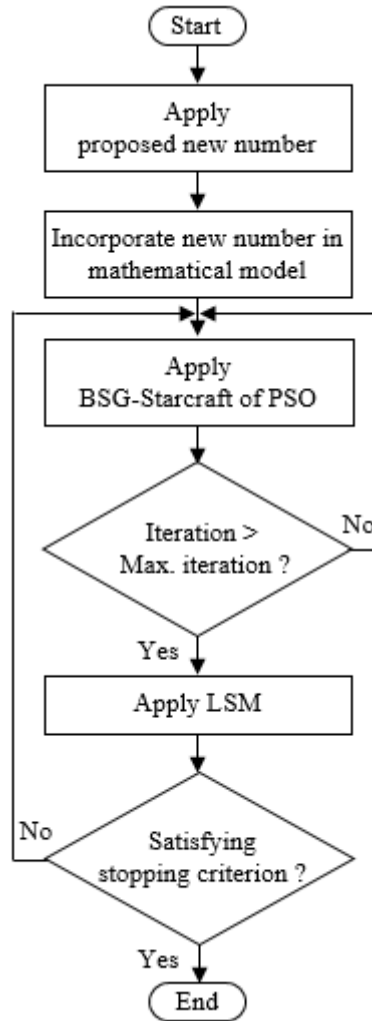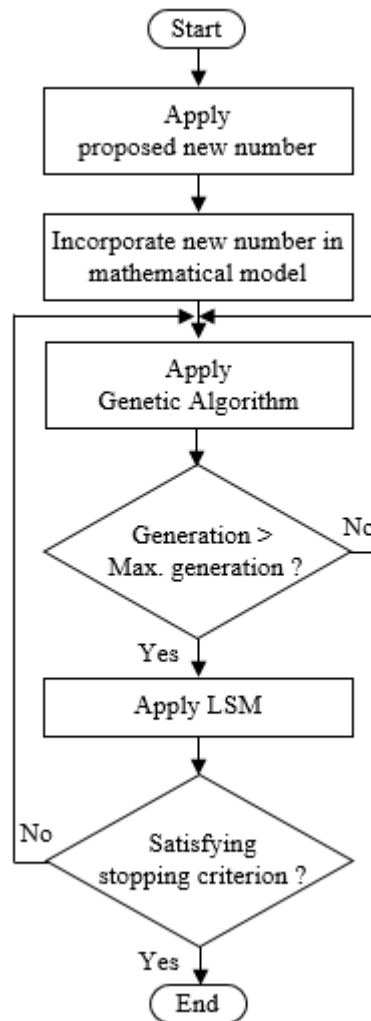
Fig. 4.3 Procedure for determining frictional characteristic curves of human ocular surfaces

in using proposed new number by employing the Genetic Algorithm and LSM

77

4.3 Frictional Characteristic Curves of Human Ocular Surfaces

4.3.1 Determined by Using Hersey Number in Employing LSM

Figure 4.4 shows the frictional characteristic curve on the cornea and bulbar conjunctiva of subject A determined by using Hersey Number in employing LSM. As for the subject A, by using the Hersey Number in employing the LSM, the obtained frictional characteristic curve shows a concave-downward characteristic. Frictional coefficients on both the cornea and bulbar conjunctiva fall outside the fluid lubrication region and the mixed lubrication region.

Fig. 4.4 Frictional characteristic curve on cornea and bulbar conjunctiva of subject A determined by using Hersey Number in employing LSM

Figure 4.5 shows the frictional characteristic curve on the cornea and bulbar conjunctiva of subject B determined by using Hersey Number in employing LSM. As for the subject B, by using the Hersey Number in employing the LSM, the obtained frictional characteristic curve shows a downward-sloping characteristic. Frictional coefficients on both the cornea and bulbar conjunctiva fall within the mixed lubrication where a part of the eyelid and ocular surface is supported by the tear layer, and in the other part, the eyelid surface may be in contact with the ocular surface.

Fig. 4.5 Frictional characteristic curve on cornea and bulbar conjunctiva of

subject B determined by using Hersey Number in employing LSM

Figure 4.6 shows the frictional characteristic curve on the cornea and bulbar conjunctiva of subject C determined by using Hersey Number in employing LSM. As for the subject C, by using the Hersey Number in employing the LSM, the obtained frictional characteristic curve shows a concave-downward characteristic. Frictional coefficients on both the cornea and bulbar conjunctiva fall outside the fluid lubrication region and the mixed lubrication region.

Fig. 4.6 Frictional characteristic curve on cornea and bulbar conjunctiva of

subject C determined by using Hersey Number in employing LSM

Figure 4.7 shows the frictional characteristic curve on the cornea and bulbar conjunctiva of subject D determined by using Hersey Number in employing LSM. As for the subject D, by using the Hersey Number in employing the LSM, the obtained frictional characteristic curve shows a concave-upward characteristic. The frictional coefficients on the cornea fall within the fluid lubrication where the eyelid and the cornea are fully separated by the tear layer. Frictional coefficients on the bulbar conjunctiva fall within the mixed lubrication where a part of the eyelid and ocular surface is supported by the tear layer, and in the other part, the eyelid surface may be in contact with the ocular surface.

Fig. 4.7 Frictional characteristic curve on cornea and bulbar conjunctiva of subject D determined by using Hersey Number in employing LSM

Figure 4.8 shows the frictional characteristic curve on the cornea and bulbar conjunctiva of subject E determined by using Hersey Number in employing LSM. As for the subject E, by using the Hersey Number in employing the LSM, the obtained frictional characteristic curve shows a concave-downward characteristic. Frictional coefficients on both the cornea and bulbar conjunctiva fall outside the fluid lubrication region and the mixed lubrication region.
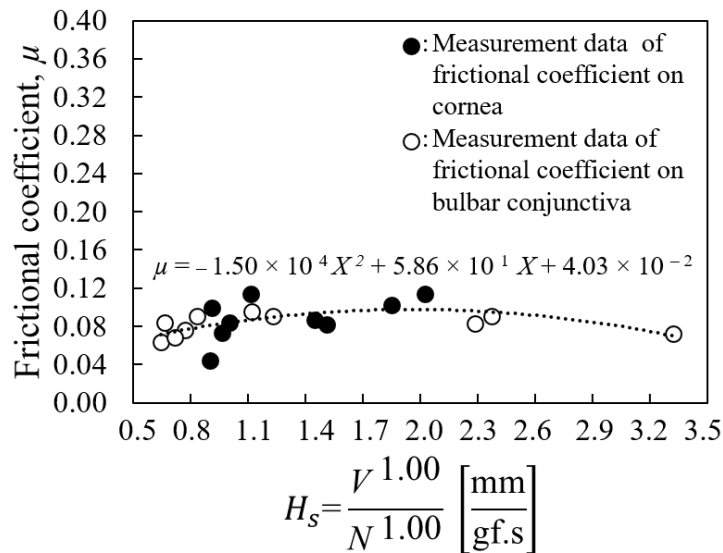
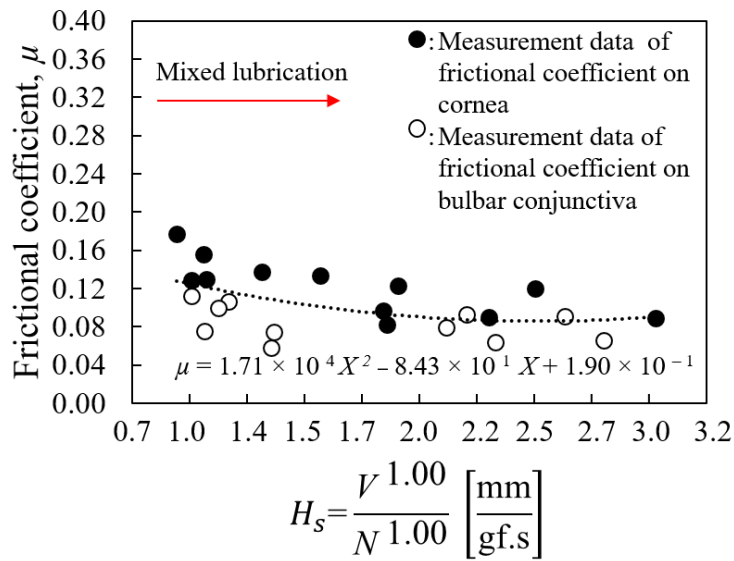$$H_s = \frac{V\ 1.00}{N\ 1.00} \left[\frac{mm}{gf.s}\right]$$
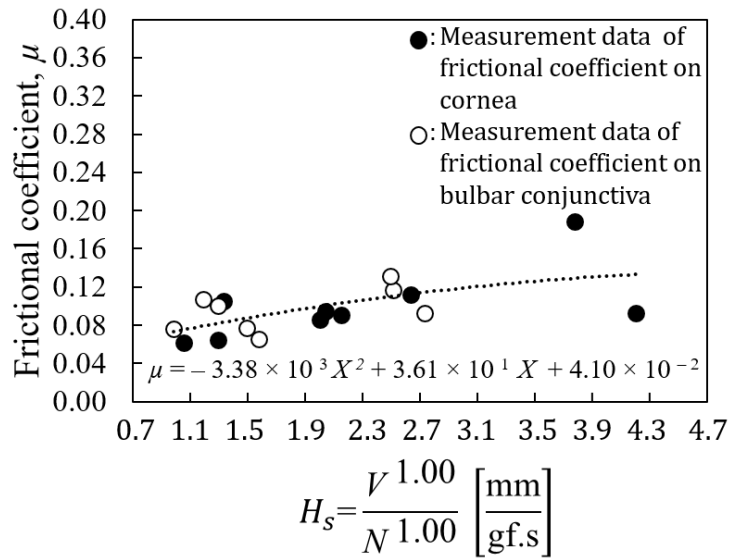
Fig. 4.8 Frictional characteristic curve on cornea and bulbar conjunctiva of

subject E determined by using Hersey Number in employing LSM

Figure 4.9 shows the frictional characteristic curve on the cornea and bulbar conjunctiva of

subject F determined by using Hersey Number in employing LSM. As for the subject F, by using

the Hersey Number in employing the LSM, the obtained frictional characteristic curve shows a

concave-downward characteristic. Frictional coefficients on both the cornea and bulbar conjunctiva

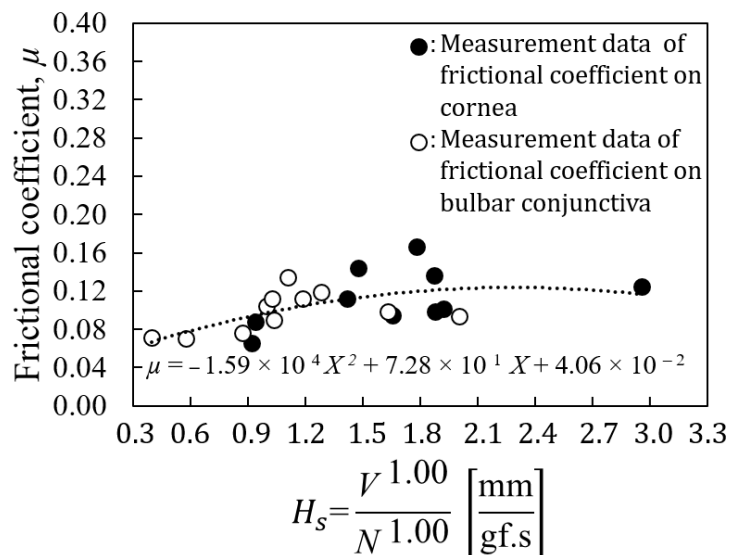fall outside the fluid lubrication region and the mixed lubrication region.
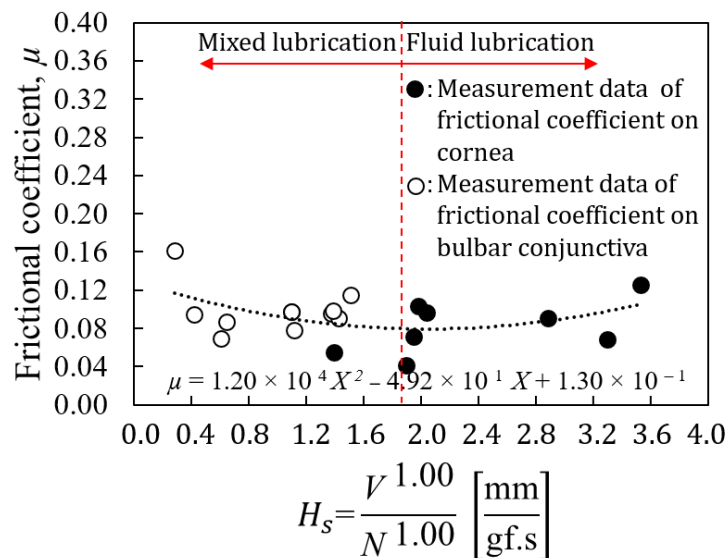

$$H_s = \frac{V\ 1.00}{N\ 1.00} \left[\frac{mm}{gf.s}\right]$$
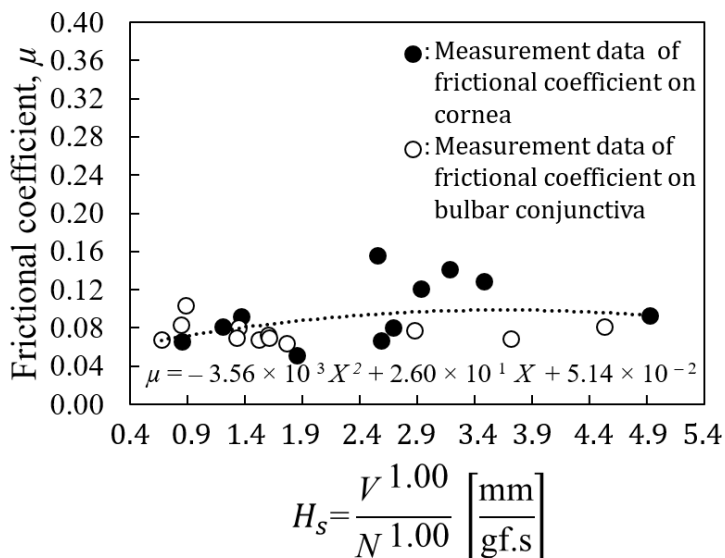
Fig. 4.9 Frictional characteristic curve on cornea and bulbar conjunctiva of

subject F determined by using Hersey Number in employing LSM

81

4.3.2 Determined by Using Proposed New Number in Employing BSG-Starcraft of PSO and LSM

Figures 4.10 shows the example of the frictional characteristic curve of the cornea and bulbar conjunctiva in fluid lubrication region of subject A calculated by using BSG-Starcraft of PSO and LSM. The frictional characteristic curve is described based on the measured data obtained from the subject A. The calculations were carried out using the computational program of the BSG-Starcraft of PSO and LSM by setting the number, n_s = 20 of particles in a swarm. The parameters, $p_2 = 1.00$ and $p_3 = 1.00$ were obtained when the objection function value, $F_i^j = 0.068$. The objective function value, $F_i^j = 0.068$ was achieved within the maximum iteration number, $j_{max} = 200$. As for the subject A, the frictional coefficients on both cornea and bulbar conjunctiva fall within the fluid lubrication where the eyelid and ocular surfaces are fully separated by the tear layer. Then the curve in the fluid lubrication shows an upward-sloping characteristic.

Fig.4.10 Example of frictional characteristic curve of cornea and bulbar conjunctiva in fluid lubrication region of subject A calculated by using BSG-Starcraft of PSO and LSM $(0.04 < \mu < 0.11; \ \bar{\mu} = 0.08)$

Figures 4.11 shows the example of the frictional characteristic curve of the cornea and bulbar conjunctiva in mixed lubrication region of subject B calculated by using BSG-Starcraft of PSO and LSM. The frictional characteristic curve is described based on the measured data obtained from the subject B. The calculations were carried out using the computational program of the BSG-Starcraft of PSO and LSM by setting the number, n_s = 20 of particles in a swarm. The parameters, $p_2 = 0.82$ and $p_3 = 0.33$ were obtained when the objection function value, $F_i^j = 0.125$. The objective function value, $F_i^j = 0.125$ was achieved within the maximum iteration number, $j_{max} = 200$. As for the subject B, the frictional coefficients on both cornea and bulbar conjunctiva fall within the mixed lubrication where a part of the eyelid and ocular surfaces is supported by the tear layer, and in the other part, the eyelid surface may be in contact with the ocular surface. Then the curve in the mixed lubrication shows a downward-sloping characteristic.

Fig. 4.11 Example of frictional characteristic curve of cornea and bulbar conjunctiva in mixed lubrication region of subject B calculated by using BSG-Starcraft of PSO and LSM $(0.06 < \mu < 0.18; \bar{\mu} = 0.10)$

Figures 4.12 shows the example of the frictional characteristic curve of the cornea and bulbar conjunctiva in fluid lubrication region of subject C calculated by using BSG-Starcraft of PSO and LSM. The frictional characteristic curve is described based on the measured data obtained from the subject C. The calculations were carried out using the computational program of the BSG-Starcraft of PSO and LSM by setting the number, $n_s = 20$ of particles in a swarm. The parameters, $p_2 = 0.39$ and $p_3 = 0.85$ were obtained when the objection function value, $F_i^j = 0.097$. The objective function value, $F_i^j = 0.097$ was achieved within the maximum iteration number, $j_{max} = 200$. As for the subject C, the frictional coefficients on both cornea and bulbar conjunctiva fall within the fluid lubrication where the eyelid and ocular surfaces are fully separated by the tear layer. Then the curve in the fluid lubrication shows an upward-sloping characteristic.
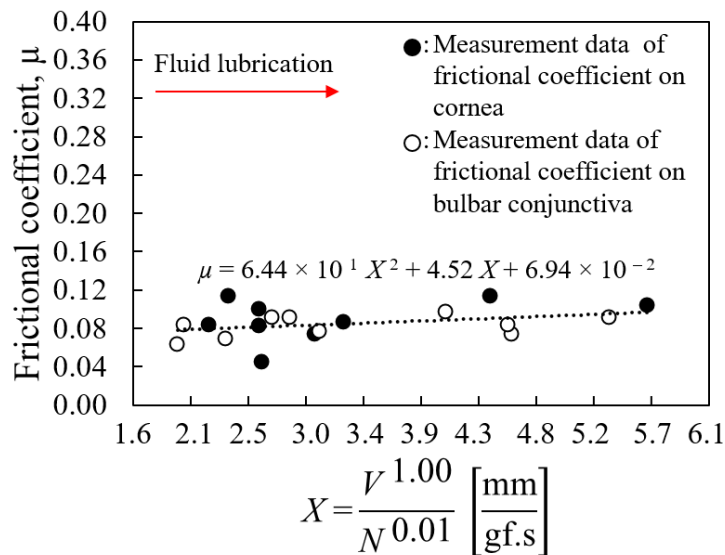

$$X = \frac{V^{0.39}}{N^{0.85}} \left[\frac{\text{mm}}{\text{gf.s}}\right]$$

Fig. 4.12 Example of frictional characteristic curve of cornea and bulbar conjunctiva in fluid lubrication region of subject C calculated by using BSG-Starcraft of PSO and LSM $(0.07 < \mu < 0.17; \ \overline{\mu} = 0.11)$

Figures 4.13 shows the example of the frictional characteristic curve of the cornea and bulbar conjunctiva in mixed and fluid lubrication regions of subject D calculated by using BSG-

Starcraft of PSO and LSM. The frictional characteristic curve is described based on the measured data obtained from the subject D. The calculations were carried out using the computational program of the BSG-Starcraft of PSO and LSM by setting the number, $n_s = 20$ of particles in a swarm. The parameters, $p_2 = 0.97$ and $p_3 = 0.62$ were obtained when the objection function value, $F_i^j = 0.111$. The objective function value, $F_i^j = 0.110$ was achieved within the maximum iteration number, $j_{max} = 200$. As for the subject D, the concave upward curve was obtained as the frictional characteristic one. The frictional coefficients on the cornea fall within the fluid lubrication where the eyelid and the cornea are fully separated by the tear layer. Then the curve in the fluid lubrication shows an upward-sloping characteristic. The frictional coefficients on the bulbar conjunctiva fall within the mixed lubrication where a part of the eyelid and bulbar conjunctiva is supported by the tear layer, and in the other part, the eyelid surface may be in contact with the bulbar conjunctiva. Then the curve in the mixed lubrication shows a downward-sloping characteristic.
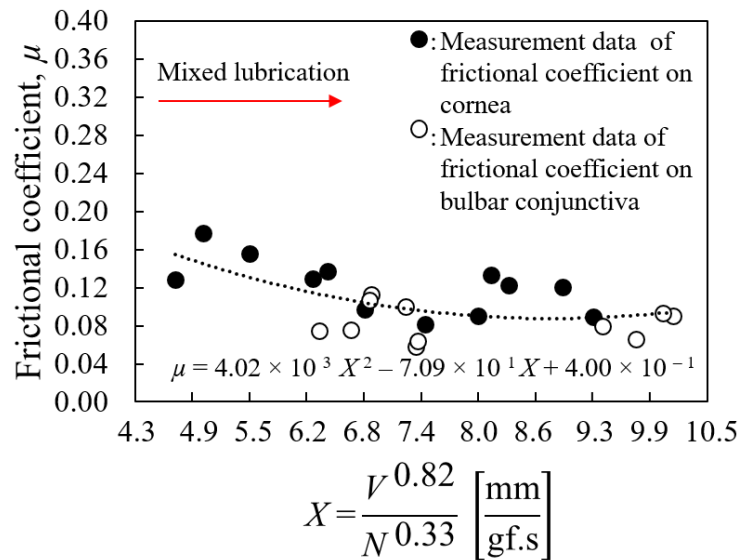

Fig. 4.13 Example of frictional characteristic curve of cornea and bulbar conjunctiva in mixed and fluid lubrication regions of subject D calculated by using BSG-Starcraft of PSO and LSM $(0.04 < \mu < 0.16;\ \overline{\mu} = 0.09)$

Figures 4.14 shows the example of the frictional characteristic curve of the cornea and bulbar conjunctiva in fluid lubrication region of subject E calculated by using BSG-Starcraft of PSO and LSM. The frictional characteristic curve is described based on the measured data obtained from the subject E. The calculations were carried out using the computational program of the BSG-Starcraft of PSO and LSM by setting the number, n_s = 20 of particles in a swarm. The parameters, $p_2 = 0.38$ and $p_3 = 0.49$ were obtained when the objection function value, $F_i^j = 0.097$. The objective function value, $F_i^j = 0.097$ was achieved within the maximum iteration number, $j_{max} = 200$. As for the subject E, the frictional coefficients on both cornea and bulbar conjunctiva fall within the fluid lubrication where the eyelid and ocular surfaces are fully separated by the tear layer. Then the curve in the fluid lubrication shows an upward-sloping characteristic.
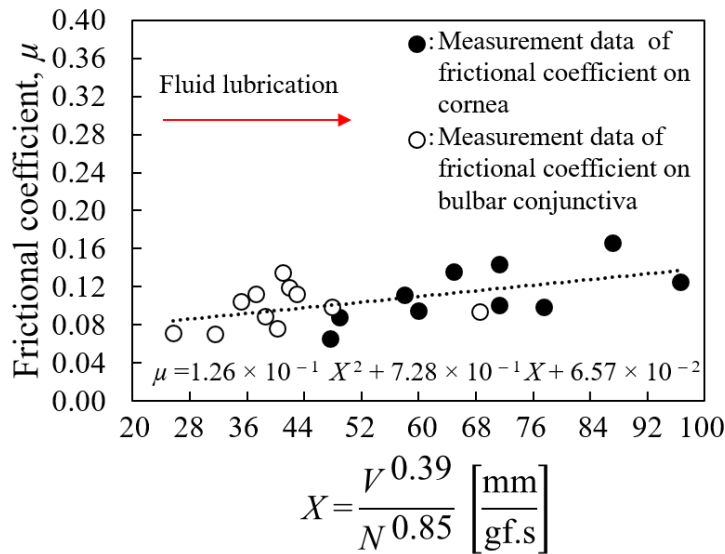

Fig. 4.14 Example of frictional characteristic curve of cornea and bulbar conjunctiva in fluid lubrication region of subject E calculated by using BSG-Starcraft of PSO and LSM $(0.04 < \mu < 0.20;\ \bar{\mu} = 0.10)$

Figures 4.15 shows the example of the frictional characteristic curve of the cornea and bulbar conjunctiva in fluid lubrication region of subject F calculated by using BSG-Starcraft of PSO and LSM. The frictional characteristic curve is described based on the measured data obtained from the subject F. The calculations were carried out using the computational program of the BSG-Starcraft of PSO and LSM by setting the number, n_s = 20 of particles in a swarm. The parameters, $p_2 = 0.65$ and $p_3 = 0.16$ were obtained when the objection function value, $F_i^j = 0.110$. The objective function value, $F_i^j = 0.109$ was achieved within the maximum iteration number, $j_{max} = 200$. As for the subject F, the frictional coefficients on both cornea and bulbar conjunctiva fall within the fluid lubrication where the eyelid and ocular surfaces are fully separated by the tear layer. Then the curve in the fluid lubrication shows an upward-sloping characteristic.
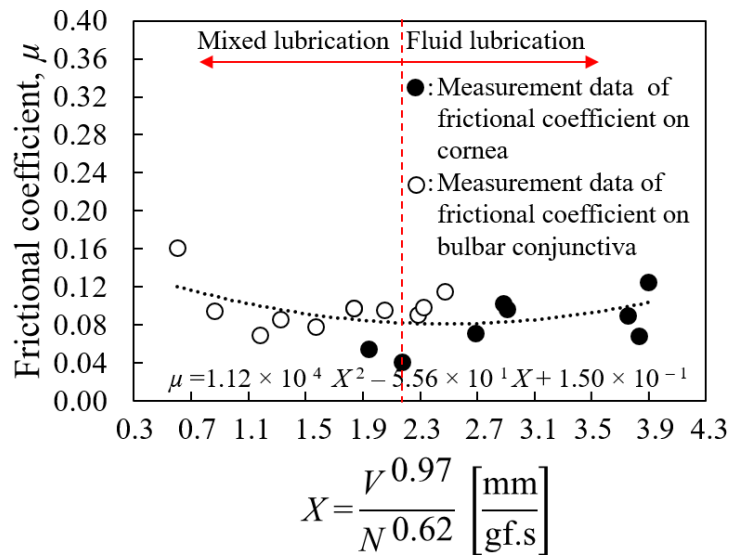

Fig. 4.15 Example of frictional characteristic curve of cornea and bulbar conjunctiva in fluid lubrication region of subject F calculated by using BSG-Starcraft of PSO and LSM

$(0.05 < \mu < 0.16; \ \overline{\mu} = 0.09)$

4.3.3 Determined by Using Proposed New Number in Employing Genetic Algorithm and LSM

Figures 4.16 shows the example of the frictional characteristic curve of the cornea and bulbar conjunctiva in fluid lubrication region of subject A calculated by using Genetic Algorithm and LSM. The frictional characteristic curve is described based on the measured data obtained from the subject A. The calculations were carried out using the computational program of the genetic algorithm and LSM by setting the number of generation = 1000, the number of population =100, the mutation rate = 0.05. The parameters, p_2 = 1.00 and p_3 = 1.00 were obtained when the fitness function value, J_i = 95.39. As for the subject A, the frictional coefficients on both cornea and bulbar conjunctiva fall within the fluid lubrication where the eyelid and ocular surfaces are fully separated by the tear layer. Then the curve in the fluid lubrication shows an upward-sloping characteristic.
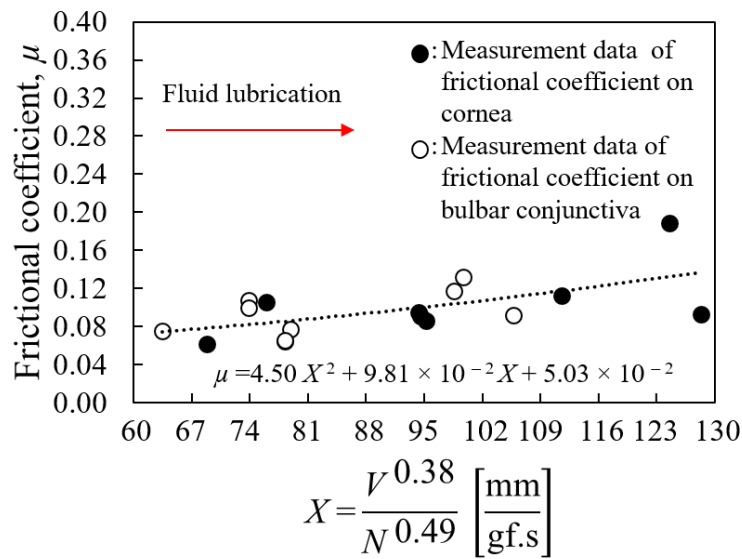

$$X = \frac{V^{0.98}}{N^{0.01}} \left[\frac{mm}{gf.s}\right]$$
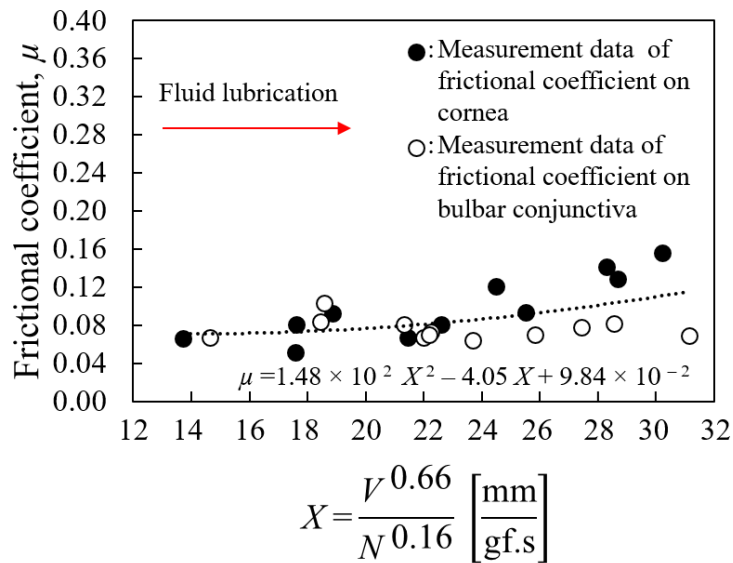
Fig. 4.16 Example of frictional characteristic curve of cornea and bulbar conjunctiva in fluid lubrication region of subject A calculated by using Genetic Algorithm and LSM

$(0.04 < \mu < 0.11; \ \bar{\mu} = 0.08)$

Figures 4.17 shows the example of the frictional characteristic curve of the cornea and bulbar conjunctiva in mixed lubrication region of subject B calculated by using Genetic Algorithm and LSM. The frictional characteristic curve is described based on the measured data obtained from the subject B. The calculations were carried out using the computational program of the Genetic Algorithm and LSM by setting the number of generation = 1000, the number of population =100, the mutation rate = 0.05. The parameters, p_2 = 0.65 and p_3 = 0.48 were obtained when the fitness function value, J_i = 90.34. As for the subject B, the frictional coefficients on both cornea and bulbar conjunctiva fall within the mixed lubrication where a part of the eyelid and ocular surfaces is supported by the tear layer, and in the other part, the eyelid surface may be in contact with the ocular surface. Then the curve in the mixed lubrication shows a downward-sloping characteristic.

Fig. 4.17 Example of frictional characteristic curve of cornea and bulbar conjunctiva in mixed lubrication region of subject B calculated by using Genetic Algorithm and LSM $(0.06 < \mu < 0.18; \ \overline{\mu} = 0.10)$

Figures 4.18 shows the example of the frictional characteristic curve of the cornea and bulbar conjunctiva in fluid lubrication region of subject C calculated by using Genetic Algorithm and LSM. The frictional characteristic curve is described based on the measured data obtained from the subject C. The calculations were carried out using the computational program of the Genetic Algorithm and LSM by setting the number of generation = 1000, the number of population =100, the mutation rate = 0.05. The parameters, p_2 = 0.04 and p_3 = 0.83 were obtained when the fitness function value, J_i = 92.98. As for the subject C, the frictional coefficients on both cornea and bulbar conjunctiva fall within the fluid lubrication where the eyelid and ocular surfaces are fully separated by the tear layer. Then the curve in the fluid lubrication shows an upward-sloping characteristic.
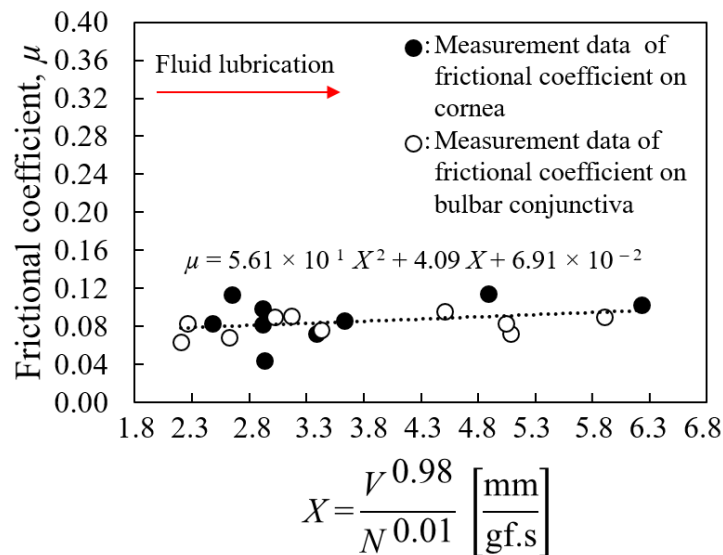

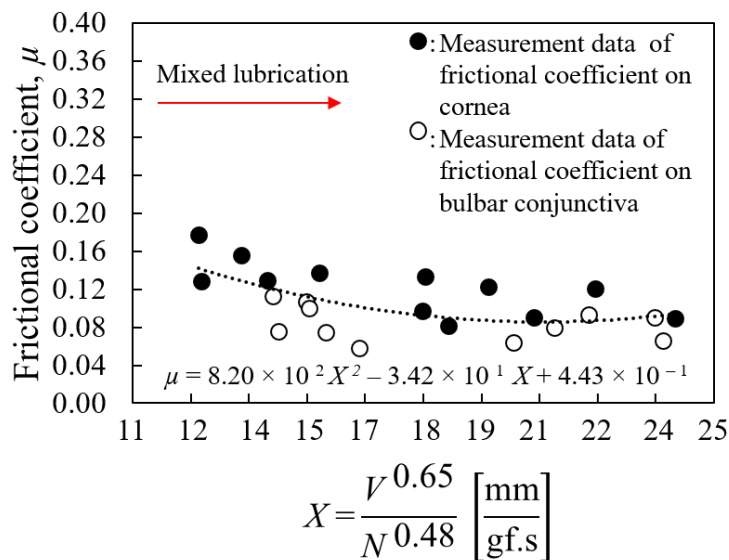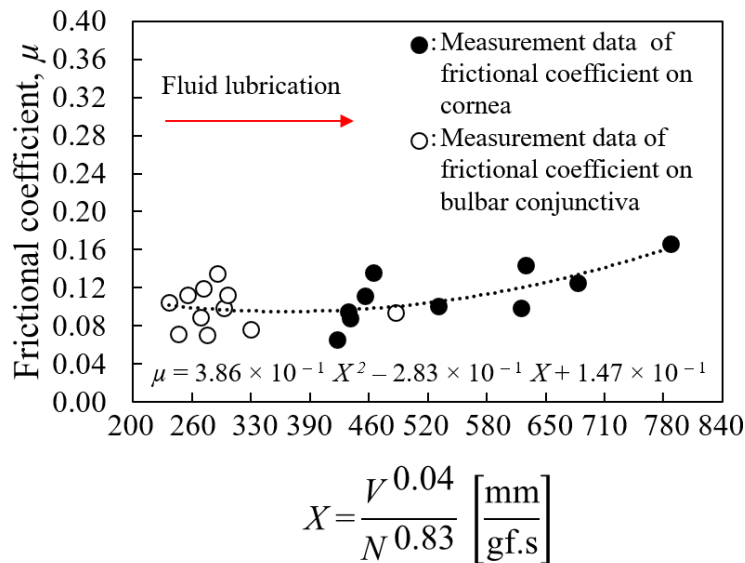$$X = \frac{V^{0.04}}{N^{0.83}} \left[\frac{\text{mm}}{\text{gf.s}}\right]$$

Fig. 4.18 Example of frictional characteristic curve of cornea and bulbar conjunctiva in fluid lubrication region of subject C calculated by using Genetic Algorithm and LSM

$(0.07 < \mu < 0.17;\ \overline{\mu} = 0.11)$

Figures 4.19 the example of the frictional characteristic curve of the cornea and bulbar conjunctiva in mixed and fluid lubrication regions of subject D calculated by using Genetic Algorithm and LSM. The frictional characteristic curve is described based on the measured data obtained from the subject D. The calculations were carried out using the computational program of the Genetic Algorithm and LSM by setting the number of generation = 1000, the number of population =100, the mutation rate = 0.05. The parameters, p_2 = 0.94 and p_3 = 0.03 were obtained when the fitness function value, J_i = 93.38. As for the subject D, the concave upward curve was obtained as the frictional characteristic one. The frictional coefficients on the cornea fall within the fluid lubrication where the eyelid and the cornea are fully separated by the tear layer. Then the curve in the fluid lubrication shows an upward-sloping characteristic. The frictional coefficients on the bulbar conjunctiva fall within the mixed lubrication where a part of the eyelid and bulbar conjunctiva is supported by the tear layer, and in the other part, the eyelid surface may be in contact with the bulbar conjunctiva. Then the curve in the mixed lubrication shows a downward-sloping characteristic.

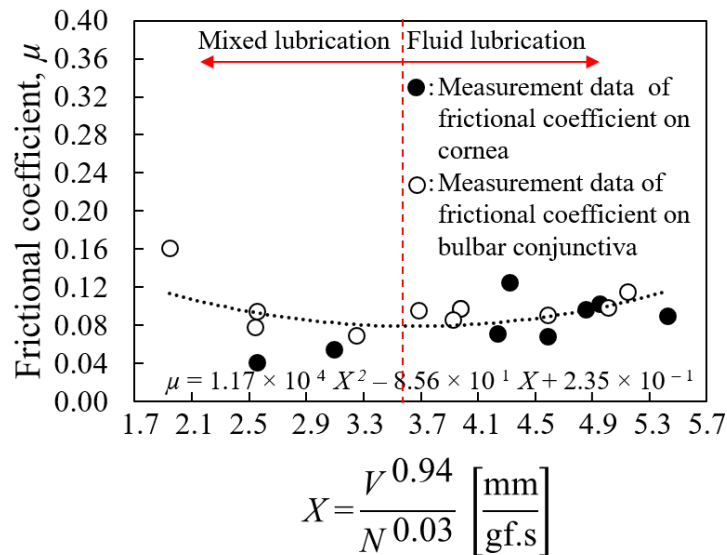$$X = \frac{V^{0.94}}{N^{0.03}} \left[\frac{mm}{gf.s}\right]$$

Fig. 4.19 Example of frictional characteristic curve of cornea and bulbar conjunctiva in mixed and fluid lubrication regions of subject D calculated by using Genetic Algorithm and LSM ($0.04 < \mu < 0.16$; $\bar{\mu}$= 0.09)

Figures 4.20 shows the example of the frictional characteristic curve of the cornea and bulbar conjunctiva in fluid lubrication region of subject E calculated by using Genetic Algorithm and LSM. The frictional characteristic curve is described based on the measured data obtained from the subject E. The calculations were carried out using the computational program of the Genetic Algorithm and LSM by setting the number of generation = 1000, the number of population =100, the mutation rate = 0.05. The parameters, $p_2 = 0.42$ and $p_3 = 0.60$ were obtained when the fitness function value, $J_i = 93.77$. As for the subject E, the frictional coefficients on both cornea and bulbar conjunctiva fall within the fluid lubrication where the eyelid and ocular surfaces are fully separated by the tear layer. Then the curve in the fluid lubrication shows an upward-sloping characteristic.

$$X = \frac{V^{0.42}}{N^{0.60}} \left[\frac{mm}{gf.s}\right]$$

Fig. 4.20 Example of frictional characteristic curve of cornea and bulbar conjunctiva in fluid lubrication region of subject E calculated by using Genetic Algorithm and LSM

$(0.06 < \mu < 0.19; \ \overline{\mu} = 0.10)$

Figures 4.21 shows the example of the frictional characteristic curve of the cornea and bulbar conjunctiva in fluid lubrication region of subject F calculated by using Genetic Algorithm and LSM. The frictional characteristic curve is described based on the

measured data obtained from the subject F. The calculations were carried out using the computational program of the Genetic Algorithm and LSM by setting the number of generation = 1000, the number of population =100, the mutation rate = 0.05. The parameters, p_2 = 0.38 and p_3 = 0.28 were obtained when the fitness function value, J_i = 92.00. As for the subject F, the frictional coefficients on both cornea and bulbar conjunctiva fall within the fluid lubrication where the eyelid and ocular surfaces are fully separated by the tear layer. Then the curve in the fluid lubrication shows an upward-sloping characteristic.
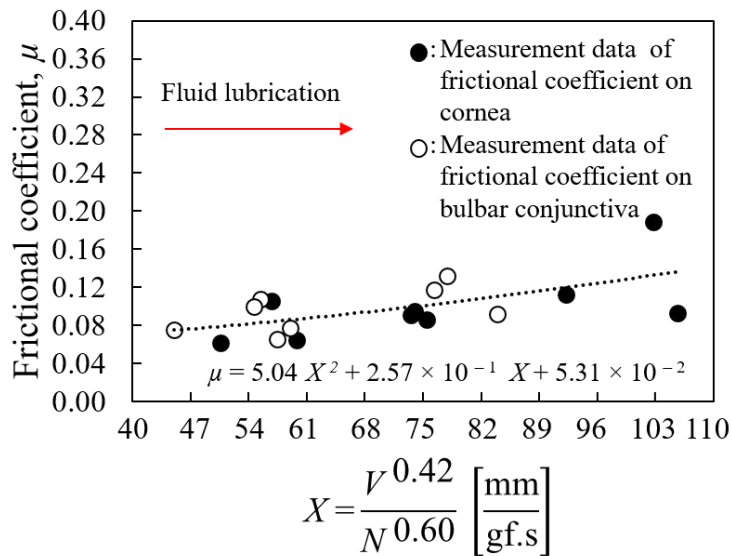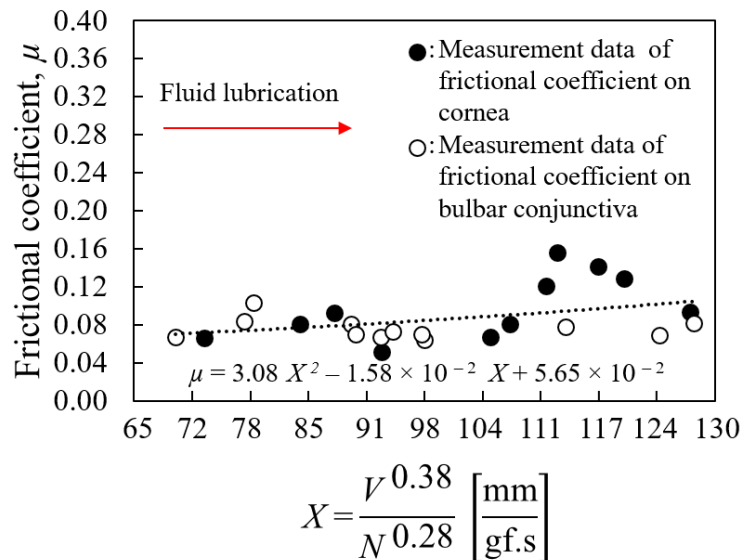

Fig. 4.21 Example of frictional characteristic curve of cornea and bulbar conjunctiva in fluid lubrication region of subject F calculated by using Genetic Algorithm and LSM

$(0.05 < \mu < 0.16;\ \overline{\mu} = 0.09)$

In this research, similar to the subject A, the frictional characteristic curves on the cornea and bulbar conjunctiva of subjects C, E, and F determined by using the Hersey Number in employing the LSM show the concave-downward characteristic. However, the frictional characteristic curves on the cornea and bulbar conjunctiva of subjects C, E, and F determined by using the proposed new number in employing the BSG-Starcraft of

PSO and LSM show the upward-sloping characteristic. The upward-sloping characteristic curves of the frictional coefficients on the cornea and bulbar conjunctiva of subjects C, E, and F also obtained by using the proposed new number in employing the Genetic Algorithm and LSM.

4.4 Conclusion

The summary of the results is shown below.

(1) The appropriate parameters that the friction characteristic curves of the human ocular surface can be arranged had been obtained.

(2) The frictional characteristic curves had been determined by using three methods: the Hersey Number in employing LSM, the proposed new number in employing the BSG-Starcraft of PSO and LSM, and the proposed new number in employing the Genetic Algorithm and LSM. Then the frictional characteristic curves had been compared.

(3) The frictional characteristic curves obtained by using the three methods on both the mixed lubrication and lubrication containing the mixed and fluid ones have similar patterns, namely a downward-sloping characteristic and a concave-upward characteristic, respectively. However, for the fluid lubrication, the frictional characteristic curves obtained by using the Hersey Number shows a concave-downward characteristic, while those obtained by using the proposed new number shows an upward-sloping characteristic.

(4) In both the mixed lubrication and the lubrication containing the mixed and fluid ones, the appropriate frictional characteristic curves could be obtained for the three methods. While, in the fluid lubrication, the appropriate frictional characteristic curves could be obtained for the two methods using the proposed new number, but the appropriate ones could not be obtained for the method using the Hersey Number.

Chapter 5

Conclusions

A new ocular surface tribometer to measure normal force, frictional force and displacement of the probe on human ocular surfaces had been developed in this research. An electrostatic capacitive sensor as a two-axis force sensor had been used in the developed ocular surface tribometer. A new data logger software had been developed that capable to synchronize in measuring normal forces, frictional forces and displacements of the probe. Then using the developed ocular surface tribometer, the measurements of normal forces, frictional forces, and displacements of the probe had been successfully conducted on six healthy subjects. The developed data logger software had been used to process the measured data of normal forces, frictional forces, and displacements of the probe. The measured data and the calculated results have been presented.

A new number relating to the tear viscosity, blink velocity, and palpebral pressure had been proposed. A mathematical model describing frictional coefficient of the human ocular surface by incorporating the proposed new number had also been proposed in this research. Computational codes employing a combination of BSG-Starcraft of PSO and LSM had been developed to find the optimal parameters in the mathematical model for determining frictional characteristics of human ocular surfaces.

The frictional characteristics of human ocular surfaces had been classified into three types: the fluid lubrication where the eyelid and ocular surfaces are fully separated by the tear layer, the mixed lubrication where a part of the eyelid and ocular surfaces is

supported by the tear layer and in the other part, the eyelid surface may be in contact with the ocular surface, and the lubrication containing both the mixed and fluid ones.

A comparison of frictional characteristic curves of human ocular surfaces determined by using the Hersey Number and the proposed new number has been examined. The frictional characteristic curves have been determined by using three methods: the Hersey Number in employing LSM, the proposed new number in employing the BSG-Starcraft of PSO and LSM, and the proposed new number in employing the Genetic Algorithm and LSM.

The frictional characteristic curves obtained by using the three methods on both the mixed lubrication and lubrication containing the mixed and fluid ones have similar patterns, namely a downward-sloping characteristic and a concave-upward characteristic, respectively. However, for the fluid lubrication, the frictional characteristic curves obtained by using the Hersey Number shows a concave-downward characteristic, while those obtained by using the proposed new number shows an upward-sloping characteristic.

In both the mixed lubrication and the lubrication containing the mixed and fluid ones, the appropriate frictional characteristic curves could be obtained for the three methods. While, in the fluid lubrication, the appropriate frictional characteristic curves could be obtained for the two methods using the proposed new number, but the appropriate ones could not be obtained for the method using the Hersey Number.

References

[1] Wilson, T., Aeschlimann, R., Tosatti, S., Toubouti, Y., Kakkassery, J. and Lorenz, K.O., 2015. Coefficient of friction of human corneal tissue. *Cornea, 34(9)*, pp.1179-1185.

[2] Roba, M., Duncan, E.G., Hill, G.A., Spencer, N.D. and Tosatti, S.G.P., 2011. Friction measurements on contact lenses in their operating environment. *Tribology Letters*, *44*(3), p.387.

[3] Rennie, A.C., Dickrell, P.L. and Sawyer, W.G., 2005. Friction coefficient of soft contact lenses: measurements and modeling. *Tribology Letters*, *18*(4), pp.499-504.

[4] Dunn, A.C., Urueña, J.M., Puig, E., Perez, V.L. and Sawyer, W.G., 2013. Friction coefficient measurement of an in vivo murine cornea. *Tribology Letters*, *49*(1), pp.145-149.

[5] Jones, M.B., Fulford, G.R., Please, C.P., McElwain, D.L.S. and Collins, M.J., 2008. Elastohydrodynamics of the eyelid wiper. *Bulletin of Mathematical Biology*, *70*(2), pp.323-343.

[6] Dunn, A.C., Tichy, J.A., Urueña, J.M. and Sawyer, W.G., 2013. Lubrication regimes in contact lens wear during a blink. *Tribology International*, *63*, pp.45-50.

[7] Pult, H., Tosatti, S.G., Spencer, N.D., Asfour, J.M., Ebenhoch, M. and Murphy, P.J., 2015. Spontaneous blinking from a tribological viewpoint. *The ocular surface*, *13*(3), pp.236-249.

[8] Okamoto, S., Pranoto, S., Ohwaki, Y., Lee, J.H., Shiraishi, A., Sakane, Y., Ohta, K. and Ohashi, Y., 2016. Development of a Physical Apparatus and Computational Program Employing a Genetic Algorithm and Least-Squares Method for Measuring the Frictional Coefficient of the Human Ocular Surface. In *Proceedings of 3rd International Conference on Biomedical Engineering and Systems (ICBES'16).*

[9] Hamrock, B.J., Schmid, S.R. and Jacobson, B.O., 2004. *Fundamentals of fluid film lubrication*. CRC press.

[10] Schaumberg, D.A., Dana, R., Buring, J.E. and Sullivan, D.A., 2009. Prevalence of dry eye disease among US men: estimates from the Physicians' Health Studies. *Archives of ophthalmology*, *127*(6), pp.763-768.

[11] McGinnigle, S., Naroo, S.A. and Eperjesi, F., 2012. Evaluation of dry eye. *Survey of ophthalmology*, *57*(4), pp.293-316.

[12] Navascues-Cornago, M., Maldonado-Codina, C. and Morgan, P.B., 2014. Mechanical sensitivity of the human conjunctiva. *Cornea*, *33*(8), pp.855-859.

[13] Johnson, M.E. and Murphy, P.J., 2004. Changes in the tear film and ocular surface

from dry eye syndrome. *Progress in retinal and eye research*, *23*(4), pp.449-474.

[14] Yoshioka, E., Yamaguchi, M., Shiraishi, A., Kono, T., Ohta, K. and Ohashi, Y., 2015. Influence of eyelid pressure on fluorescein staining of ocular surface in dry eyes. *American journal of ophthalmology*, *160*(4), pp.685-692.

[15] Kojima, T., Ishida, R., Dogru, M., Goto, E., Takano, Y., Matsumoto, Y., Kaido, M., Ohashi, Y. and Tsubota, K., 2004. A new noninvasive tear stability analysis system for the assessment of dry eyes. *Investigative ophthalmology & visual science*, *45*(5), pp.1369-1374.

[16] Acosta, M.C., Gallar, J. and Belmonte, C., 1999. The influence of eye solutions on blinking and ocular comfort at rest and during work at video display terminals. *Experimental eye research*, *68*(6), pp.663-669.

[17] Rosenfield, M., 2011. Computer vision syndrome: a review of ocular causes and potential treatments. *Ophthalmic and Physiological Optics*, *31*(5), pp.502-515.

[18] Patel, S., Henderson, R., Bradley, L., Galloway, B. and Hunter, L., 1991. Effect of visual display unit use on blink rate and tear stability. *Optom Vis Sci*, *68*(11), pp.888-892.

[19] Le, Q., Zhou, X., Ge, L., Wu, L., Hong, J. and Xu, J., 2012. Impact of dry eye syndrome on vision-related quality of life in a non-clinic-based general population. *BMC ophthalmology*, *12*(1), p.22.

[20] Uchino, M. and Schaumberg, D.A., 2013. Dry eye disease: impact on quality of life and vision. *Current ophthalmology reports*, *1*(2), pp.51-57.

[21] Schaumberg, D.A., Sullivan, D.A., Buring, J.E. and Dana, M.R., 2003. Prevalence of dry eye syndrome among US women. *American journal of ophthalmology*, *136*(2), pp.318-326.

[22] Sullivan, D.A., Hammitt, K.M., Schaumberg, D.A., Sullivan, B.D., Begley, C.G., Gjorstrup, P., Garrigue, J.S., Nakamura, M., Quentric, Y., Barabino, S. and Dalton, M., 2012. Report of the TFOS/ARVO symposium on global treatments for dry eye disease: an unmet need. *The ocular surface*, *10*(2), pp.108-116.

[23] Lemp, M.A., Bron, A.J., Baudouin, C., del Castillo, J.M.B., Geffen, D., Tauber, J., Foulks, G.N., Pepose, J.S. and Sullivan, B.D., 2011. Tear osmolarity in the diagnosis and management of dry eye disease. *American journal of ophthalmology*, *151*(5), pp.792-798.

[24] Grubbs Jr, J.R., Tolleson-Rinehart, S., Huynh, K. and Davis, R.M., 2014. A review of quality of life measures in dry eye questionnaires. *Cornea*, *33*(2), p.215.

[25] Paulsen, A.J., Cruickshanks, K.J., Fischer, M.E., Huang, G.H., Klein, B.E., Klein, R. and Dalton, D.S., 2014. Dry eye in the beaver dam offspring study: prevalence, risk factors, and health-related quality of life. *American journal of ophthalmology*, *157*(4), pp.799-806.

[26] Uchino, M., Uchino, Y., Dogru, M., Kawashima, M., Yokoi, N., Komuro, A.,

Sonomura, Y., Kato, H., Kinoshita, S., Schaumberg, D.A. and Tsubota, K., 2014. Dry eye disease and work productivity loss in visual display users: the Osaka study. *American journal of ophthalmology*, *157*(2), pp.294-300.

[27] Phadatare, S.P., Momin, M., Nighojkar, P., Askarkar, S. and Singh, K.K., 2015. A comprehensive review on dry eye disease: diagnosis, medical management, recent developments, and future challenges. *Advances in Pharmaceutics*, *2015*.

[28] Javadi, M.A. and Feizi, S., 2011. Dry eye syndrome. *Journal of ophthalmic & vision research*, *6*(3), p.192.

[29] Pult, H., Purslow, C. and Murphy, P.J., 2011. The relationship between clinical signs and dry eye symptoms. *Eye*, *25*(4), p.502.

[30] Ibrahim, O.M., Dogru, M., Takano, Y., Satake, Y., Wakamatsu, T.H., Fukagawa, K., Tsubota, K. and Fujishima, H., 2010. Application of visante optical coherence tomography tear meniscus height measurement in the diagnosis of dry eye disease. *Ophthalmology*, *117*(10), pp.1923-1929.

[31] Kamao, T., Yamaguchi, M., Kawasaki, S., Mizoue, S., Shiraishi, A. and Ohashi, Y., 2011. Screening for dry eye with newly developed ocular surface thermographer. *American journal of ophthalmology*, *151*(5), pp.782-791.

[32] Pult, H., Purslow, C. and Murphy, P.J., 2011. The relationship between clinical signs and dry eye symptoms. *Eye*, *25*(4), p.502.

[33] Pult, H., Riede-Pult, B.H. and Murphy, P.J., 2013. The relation between blinking and conjunctival folds and dry eye symptoms. *Optometry and Vision Science*, *90*(10), pp.1034-1039.

[34] Shaw, A.J., Collins, M.J., Davis, B.A. and Carney, L.G., 2010. Eyelid pressure and contact with the ocular surface. *Investigative ophthalmology & visual science*, *51*(4), pp.1911-1917.

[35] Sakai, E., Shiraishi, A., Yamaguchi, M., Ohta, K. and Ohashi, Y., 2012. Blepharo-tensiometer: new eyelid pressure measurement system using tactile pressure sensor. *Eye & contact lens*, *38*(5), pp.326-330.

[36] Francis, I.C., Stapleton, F., Ehrmann, K. and Coroneo, M.T., 2006. Lower eyelid tensometry in younger and older normal subjects. *Eye*, *20*(2), p.166.

[37] Ehrmann, K., Francis, I. and Stapleton, F., 2001. A novel instrument to quantify the tension of upper and lower eyelids. *Contact Lens and Anterior Eye*, *24*(2), pp.65-72.

[38] Mohammed, Z., Maidin, M.H.H. and Mohd-Ali, B., 2012. Lid wiper epitheliopathy in subjects with and without dry eye symptoms in Kuala Lumpur–a pilot study. *Archives Des Sciences*, *65*(10).

[39] Korb, D.R., Herman, J.P., Blackie, C.A., Scaffidi, R.C., Greiner, J.V., Exford, J.M. and Finnemore, V.M., 2010. Prevalence of lid wiper epitheliopathy in subjects with dry eye signs and symptoms. *Cornea*, *29*(4), pp.377-383.

[40] Shaw, A.J., 2009. *Eyelid pressure on the cornea* (Doctoral dissertation, Queensland University of Technology).

[41] Wan, T., Jin, X., Lin, L., Xu, Y. and Zhao, Y., 2016. Incomplete blinking may attribute to the development of meibomian gland dysfunction. *Current eye research*, *41*(2), pp.179-185.

[42] Korb, D.R., Herman, J.P., Greiner, J.V., Scaffidi, R.C., Finnemore, V.M., Exford, J.M., Blackie, C.A. and Douglass, T., 2005. Lid wiper epitheliopathy and dry eye symptoms. *Eye & Contact Lens*, *31*(1), pp.2-8.

[43] Berry, M., Pult, H., Purslow, C. and Murphy, P.J., 2008. Mucins and ocular signs in symptomatic and asymptomatic contact lens wear. *Optometry and Vision Science*, *85*(10), pp.E930-E938.

[44] Sterner, O., Karageorgaki, C., Zürcher, M., Zürcher, S., Scales, C.W., Fadli, Z., Spencer, N.D. and Tosatti, S.G., 2017. Reducing friction in the eye: a comparative study of lubrication by surface-anchored synthetic and natural ocular mucin analogues. *ACS applied materials & interfaces*, *9*(23), pp.20150-20160.

[45] Cher, I., 2003. Blink-related microtrauma: when the ocular surface harms itself. *Clinical & experimental ophthalmology*, *31*(3), pp.183-190.

[46] Yee, R.W., Sperling, H.G., Kattek, A., Paukert, M.T., Dawson, K., Garcia, M. and Hilsenbeck, S., 2007. Isolation of the ocular surface to treat dysfunctional tear syndrome associated with computer use. *The ocular surface*, *5*(4), pp.308-315.

[47] Rosenfield, M., 2011. Computer vision syndrome: a review of ocular causes and potential treatments. *Ophthalmic and Physiological Optics*, *31*(5), pp.502-515.

[48] Le, Q., Zhou, X., Ge, L., Wu, L., Hong, J. and Xu, J., 2012. Impact of dry eye syndrome on vision-related quality of life in a non-clinic-based general population. *BMC ophthalmology*, *12*(1), p.22.

[49] Foulks, G.N., Lemp, M., Jester, J., Sutphin, J., Murube, J. and Novack, G., 2007. report of the international dry eye workshop (DEWS). *Ocul Surf*, *5*(2), pp.65-204.

[50] Stevenson, W., Chauhan, S.K. and Dana, R., 2012. Dry eye disease: an immune-mediated ocular surface disorder. *Archives of ophthalmology*, *130*(1), pp.90-100.

[51] Veres, A., Tapasztó, B., Kosina-Hagyó, K., Somfai, G.M. and Németh, J., 2011. Imaging lid-parallel conjunctival folds with OCT and comparing its grading with the slit lamp classification in dry eye patients and normal subjects. *Investigative ophthalmology & visual science*, *52*(6), pp.2945-2951.

[52] Lin, Z., Liu, X., Zhou, T., Wang, Y., Bai, L., He, H. and Liu, Z., 2011. A mouse dry eye model induced by topical administration of benzalkonium chloride. *Molecular vision*, *17*, p.257.

[53] Cobb, J.A., Dunn, A.C., Kwon, J., Sarntinoranont, M., Sawyer, W.G. and Tran-Son-Tay, R., 2008. A novel method for low load friction testing on living cells. *Biotechnology letters*, *30*(5), pp.801-806.

[54] Dunn, A.C., Cobb, J.A., Kantzios, A.N., Lee, S.J., Sarntinoranont, M., Tran-Son-Tay, R. and Sawyer, W.G., 2008. Friction coefficient measurement of hydrogel materials on living epithelial cells. *Tribology Letters*, *30*(1), p.13.

[55] Chamoret, D., Salmon, S., Di Cesare, N. and Xu, Y.J., 2014, May. BSG-Starcraft radius improvements of particle swarm optimization algorithm: An application to ceramic matrix composites. In *International Conference on Swarm Intelligence Based Optimization* (pp. 166-174). Springer, Cham.

[56] Xu, Y.J., Padayodi, E., Bahrani, S.A. and Chamoret, D., 2014. Minimizing Thermal Residual Stresses in Ceramic Matrix Composite by BSG-Starcraft Radius PSO. *International Journal of Advanced Design and Manufacturing Technology*, *7*(2), p.21.

[57] Satyobroto, T., 2011. Mathematical modelling and applications of particle swarm optimization. *School of Engineering, Blekinge Institute of Technology*.

[58] Salmon, S., 2011. Particle swarm optimization in Scilab.

[59] Kennedy, J., 2011. Particle swarm optimization. In *Encyclopedia of machine learning* (pp. 760-766). Springer US.

[60] Liu, D.P., 2006, August. Parameter identification for LuGre friction model using genetic algorithms. In *Machine Learning and Cybernetics, 2006 International Conference on* (pp. 3419-3422). IEEE.

[61] Verge, M., 2005. Friction identification with genetic algorithms. *IFAC Proceedings Volumes*, *38*(1), pp.560-565.

[62] Gleghorn, J.P. and Bonassar, L.J., 2008. Lubrication mode analysis of articular cartilage using Stribeck surfaces. *Journal of biomechanics*, 41(9), pp.1910-1918.

[63] Kalin, M., Velkavrh, I. and Vižintin, J., 2009. The Stribeck curve and lubrication design for non-fully wetted surfaces. *Wear,* 267(5-8), pp.1232-1240.

List of Papers

International Journals (Full papers with reviews)

1. "Determining Frictional Characteristics of Human Ocular Surfaces by Employing BSG-Starcraft of Particle Swarm Optimization", Sarwo Pranoto, Shingo Okamoto, Jae Hoon Lee, Atsushi Shiraishi, Yuri Sakane, and Yuichi Ohashi, *Journal of Biomedical Engineering and Biosciences (JBEB),* Vol. 4, pp. 43 – 51, 2017.

2. "Development of Ocular Surface Tribometer and Frictional Characteristics of Human Ocular Surface", Sarwo Pranoto, Shingo Okamoto, Ryoichiro Kataoka, Jae Hoon Lee, Atsushi Shiraishi, Yuri Sakane, Masahiko Yamaguchi, and Yuichi Ohashi, *International Journal of Bioscience, Biochemistry and Bioinformatics (IJBBB),* Vol. 8, No. 2, April 2018.

Proceeding of International Conference (Full paper with review)

1. "Development of Ocular Surface Tribometer and Frictional Characteristics of Human Ocular Surface", Sarwo Pranoto, Shingo Okamoto, Ryoichiro Kataoka, Jae Hoon Lee, Atsushi Shiraishi, Yuri Sakane, Masahiko Yamaguchi, and Yuichi Ohashi, *Proceeding of 8th International Conference on Bioscience, Biochemistry and Bioinformatics (ICBBB),* January 18-20, 2018, Tokyo, Japan.

2. "Comparison of Frictional Characteristic Curves of Human Ocular Surface Determined by Using Hersey Number and Proposed New Number", Sarwo Pranoto, Shingo Okamoto, Jae Hoon Lee, Atsushi Shiraishi, Yuri Sakane, Masahiko Yamaguchi, and Yuichi Ohashi, *Proceeding of 4th World Congress on Electrical Engineering and Computer Systems and Sciences (EECSS'18),* August 21-23, 2018, Madrid, Spain.

Acknowledgments

Curriculum Vitae

Name	:	Sarwo Pranoto
Place/Date of Birth	:	Cilacap, Indonesia / June 20, 1980
Gender	:	Male
Background of Education		
1. Master (M.Eng)	:	Electrical and Computer System Engineering, Faculty of Engineering, Monash University, Australia (2008-2009)
2. Bachelor (B.Eng)	:	Electrical Engineering, Faculty of Engineering, Gadjah Mada University, Indonesia (1998-2003)
Occupation	:	Lecturer
Institution	:	State Polytechnic of Ujung Pandang, Indonesia
Department	:	Electrical Engineering
Study Program	:	Electrical Engineering
Personal Email Address	:	sarwo.pranoto@gmail.com